Studies on Controller Networks

Dissertation

Submitted in Partial Fulfillment of the Requirements
for the Degree of Doctor of Informatics

Shinsaku Izumi

Department of Systems Science
Graduate School of Informatics
Kyoto University

Abstract

While feedback systems using a single controller have been mainly considered in the systems and control field, systems with networked controllers, *i.e.,* a controller network, have received much attention in recent years. In such systems, the nodes of the network cooperatively determine control inputs by sharing information with their neighbors. This scheme enables us to make control systems robust against failures. Furthermore, the controller network has great potential for engineering applications, *e.g.,* wireless control systems, smart grids, and multi-robot systems.

The main purpose of this thesis is to give solutions to some problems in the controller network design. More precisely, we address the following problems.

First, we consider a problem of finding a controller network to stabilize linear plants under the assumption that its network topology is fixed but unknown. As a solution to the problem, a controller network acting as a state feedback controller is proposed. We then prove that the resulting feedback system is stable if the gains of networked controllers are appropriately chosen. With this result, we can obtain a controller network which is robust against changes in the network topology. In addition, the relation between the stabilizing gain and the network topology is clarified, which provides useful information to design the gain in an easy way.

Second, we provide a framework of real-time pricing, *i.e.,* to control the total power consumption of consumers by changing power prices in real-time, based on the controller network. In the proposed framework, each power source has a local controller, and estimates the total power consumption by exchanging information on the required power with its neighbors. The problem addressed here is to design the local controllers and a power price controller such that the total power consumption tracks a given reference input under a constraint on the range of the power price. For this problem, we first derive a necessary condition for its solvability. This enables us to estimate the price needed to achieve tracking a given reference input. Then, we propose a solution to the problem and show that it achieves the real-time pricing. With this result, we can achieve the real-time pricing without collecting information on the power consumption from all the consumers.

Finally, we address a problem of designing a controller network for the robotic mass games, that is, to let robots organize themselves into a formation displaying a given grayscale image. By fusing ideas of the coverage control and the halftone image processing, we derive a solution to the problem. The performance of our solution is demonstrated by numerical experiments with standard images. Moreover, we give extensions to the cases of r-disk proximity networks and a variable number of player robots. The former enables us to achieve the mass games even though the communication range of the robots is limited. The latter improves the visual quality of the resulting formations.

Acknowledgements

I would like to express my heartfelt appreciation to everyone who has supported and encouraged this work in various ways.

First of all, I would like to express my sincere gratitude to Professor Toshiharu Sugie for providing a valuable opportunity to work toward a Ph.D. degree in his laboratory. He has provided favorable working environment for me. In addition, he has given patient guidance and constant encouragement to me. Without such support, this thesis would never be completed.

Secondly, I wish to thank Professor Yoshito Ohta and Professor Toshiyuki Ohtsuka for being the committee members of this dissertation and for their critical comments.

Thirdly, I would like to appreciate Dr. Shun-ichi Azuma for his valuable advice and encouragement. I have learned skills of logical thinking and academic writing from him. These skills are useful to complete this thesis. Moreover, he has given me great opportunities for studying many interesting topics. This thesis includes some of the topics.

Fourthly, I would like to thank Dr. Ichiro Maruta for his a lot of support. In particular, he has advised me on techniques of computer programming. Numerical experiments in this thesis have been performed based on the advice.

Fifthly, I would like to thank the former and current members of Mechanical Systems Control Laboratory of Kyoto University. Dr. Kazunori Sakurama, Dr. Yuki Minami, Dr. Ryosuke Morita, and Dr. Kazuhiro Sato have given me useful advice and encouragement. Also, I have enjoyed the time with the members of the laboratory, which has given me moral support.

Finally, I am grateful to my parents Hisashi and Hiromi Izumi for their patient and warm encouragement.

Shinsaku Izumi
Kyoto University
December 2014

Contents

Notation

The following notation is used in this thesis.

$\mathbb{R}$	real number field
$\mathbb{R}_+$	set of positive real numbers
$\mathbb{R}_{0+}$	set of nonnegative real numbers
$\mathbb{C}$	complex number field
i	imaginary unit, *i.e.,* $\mathrm{i} := \sqrt{-1}$
1_n	$n \times 1$ vector whose elements are one
I_n	$n \times n$ identity matrix
$0_{n\times m}$ (or simply 0)	$n \times m$ zero matrix
$M^\top$	transpose of the matrix M
M^{-1}	inverse of the matrix M
$[M]_{ij}$	(i, j)-element of the matrix M
$\mathrm{diag}(x_1, x_2, \ldots, x_n)$	diagonal matrix whose i-th diagonal element is the number x_i
$\mathrm{diag}(M_1, M_2, \ldots, M_n)$	block diagonal matrix whose i-th diagonal block is the matrix M_i
$\lambda_i(M)$	eigenvalue of the matrix M with the i-th smallest modulus
$\Lambda(M)$	diagonal matrix whose i-th diagonal element is the eigenvalue $\lambda_i(M)$ of the matrix M, *i.e.,* $\Lambda(M) := \mathrm{diag}(\lambda_1(M), \lambda_2(M), \ldots, \lambda_n(M)) \in \mathbb{C}^{n\times n}$
$\Lambda_{-i}(M)$	$\mathrm{diag}(\lambda_1(M), \ldots, \lambda_{i-1}(M), \lambda_{i+1}(M), \ldots, \lambda_n(M)) \in \mathbb{C}^{(n-1)\times(n-1)}$
$\|x\|$	Euclidean norm of the vector x
$\|M\|$	Euclidean norm of the matrix M
$\|M\|_p$	induced p-norm of the matrix M

$\mathrm{Re}(z)$	real part of the complex number z
$\emptyset$	empty set
$\mathbb{B}(c, r)$	closed disk of center c and radius r, *i.e.*, $\mathbb{B}(c, r) := \{x \in \mathbb{R}^2 \mid \|x - c\| \le r\}$
$\lvert\mathbb{S}\rvert$	cardinality of the set $\mathbb{S}$
$\mathrm{bd}(\mathbb{S})$	boundary of the set $\mathbb{S}$
$\mathrm{diam}(\mathbb{S})$	diameter of the set $\mathbb{S}$, that is, $\mathrm{diam}(\mathbb{S}) := \max_{(p,q)\in\mathbb{S}\times\mathbb{S}} \|p - q\|$

The following notation is also defined.

- For the vectors $x_1, x_2, \ldots, x_n \in \mathbb{R}^m$ and the set $\mathbb{I} := \{i_1, i_2, \ldots, i_\ell\} \subseteq \{1, 2, \ldots, n\}$, let $[x_i]_{i\in\mathbb{I}} := [x_{i_1}^\top \; x_{i_2}^\top \; \cdots \; x_{i_\ell}^\top]^\top \in \mathbb{R}^{\ell m}$.
- For the numbers $a \in \mathbb{R}_+$ and $x \in \mathbb{R}$, the saturation function is defined as

$$\mathrm{sat}_a(x) := \begin{cases} a & \text{if } a < x, \\ x & \text{if } 0 \le x \le a, \\ 0 & \text{if } x < 0. \end{cases}$$

- For the bounded and nonzero-measure set $\mathbb{S} \subset \mathbb{R}^2$ and the function $f : \mathbb{R}^2 \to \mathbb{R}_{0+}$, let

$$\mathrm{cent}(\mathbb{S}, f) := \frac{\int_{\mathbb{S}} s f(s) ds}{\int_{\mathbb{S}} f(s) ds}.$$

  This represents the weighted centroid of the set $\mathbb{S}$.

Chapter 1

Introduction

1.1 Background

In the systems and control field, feedback systems in the form of Figure 1.1 have been mainly considered, and controller design problems have been addressed.

On the other hand, feedback systems in the form of Figure 1.2 have received much attention in recent years [1]. They include a network of controller nodes instead of the controller in the system in Figure 1.1. The controller nodes cooperatively determine control inputs by exchanging information with their neighbors. The network of the controller nodes is called here the *controller network*.

Considering the controller network is motivated by the following three facts. First, with recent advances in microcontrollers and wireless communication technologies, the controller network has become available in many practical situations. In fact, it is impractical to construct the controller network only by desktop computers and wired networks. Second, the controller network makes the resulting control system robust against failures. This is because, the control system in Figure 1.1 does not work if the controller fails, but even if some controller nodes fail in the system in Figure 1.2 the others can compensate for the failures. Finally, the controller network has great potential for engineering applications. Examples are as follows.

- **Wireless control systems.** In wireless control systems, sensors, controllers, and actuators are connected by wireless networks. With wireless technologies, we can substantially reduce costs and time needed for installation and maintenance of cables. Figure 1.3 illustrates a typical setup of the wireless control system, where the dotted lines and the arrows represent the network structure and the information flow. This consists of sensors, a controller, actuators, and communication nodes, and the control is performed over the multi-hop network [2–5]. Namely, the controller receives the signals from

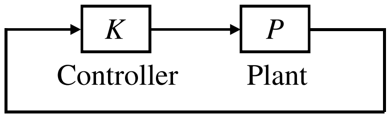

Figure 1.1: Conventional feedback system.

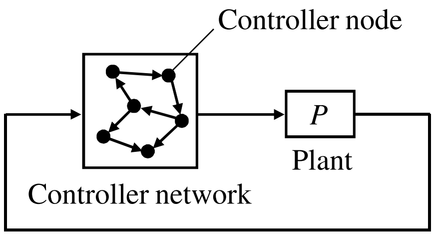

Figure 1.2: Feedback system with controller network.

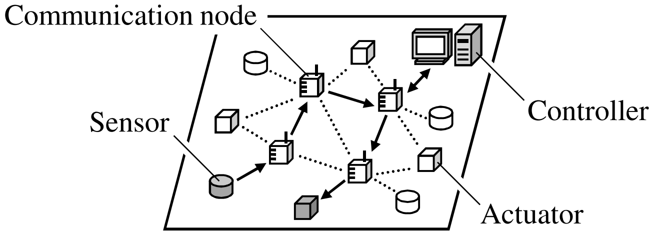

Figure 1.3: Wireless control system with multi-hop network.

the sensors through the communication nodes, and transmits control signals to the actuators through those. In this system, we can make the controller network by using the communication nodes as the controller nodes if they have processing capability. The resulting system is shown in Figure 1.4 (a).

- **Smart grids.** Smart grids are electrical grid systems with information and communication technologies. By utilizing such technologies, it is expected that we can manage a large amount of renewable energy, *e.g.,* wind power and solar power, which results in lower greenhouse gas emissions. An illustration of the smart grids is given in Figure 1.4 (b). In this system, the power sources are connected by the communication links. Then, the system can be considered as that in Figure 1.2, where the plant corresponds to, for example, the balance of power demand and supply, and the controller nodes correspond to controllers embedded in the power sources.

- **Multi-robot systems.** In multi-robot systems, robots cooperatively exe-

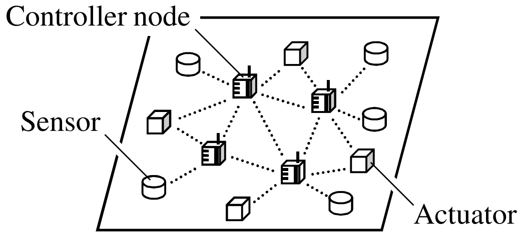

(a) Wireless control system.

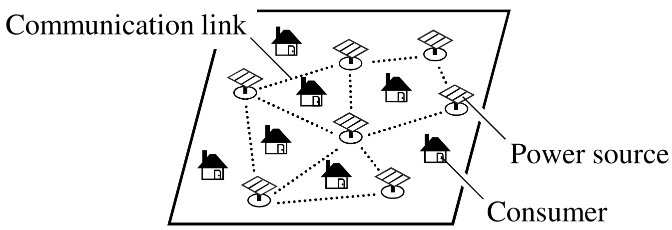

(b) Smart grid.

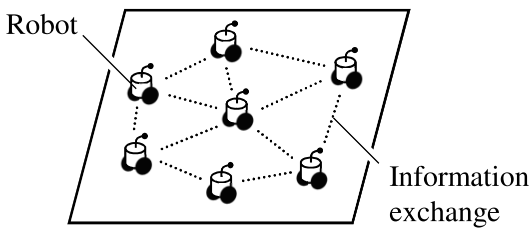

(c) Multi-robot system.

Figure 1.4: Applications of controller network.

cute a given motion coordination task by exchanging information with their neighbors. This type of system has various applications including exploration, surveillance, and hazardous material handling [6]. An illustration of the multi-robot systems is shown in Figure 1.4 (c). The information exchange among the robots is performed by sensing or communication, and as a result, a network where the robots correspond to the nodes is constructed. Then, the multi-robot system can be interpreted as the system in Figure 1.2 by regarding the behavior of the group of the robots and the embedded controllers as the plant and the controller nodes, respectively.

1.2 Previous Works

Though the concept of the controller network has recently been introduced, several studies have already been performed. The main problem is to design the controller network such that the resulting feedback system achieves desired performance. In the existing studies, this problem has been addressed in three ways, and the following results have been obtained.

- **Linear control approach.** This approach is to suppose that each controller node is a linear compensator and to apply design methods in the linear control theory. In fact, the resulting feedback system is linear if the plant is a linear system, which allows us to use such methods. In this way, some studies have been conducted. Pajic et al. [1] have proposed a design method of the controller nodes stabilizing linear plants. They have also derived conditions on the network topology such that the method is available [7]. The result in [1] has been extended to optimal control and robust control [8]. In addition, Miao et al. [9] have provided a scheme to implement a given linear compensator as a controller network.

- **Neural network approach.** In the neural network approach, the controller network is designed as a neural network controller (see, *e.g.,* [10]), where each controller node corresponds to each neuron. By this approach, a controller network for nonlinear plants has been derived [11]. After that, an H_∞ controller network has been presented [12].

- **Distributed state estimation approach.** The distributed state estimation approach is to estimate the state of the plant by sharing information between the controller nodes, and to perform feedback control based on the estimate. In [13], an H_∞ controller network based on this approach has been derived.

While such results have been obtained, there are two problems to be addressed. First, the network topology is assumed to be fixed in the existing studies, but the network topology often changes in a real situation. For example, when a wireless network is adopted to connect the controller nodes, radio frequency interference causes failures of the communication links, which results in a topology change. If such a topology change occurs for the existing controller networks, the resulting feedback systems may be unstable. Second, most of the existing controller networks are not scalable; namely, it is difficult to apply them to large-scale systems such as smart grids. In fact, in the linear control approach, the controller nodes are treated in a discriminate way, which implies that we have to provide a dedicated controller for each of many controller nodes. Also, in the distributed state estimation approach, the state vector of each controller node has the size of that of the plant, and so a large amount of memory is needed for large-scale plants.

Meanwhile, from the viewpoint of the multi-robot control, the controller network has been investigated. The main problem is to find a controller network for achieving a given motion-coordination task. Examples of the task are as follows.

- **Rendezvous [14–21]:** All the robots move to a common point as shown in Figure 1.5 (a).

- **Coverage [22–28]:** The robots are steered so that the sizes of the robots' occupied areas are equal in some sense. An example is shown in Figure 1.5 (b) where the regions separated by the dotted lines correspond to the robots' occupied areas.

- **Flocking [29–35]:** The robots exhibit a behavior like bird flocking or fish schooling. Figure 1.5 (c) illustrates an example.

This problem is different from the above one in the sense that the target system and the purpose are limited to the multi-robot system and the motion-coordination, respectively. From this standpoint, many results have been obtained so far (see *e.g.,* [36, 37] and references therein).

In various topics of the multi-robot control, formation control, *i.e.,* making the robots move so that the configuration becomes a desired shape, has been an active research topic in the systems and control community. The existing studies on the formation control have been pursued to achieve formations given as

- specific geometric patterns (*e.g.,* lines, circles, and polygons) [38–42],

- distances between the robots [43–50],

- relative positions between the robots [51–57].

This implies that rather simple formations by at most several tens of robots have been mainly considered. In fact, if the number of robots is large and the desired formation is not regular, it is difficult to calculate the distances or the relative positions between the robots in the desired formation. For example, the formation control to achieve formations displaying pictures has great potential for entertainment applications, but it is not easy to specify such formations as the distances or the relative positions between robots. This suggests us to develop a framework for complex formations by large-scale robotic systems.

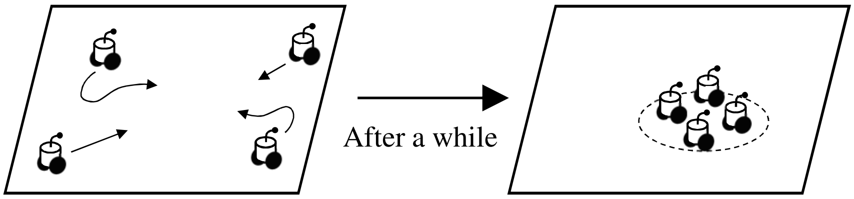

(a) Rendezvous.

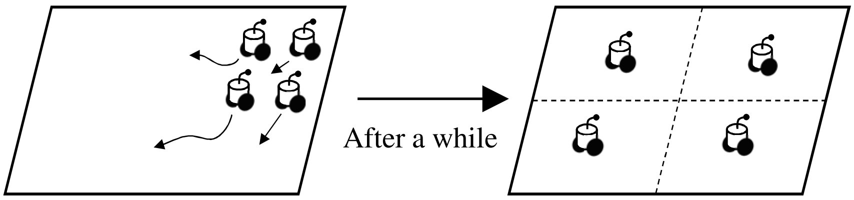

(b) Coverage.

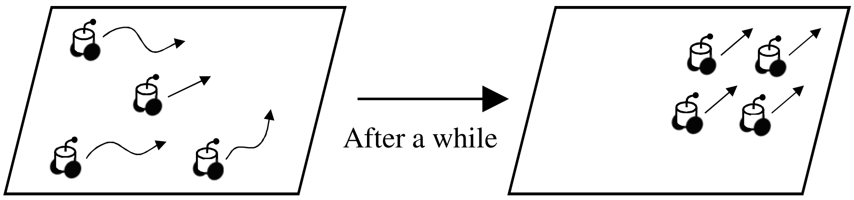

(c) Flocking.

Figure 1.5: Examples of motion-coordination task.

1.3 Purposes and Contributions

The main aim of this thesis is to give solutions to some problems in the controller network design. More precisely, we develop

1) a controller network that is *scalable* and *robust* against changes in the network topology,

2) a controller network for *real-time pricing* [58] in the smart grids,

3) a controller network to achieve formations displaying *grayscale images*.

The reasons for considering the first and third ones are as described in Section 1.2. The second one is, meanwhile, motivated by the fact that, to our best knowledge, there is no result on the controller network for the real-time pricing, *i.e.,* to control the power consumption of consumers by changing power prices in real-time. The detailed motivation will be given in Chapter 4.

For this purpose, we focus on the following three topics.

1. Stabilization by controller networks

In this topic, we consider the feedback system in Figure 1.6, which is composed of a single-input plant, sensor nodes, controller nodes, and an actuator node. For this system, we suppose that the network topology belongs to a prespecified set but the detail (which element it is) is *unknown*, and assume that all the controller nodes are the *same*. Then, the problem considered here is to find sensor nodes, controller nodes, and an actuator node, stabilizing the resulting feedback system. Since the network topology is assumed to be unknown, the solution can stabilize the feedback system even if the topology changes. Furthermore, by the assumption that all the controller nodes are the same, we can deal with them in an indiscriminate manner, which makes the solution scalable.

For this problem, the thesis makes the following two contributions. First, we present a solution to the stabilization problem. It is given as the nodes such that the entire network acts as a state feedback controller by a consensus protocol [59]. We then prove that the resulting feedback system is stable if the gains are appropriately selected. The key idea behind this result is to introduce a *parameterized* coordinate transformation and characterize the parameter in terms of the stability. If a fixed coordinate transformation is applied in the same way, we can only show the stability for some specific plants. However, by introducing the parameterized one and reducing the stabilization problem to that of finding a range of the parameter, we can prove the stability for all controllable plants. Second, the relation between the stabilizing gain and the network topology is clarified. As a result, it is shown that a large gain will be needed for the stabilization if the network among the controller nodes is sparse. This implies that we should design the gain only for the sparsest network in the prespecified set, which substantially reduces the development time of the controller network.

2. Reference tracking by controller networks for real-time pricing

A real-time pricing system based on the controller network is shown in Figure 1.7, which is composed of consumers, power sources, and a power price controller. In this system, each power source has a local controller, and it acts as a distributed estimator for the power consumption. That is, each power source estimates the total power consumption by exchanging information on the required power with its neighbors. The power price controller receives it from the neighbor power sources, and determines the power price. For this system, the following problem is considered: when a reference input, an upper bound of the power price, and a network topology are given, find local controllers and a power price controller

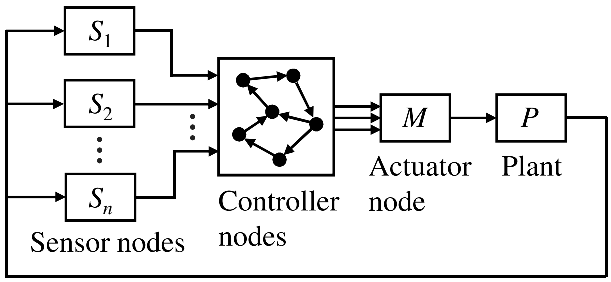

Figure 1.6: Feedback system considered in topic 1.

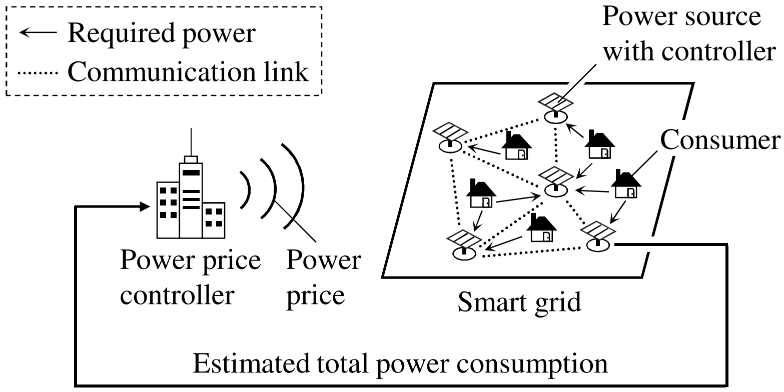

Figure 1.7: Real-time pricing system considered in topic 2.

such that the total power consumption tracks the given reference input. To our best knowledge, such a problem has never been handled so far.

The contributions for this problem are summarized as follows. The first one is to derive a necessary condition for solving the design problem of the real-time pricing system. The condition is given as an inequality in terms of the reference input and the upper bound of the power price. This enables us to estimate the price needed to achieve tracking a given reference input. The second contribution is to give a solution to the design problem. It is composed of local controllers based on a consensus protocol and a proportional and integral type power price controller. We then prove that the solution achieves the real-time pricing by appropriately selecting the gains. The key idea behind this result is to extend the result for topic 1 to the integral control for achieving the reference tracking.

It should be stressed that we do not just apply the result for topic 1 to the real-time pricing. In fact, as described above, we extend the previous result to integral control for solving the tracking problem. As a result, we can obtain the appropriate gains of the resulting controller network without the exact information on the consumers. This is an advantage when the real-time pricing is applied to large-scale communities. Meanwhile, since using the integrator increases the dimension of the entire system, the analysis technique based on a coordinate transformation, proposed in topic 1, is not directly available for the proof of the convergence. So, we perform a new coordinate transformation by utilizing special properties of the consumers, from which a convergence result is obtained. Also in this respect, the result obtained here is not a straightforward consequence of the previous one.

3. Robotic mass games by controller networks

In this topic, the multi-robot system in Figure 1.4 (c) is handled. For this system, the following problem is addressed: when a grayscale image is given, find local controllers embedded in the robots, achieving a formation displaying the image. Such a formation control problem is called here the *mass game* problem and it is illustrated in Figure 1.8. The motivation for the mass game problem is that this problem has a different kind of difficulty from those of the existing ones. In fact, information on the desired formation is only the image, and the desired position of each robot is not explicitly specified. Then, we have to represent the grayscale information, *i.e.,* interlevel information, of the image as a formation by a finite number of robots. This type of multi-robot problem is novel.

For this problem, the contributions of the thesis are as follows. First, a solution to the mass game problem is provided. It is given by combining ideas of the *coverage control* [23] and the *halftone image processing* (see, *e.g.,* [60]). The performance is verified in the same way as that in the image processing area. More precisely, by numerical experiments with the standard images [61], it is demonstrated that the solution achieves formations displaying given grayscale images. Second, we extend the above result to the case of *r-disk proximity networks* [62]. The above result may require that each robot communicates with distant others, and so it is difficult to apply the result to real robots with limited communication range. However, with this result, we can achieve the mass games even in the situation where communication range constraints are imposed for robots. Finally, we present an extension to the case of a *variable* number of player robots. The above two results are for the mass game with a *fixed* number of player robots, and it is assumed in them that all the robots participate in the mass game even for a bright image which only needs a few robots. This results in a critical drawback that the brightness of the resulting image does not agree with that of the given image. Meanwhile, the controller network proposed here classifies the robots into a player group and a nonplayer group in a distributed manner, and so the resulting image always agrees with the given image. This difference will be demonstrated in Chapter 5, and it will be shown that the controller network proposed here improves approximately up to 8.6 dB in the peak signal to noise ratio [63].

We would like to emphasize the novelty of the result obtained here. The result

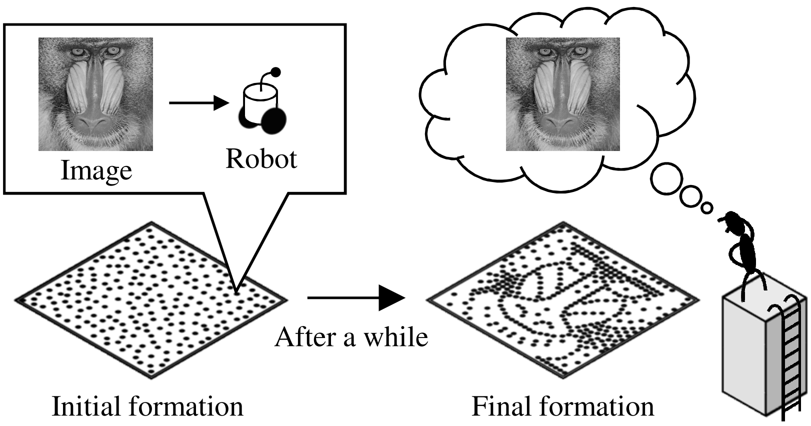

Figure 1.8: Mass game by robots.

here is given by fusing techniques from the control area and the image processing area. From a technical point of view, there is no multi-robot control method utilizing image processing techniques.

1.4 Organization of Thesis

This thesis is organized as follows.

Chapter 2 presents a mathematical framework of the controller network. We first introduce some notions of the graph theory in order to describe the network by a graph. Then, systems with the controller network are mathematically expressed, and a design problem of the controller network is formulated.

Chapter 3 gives a controller network for stabilization. First, a design problem of the controller network is formulated. As a solution the problem, we propose a controller network such that the entire network acts as a state feedback controller by a consensus protocol. We then derive conditions on the gains for the stability of the resulting feedback system. In addition, the relation between the stabilizing gain and the network topology is clarified.

Chapter 4 presents a tracking controller network for the real-time pricing. To this end, we first formulate the tracking problem for the real-time pricing system. For this problem, a necessary condition for the solvability is derived. In addition, we propose consensus-based local controllers and a proportional and integral type power price controller, and prove that these solve the problem.

Chapter 5 gives controller networks for the mass games. First, the mass game problem is stated. Next, as elemental techniques, we introduce the coverage control and the halftone image processing. Based on these, a controller network for the mass games is proposed. The performance of the proposed controller network is demonstrated by numerical experiments with the standard images. In addition to this, we give extensions to the cases of r-disk proximity networks and a variable number of player robots.

Chapter 6 concludes this thesis.

Chapter 2

Controller Networks

In this chapter, we present a mathematical framework of the controller network. First, some notions of the graph theory are introduced [37, 62] because graphs are a useful tool for expressing the network. Then, we provide a system description, and show a general form of the design problem of the controller network. In addition, we explain the relation between the general design problem and the problems addressed in the following chapters.

2.1 Graph Theory

Graphs are composed of *nodes* and *edges*, and they, for example, are expressed by circles and arrows as shown in Figure 2.1. The set of the nodes is called the *node set*, and is represented by $\mathbb{I}$. In a similar way, we refer to the set of the edges as the *edge set*, and represent it by $\mathbb{E}$. The edge set $\mathbb{E}$ is a set of ordered pairs of the nodes, that is, $\mathbb{E} \subseteq \mathbb{I} \times \mathbb{I}$. Then, a graph is expressed by $G = (\mathbb{I}, \mathbb{E})$. For instance, the graph in Figure 2.1 is denoted by $G = (\mathbb{I}, \mathbb{E})$ for $\mathbb{I} := \{1, 2, \ldots, 5\}$ and $\mathbb{E} := \{(1, 2), (2, 3), (3, 4), (3, 5), (5, 1), (5, 2)\}$.

Next, let us introduce two notions used in this thesis. A graph $G' = (\mathbb{I}', \mathbb{E}')$ is said to be a *subgraph* of a graph $G = (\mathbb{I}, \mathbb{E})$ if $\mathbb{I}' \subset \mathbb{I}$ and $\mathbb{E}' \subset \mathbb{E}$. An example is shown in Figure 2.2 where a subgraph of the graph in Figure 2.2 (a) is given in Figure 2.2 (b). Meanwhile, a graph is said to be *strongly connected* if there is a path between any two nodes. For example, the graph in Figure 2.3 is strongly connected, but that in Figure 2.1 is not.

Finally, the *graph Laplacian* L of a graph $G = (\mathbb{I}, \mathbb{E})$ is defined as a matrix

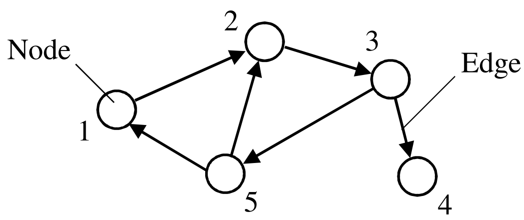

Figure 2.1: Example of graph

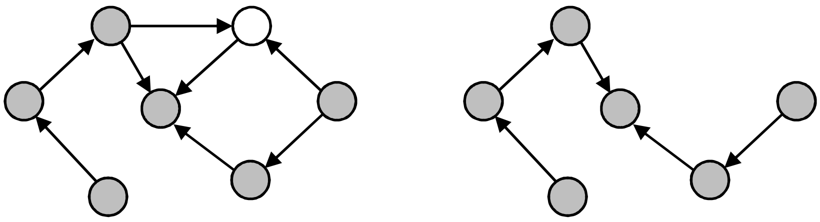

(a) (b)

Figure 2.2: Two graphs.

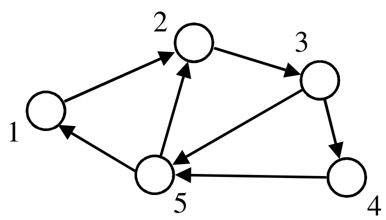

Figure 2.3: Strongly connected graph

whose (i, j)-element is given by

$$[L]_{ij} := \begin{cases} -1 & \text{if } (j, i) \in \mathbb{E}, \\ d_i & \text{if } i = j, \\ 0 & \text{otherwise} \end{cases} \tag{2.1}$$

where $d_i \in \mathbb{R}_{0+}$ is the *in-degree* of node i, *i.e.,* the number of the nodes connected to it. For instance, the graph Laplacian L of the graph in Figure 2.1 is defined as

$$L := \begin{bmatrix} 1 & 0 & 0 & 0 & -1 \\ -1 & 2 & 0 & 0 & -1 \\ 0 & -1 & 1 & 0 & 0 \\ 0 & 0 & -1 & 1 & 0 \\ 0 & 0 & -1 & 0 & 1 \end{bmatrix}.$$

For the graph Laplacian L, the following properties are important in this thesis.

(L1) The graph Laplacian L has a zero eigenvalue, and the corresponding eigenvector is the vector whose elements are one, *i.e.,*

$$L1_n = 0_{n\times 1} \tag{2.2}$$

for $L \in \mathbb{R}^{n\times n}$.

(L2) For the graph, assume that there exists an edge from node j to node i if there exists an edge from node i to node j. Then, L is positive-semidefinite, *i.e.,*

$$0 \leq \lambda_2(L) \leq \lambda_3(L) \leq \cdots \leq \lambda_n(L). \tag{2.3}$$

Moreover, L has the vector whose elements are one as a left eigenvector for the zero eigenvalue, that is,

$$1_n^\top L = 0_{1\times n}. \tag{2.4}$$

(L3) If the graph is strongly connected, then the zero eigenvalue of L is isolated, *i.e.,* $\lambda_2(L) \neq 0$.

2.2 Control Systems with Controller Networks

Now, we mathematically describe systems with the controller network.

Consider the feedback system Σ in Figure 2.4, composed of an ℓ-input m-output plant, m sensor nodes, n controller nodes, and ℓ actuator nodes.

The plant P is a dynamical system whose input and output are $u(t) \in \mathbb{R}^\ell$ and $y(t) \in \mathbb{R}^m$. The sensor node S_i ($i \in \{1, 2, \ldots, m\}$) is given by

$$S_i : \begin{cases} \dot{\xi}_{Si}(t) = \sigma_{i1}(\xi_{Si}(t), y_i(t)), \\ z_i(t) = \sigma_{i2}(\xi_{Si}(t), y_i(t)) \end{cases} \tag{2.5}$$

where $\xi_{Si}(t) \in \mathbb{R}^{N_S}$ is the state, $y_i(t) \in \mathbb{R}$ is the input, that is, the i-th element of $y(t)$, $z_i(t) \in \mathbb{R}^p$ is the output, and $\sigma_{i1} : \mathbb{R}^{N_S} \times \mathbb{R} \to \mathbb{R}^{N_S}$ and $\sigma_{i2} : \mathbb{R}^{N_S} \times \mathbb{R} \to \mathbb{R}^p$ are functions. The controller node K_i ($i \in \{1, 2, \ldots, n\}$) is of the form

$$K_i : \begin{cases} \dot{\xi}_{Ki}(t) = \kappa_{i1}(\xi_{Ki}(t), [z_j(t)]_{j\in\mathbb{N}_{Ki}^S}, [v_j(t)]_{j\in\mathbb{N}_{Ki}}), \\ v_i(t) = \kappa_{i2}(\xi_{Ki}(t), [z_j(t)]_{j\in\mathbb{N}_{Ki}^S}, [v_j(t)]_{j\in\mathbb{N}_{Ki}}) \end{cases} \tag{2.6}$$

where $\xi_{Ki}(t) \in \mathbb{R}^{N_K}$ is the state, $[z_j(t)]_{j\in\mathbb{N}_{Ki}^S} \in \mathbb{R}^{p|\mathbb{N}_{Ki}^S|}$ and $[v_j(t)]_{j\in\mathbb{N}_{Ki}} \in \mathbb{R}^{q|\mathbb{N}_{Ki}|}$ are the inputs, $v_i(t) \in \mathbb{R}^q$ is the output, and $\kappa_{i1} : \mathbb{R}^{N_K} \times \mathbb{R}^{p|\mathbb{N}_{Ki}^S|} \times \mathbb{R}^{q|\mathbb{N}_{Ki}|} \to \mathbb{R}^{N_K}$ and

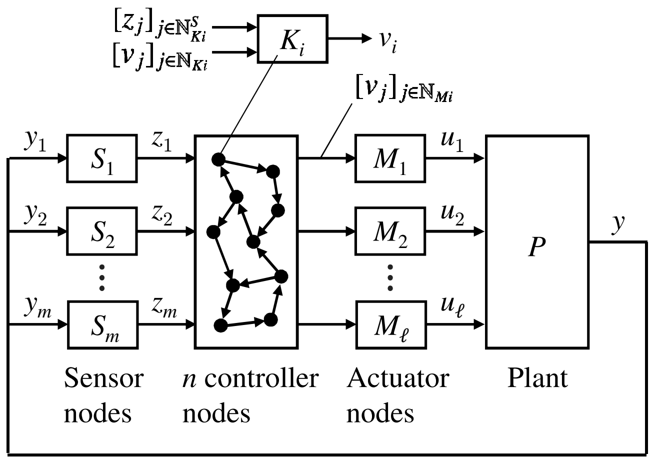

Figure 2.4: Feedback system Σ.

$\kappa_{i2} : \mathbb{R}^{N_K} \times \mathbb{R}^{p|\mathbb{N}^S_{Ki}|} \times \mathbb{R}^{q|\mathbb{N}_{Ki}|} \to \mathbb{R}^q$ are functions. The sets $\mathbb{N}^S_{Ki} \subseteq \{1, 2, \ldots, m\}$ and $\mathbb{N}_{Ki} \subseteq \{1, 2, \ldots, n\} \setminus \{i\}$ are the index sets of the *neighbors*, that is, the sensor nodes and the controller nodes sending their outputs to the controller node K_i. Finally, the actuator node M_i ($i \in \{1, 2, \ldots, \ell\}$) is given by

$$M_i : \begin{cases} \dot{\xi}_{Mi}(t) = \mu_{i1}(\xi_{Mi}(t), [v_j(t)]_{j\in\mathbb{N}_{Mi}}), \\ u_i(t) = \mu_{i2}(\xi_{Mi}(t), [v_j(t)]_{j\in\mathbb{N}_{Mi}}) \end{cases} \tag{2.7}$$

where $\xi_{Mi}(t) \in \mathbb{R}^{N_M}$ is the state, $[v_j(t)]_{j\in\mathbb{N}_{Mi}} \in \mathbb{R}^{q|\mathbb{N}_{Mi}|}$ is the input, $u_i(t) \in \mathbb{R}$ is the output, which corresponds to the i-th element of $u(t)$, and $\mu_{i1} : \mathbb{R}^{N_M} \times \mathbb{R}^{q|\mathbb{N}_{Mi}|} \to \mathbb{R}^{N_M}$ and $\mu_{i2} : \mathbb{R}^{N_M} \times \mathbb{R}^{q|\mathbb{N}_{Mi}|} \to \mathbb{R}$ is a function. The set $\mathbb{N}_{M_i} \subseteq \{1, 2, \ldots, \ell\}$ is the index set of the neighbors defined in a similar way to that for the controller nodes.

In the feedback system Σ, each sensor node S_i transmits the signal $z_i(t)$ to the neighbor controller nodes based on the measurement $y_i(t)$. The controller nodes K_i ($i = 1, 2, \ldots, n$) communicate with each other to share the information. Each actuator node M_i receives the shared information from the neighbor controller nodes, and determines the control input $u_i(t)$.

2.3 Design Problems of Controller Networks

We represent the network topology of the feedback system Σ by the graph G with the node set corresponding to S_i ($i = 1, 2, \ldots, m$), K_i ($i = 1, 2, \ldots, n$), and M_i ($i = 1, 2, \ldots, \ell$) and the edge set corresponding to the connections. Then, the problem discussed in this thesis is stated as follows: when the network topology G is given for the feedback system Σ, find sensor nodes $S_1, S_2, \ldots, S_m$, controller

Table 2.1: Relation between generalized problem and problems considered in following chapters.

	Stabilization problem (Chapter 3)	Tracking problem for real-time pricing system (Chapter 4)	Mass game problem (Chapter 5)
Σ	Generalized system	Real-time pricing system	Multi-robot system
P	Single-input linear system	Total power consumption	Group position of robots
S_i	Sensor node	Local controller in each power source	Local controller in each robot
K_i	Controller node		
M_i	Actuator node	Power price controller	
Purpose	Stabilization	Reference tracking	Mass games

nodes $K_1, K_2, \ldots, K_n$, and actuator nodes $M_1, M_2, \ldots, M_\ell$, *i.e.,* functions σ_{i1}, σ_{i2} ($i = 1, 2, \ldots, m$), κ_{i1}, κ_{i2} ($i = 1, 2, \ldots, n$), and μ_{i1}, μ_{i2} ($i = 1, 2, \ldots, \ell$), such that the system Σ achieves desired performance.

In the following chapters, this problem is considered from several viewpoints. Table 2.1 shows the relation between the problem and those addressed in the following chapters. In Chapter 3, we discuss a stabilization problem of single-input linear plants for the generalized system in Figure 1.6. Chapter 4 considers a tracking problem for the real-time pricing system in Figure 1.7, where the combination of S_i and K_i corresponds to the local controller in each power source and M_i corresponds to the power price controller. In Chapter 5, the mass game problem for the multi-robot system in Figure 1.4 (c) is handled. Here, the local controller in each robot is regarded as the collection of S_i, K_i, and M_i.

Chapter 3

Stabilization by Controller Networks

This chapter considers a design problem of the controller network for stabilization. More precisely, we address a problem of finding a controller network stabilizing linear-time invariant plants subject to the constraints that the network topology is *unknown* and all the controller nodes are the *same*. As a solution to this problem, we propose a controller network calculating a state feedback control law in a distributed manner. We then derive conditions on the gains to stabilize the resulting feedback system. This enables us to obtain a controller network which is scalable and robust against changes in the network topology. Furthermore, we clarify the relation between the stabilizing gain and the network topology, which provides useful information to design the gain in an easy way.

3.1 Problem Formulation

Consider the feedback system Σ in Figure 3.1, which is composed of a single-input m-output plant, m sensor nodes, n controller nodes, and an actuator node.

The plant P is a continuous-time linear system

$$P : \begin{cases} \dot{x}(t) = Ax(t) + Bu(t), \\ y(t) = Cx(t) \end{cases} \tag{3.1}$$

where $x(t) \in \mathbb{R}^N$ is the state, $u(t) \in \mathbb{R}$ is the input, $y(t) \in \mathbb{R}^m$ is the output, and $A \in \mathbb{R}^{N\times N}$, $B \in \mathbb{R}^{N\times 1}$, and $C \in \mathbb{R}^{m\times N}$ are constant matrices. The initial state is given as $x(0) = x_0 \in \mathbb{R}^N$.

The sensor node S_i ($i \in \{1, 2, \ldots, m\}$) is of the form

$$S_i : z_i(t) = \sigma_i(y_i(t)) \tag{3.2}$$

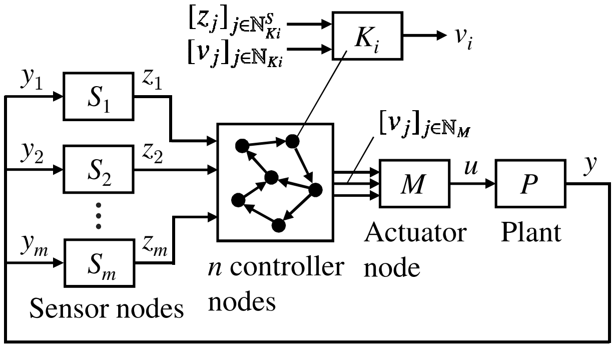

Figure 3.1: Feedback system Σ.

where $y_i(t) \in \mathbb{R}$ is the input, which corresponds to the i-th element of $y(t)$, $z_i(t) \in \mathbb{R}^p$ is the output, and $\sigma_i : \mathbb{R} \to \mathbb{R}^p$ is a function.

The controller node K_i ($i \in \{1, 2, \ldots, n\}$) is given by

$$K_i : \begin{cases} \dot{\xi}_i(t) = \kappa_1(\xi_i(t), [z_j(t)]_{j\in\mathbb{N}^S_{Ki}}, [v_j(t)]_{j\in\mathbb{N}_{Ki}}), \\ v_i(t) = \kappa_2(\xi_i(t), [z_j(t)]_{j\in\mathbb{N}^S_{Ki}}, [v_j(t)]_{j\in\mathbb{N}_{Ki}}) \end{cases} \tag{3.3}$$

where $\xi_i(t) \in \mathbb{R}$ is the state, $[z_j(t)]_{j\in\mathbb{N}^S_{Ki}} \in \mathbb{R}^{p|\mathbb{N}^S_{Ki}|}$ and $[v_j(t)]_{j\in\mathbb{N}_{Ki}} \in \mathbb{R}^{|\mathbb{N}_{Ki}|}$ are the inputs, $v_i(t) \in \mathbb{R}$ is the output, and $\kappa_1, \kappa_2 : \mathbb{R} \times \mathbb{R}^{p|\mathbb{N}^S_{Ki}|} \times \mathbb{R}^{|\mathbb{N}_{Ki}|} \to \mathbb{R}$ are functions. The sets $\mathbb{N}^S_{Ki} \subseteq \{1, 2, \ldots, m\}$ and $\mathbb{N}_{Ki} \subseteq \{1, 2, \ldots, n\} \setminus \{i\}$ are the index sets of the neighbors as defined in Chapter 2. Note that the state $\xi_i(t)$ and the output $v_i(t)$ are assumed to be scalar. This implies that the dimensions do not depend on the scale of the system Σ, *i.e.,* m, n, and N, which results in the *scalability*. In addition, the functions κ_1 and κ_2 and the initial state $\xi_i(0)$ are assumed to be the same for all the controller nodes (κ_1 and κ_2 do not have subscript i). This is also for the scalability, and the detail will be given later. Finally, we assume

$$\xi_i(0) = 0. \tag{3.4}$$

The actuator node M is given by

$$M : u(t) = \mu([v_j(t)]_{j\in\mathbb{N}_M}) \tag{3.5}$$

where $[v_j(t)]_{j\in\mathbb{N}_M} \in \mathbb{R}^{|\mathbb{N}_M|}$ is the input, $u(t) \in \mathbb{R}$ is the output, and $\mu : \mathbb{R}^{|\mathbb{N}_M|} \to \mathbb{R}$ is a function. The set $\mathbb{N}_M \subseteq \{1, 2, \ldots, n\}$ is the index set of the neighbors.

The feedback system Σ works as follows. The sensor node S_i transmits the signal $z_i(t)$ to the neighbor controller nodes based on the measurement $y_i(t)$. The controller nodes K_i ($i = 1, 2, \ldots, n$) communicate with their neighbor ones, and share compressed information on all the signals, *i.e.,* $z_i(t)$ ($i = 1, 2, \ldots, m$), as the scalar states $\xi_i(t)$ $(i = 1, 2, \ldots, n)$. The actuator node M sets the control input $u(t)$ according to the shared information.

The network topology of the feedback system Σ is represented by the graph G with the node set representing $S_1, S_2, \ldots, S_m, K_1, K_2, \ldots, K_n$, and M and the edge set representing the connections. Then, the following problem is considered.

Problem 1 For the feedback system Σ, suppose that the network topology G is unknown but is known to be an element of a given set $\mathbb{G}$. Find sensor nodes $S_1, S_2, \ldots, S_m$, controller nodes $K_1, K_2, \ldots, K_n$, and an actuator node M (*i.e.,* find functions $\sigma_1, \sigma_2, \ldots, \sigma_m, \kappa_1, \kappa_2$, and μ) such that

$$\lim_{t\to\infty} x(t) = 0_{N\times 1}, \tag{3.6}$$

$$\lim_{t\to\infty} \xi_i(t) = 0 \quad \forall i \in \{1, 2, \ldots, n\} \tag{3.7}$$

for every initial state $x_0 \in \mathbb{R}^N$. ■

Several remarks on Problem 1 are given.

First, in the problem, the stability of the feedback system Σ has to be guaranteed for an unknown network topology in the class $\mathbb{G}$. This implies that the solution can stabilize the system Σ for any network topology in $\mathbb{G}$, and thus it is robust against changes in the network topology. In exchange, this specification makes the problem challenging.

Second, as shown in (3.2) and (3.5), it is assumed here that each sensor node S_i and the actuator node M have no state variable, unlike those in the generalized problem in Chapter 2. This corresponds to the situation where they have no memory, which results in a simple solution.

Third, as aforementioned, the functions κ_1 and κ_2 and the initial state $\xi_i(0)$ are assumed to be the same for all the controller nodes. This implies that the controller nodes are handled in an indiscriminate manner, and as the result, the solution will be scalable. However, this constraint makes the problem more challenging. In contrast, since the subscript i is attached to σ, we may deal with the sensor nodes discriminately. Such a setting is quite natural because each sensor node may process information on a distinct physical quantity.

Finally, it is not possible to stabilize the feedback system Σ by collecting all the information at the actuator node and letting the actuator node act as a centralized controller. In fact, the output $v_i(t)$ of each controller node is assumed to be scalar, and thus each controller node cannot transmit the signals from all the sensor nodes, *i.e.,* $[z_1^\top(t)\ z_2^\top(t)\ \cdots\ z_m^\top(t)]^\top \in \mathbb{R}^{mp}$.

3.2 Controller Network for Stabilization

In this section, we derive a solution to Problem 1 under the several assumptions:

(A1) $C = I_N$.

(A2) For any $G \in \mathbb{G}$, the following conditions hold.

- **(A2.1)** For each $i \in \{1, 2, \ldots, m\}$, there exists a $j \in \{1, 2, \ldots, n\}$ satisfying $i \in \mathbb{N}^S_{Kj}$.
- **(A2.2)** $\mathbb{N}_M \neq \emptyset$.
- **(A2.3)** Consider the subgraph G_K of G, expressing the network topology among $K_1, K_2, \ldots, K_n$. If there exists an edge from node i to node j, then there exists an edge from node j to node i.
- **(A2.4)** The subgraph G_K is strongly connected.

The first assumption means that the state $x(t)$ is measurable. Note here that $m = N$. The second assumption is imposed for the network topology G. Conditions (A2.1) and (A2.2) guarantee that the sensor nodes, the controller nodes, and the actuator node are connected. The others imply that the communication links between the controller nodes are bidirectional and there is a path between any two controller nodes in the network.

3.2.1 Proposed Nodes

If it is possible for the actuator node M to directly obtain the information on the state $x(t)$, we can construct a state feedback control law

$$u(t) = fx(t) \tag{3.8}$$

achieving (3.6), where $f \in \mathbb{R}^{1\times N}$ is the gain. However, in order to obtain such information, the actuator node M has to communicate with most of the controller nodes K_i $(i = 1, 2, \ldots, n)$, which is practically impossible if n is large. Hence, we consider calculating an approximate value of $fx(t)$ by the sharing of information between the controller nodes.

Based on this idea, we propose the following solution to Problem 1:

$$\sigma_i(y_i(t)) := \frac{f_i}{w_i} y_i(t) \quad (i = 1, 2, \ldots, m), \tag{3.9}$$

$$\kappa_1(\xi_i(t), [z_j(t)]_{j\in\mathbb{N}_{Ki}^S}, [v_j(t)]_{j\in\mathbb{N}_{Ki}}) := g \sum_{j\in\mathbb{N}_{Ki}} \left(v_j(t) - \xi_i(t) - \sum_{k\in\mathbb{N}_{Ki}^S} z_k(t) \right), \tag{3.10}$$

$$\kappa_2(\xi_i(t), [z_j(t)]_{j\in\mathbb{N}_{Ki}^S}, [v_j(t)]_{j\in\mathbb{N}_{Ki}}) := \xi_i(t) + \sum_{j\in\mathbb{N}_{Ki}^S} z_j(t), \tag{3.11}$$

$$\mu([v_j(t)]_{j\in\mathbb{N}_M}) := \frac{n}{|\mathbb{N}_M|} \sum_{j\in\mathbb{N}_M} v_j(t) \tag{3.12}$$

where $z_i(t)$ is assumed to be scalar, $f_i \in \mathbb{R}$ is the i-th element of the gain f, $w_i \in \mathbb{R}_{0+}$ is the number of the controller nodes to which S_i sends the signal $z_i(t)$, and $g \in \mathbb{R}_+$ is the gain of the controller nodes.

The proposed nodes are interpreted as follows. From (3.3), (3.10), and (3.11), we have

$$\dot{v}_i(t) = g \sum_{j\in\mathbb{N}_{Ki}} \Big(v_j(t) - v_i(t) \Big) + \sum_{j\in\mathbb{N}_{Ki}^S} \dot{z}_j(t).$$

By regarding $\sum_{j\in\mathbb{N}_{Ki}^S} z_j(t)$ as a reference signal for the controller node K_i, it turns out that the controller nodes K_i $(i = 1, 2, \ldots, n)$ perform the dynamic consensus protocol developed in [59]. By the protocol, $v_i(t)$ $(i \in \{1, 2, \ldots, n\})$ tracks the average of the reference signals, *i.e.,* $(1/n) \sum_{i=1}^n \sum_{j\in\mathbb{N}_{Ki}^S} z_j(t)$, subject to (3.4), (A2.3), and (A2.4). The tracked signal is expressed as

$$\begin{aligned} \frac{1}{n} \sum_{i=1}^{n} \sum_{j\in\mathbb{N}_{Ki}^S} z_j(t) &= \frac{1}{n} \sum_{i=1}^{n} \sum_{j\in\mathbb{N}_{Ki}^S} \frac{f_j}{w_j} y_j(t) \\ &= \frac{1}{n} \sum_{i=1}^{m} f_i y_i(t) \\ &= \frac{1}{n} f x(t) \end{aligned}$$

where the first equality is derived by (3.2) and (3.9), the second one follows from the definitions of $\mathbb{N}_{Ki}^S$ and w_i, and the last one is given by (3.1) and (A1). Hence, (3.5) and (3.12) provide $u(t) \approx f x(t)$, and as the result, (3.6) will be satisfied if f is chosen so that all the eigenvalues of the matrix $A + Bf$ have negative real parts.

Finally, two remarks on the proposed nodes are given. First, even though the topology G is unknown, the information on w_i $(i = 1, 2, \ldots, m)$ and $|\mathbb{N}_M|$ can be obtained in a distributed manner. In fact, they are the numbers of the neighbor controller nodes of S_i $(i = 1, 2, \ldots, m)$ and M, and thus the information is available to each S_i and M. Second, since $w_i \neq 0$ for every $i \in \{1, 2, \ldots, m\}$ and $|\mathbb{N}_M| \neq 0$ under (A2.1) and (A2.2), division by zero does not occur in (3.9) and (3.12).

3.2.2 Stability Analysis

Next, we analyze the stability of the resulting feedback system Σ and derive conditions on the gains f and g for the stability.

Dynamics of Feedback System

Let $C_{KS} \in \{0,1\}^{n\times m}$ be the matrix whose (i,j)-element represents the connection between the controller node K_i and the sensor node S_j, *i.e.,*

$$[C_{KS}]_{ij} := \begin{cases} 1 & \text{if } S_j \text{ is connected to } K_i, \\ 0 & \text{otherwise.} \end{cases} \tag{3.13}$$

Similarly, $C_{MK} \in \{0,1\}^{1\times n}$ is defined as

$$[C_{MK}]_{1j} := \begin{cases} 1 & \text{if } K_j \text{ is connected to } M, \\ 0 & \text{otherwise.} \end{cases} \tag{3.14}$$

Note here that the following relations hold:

$$1_n^\top C_{KS} = [w_1 \; w_2 \; \cdots \; w_m], \tag{3.15}$$

$$C_{MK} 1_n = |\mathbb{N}_M|. \tag{3.16}$$

Moreover, the collective state of the controller nodes is denoted by $\xi(t) \in \mathbb{R}^n$, *i.e.,* $\xi(t) := [\xi_1(t)\; \xi_2(t) \; \cdots \; \xi_n(t)]^\top$.

Then, from (3.1)–(3.3), (3.5), (3.9)–(3.12), and (A1), the feedback system Σ is expressed as

$$\dot{x}_{c\ell}(t) = A_{c\ell}(f,g) x_{c\ell}(t) \tag{3.17}$$

for $x_{c\ell}(t) := [x^\top(t) \quad \xi^\top(t)]^\top \in \mathbb{R}^{N+n}$ and

$$A_{c\ell}(f,g) := \begin{bmatrix} A + \dfrac{n}{|\mathbb{N}_M|} B C_{MK} C_{KS} W^{-1} F & \dfrac{n}{|\mathbb{N}_M|} B C_{MK} \\ -gLC_{KS} W^{-1} F & -gL \end{bmatrix} \tag{3.18}$$

where $W := \mathrm{diag}(w_1, w_2, \ldots, w_m)$, $F := \mathrm{diag}(f_1, f_2, \ldots, f_N)$, and $L \in \mathbb{R}^{n\times n}$ is the graph Laplacian of G_K. Hence, the stability of the matrix $A_{c\ell}(f,g)$ corresponds to that of the feedback system Σ.

Parameterized Coordinate Transformation and Poles of Feedback System

However, due to the complicated structure of $A_{c\ell}(f, g)$, it is difficult to analyze the stability of $A_{c\ell}(f, g)$ in a direct way. Thus, we propose a *parameterized* coordinate transformation based on the special structure of $A_{c\ell}(f, g)$, which enables us to analyze the stability of the feedback system Σ.

Let

$$O := \begin{bmatrix} \frac{1}{\sqrt{n}} 1_n & Q \end{bmatrix} \tag{3.19}$$

for $Q \in \mathbb{R}^{n\times(n-1)}$ such that

$$O^\top L O = \Lambda(L). \tag{3.20}$$

Note that O is an orthogonal matrix, *i.e.,* $O^\top = O^{-1}$, and thus

$$Q^\top 1_n = 0_{(n-1)\times 1}. \tag{3.21}$$

Note also that there exists a Q satisfying (3.20) because properties (L1) and (L2) of the graph Laplacian L hold under (A2.3), $(1/\sqrt{n})1_n$ is an eigenvector for $\lambda_1(L)$ from (L1), and L is a symmetric matrix due to (L2).

Now, we propose the following transformation matrix with the parameter $\theta \in \mathbb{R}_+$:

$$T(\theta) := \begin{bmatrix} V(\tilde{A}) & 0_{N\times n} \\ \frac{1}{n}(1_n f - nC_{KS}W^{-1}F)V(\tilde{A}) & \frac{\theta}{n} O \end{bmatrix} \tag{3.22}$$

where $\tilde{A} := A + Bf$ and $V(\tilde{A})$ is the matrix whose i-th column vector is an eigenvector for $\lambda_i(\tilde{A})$ Since O is non-singular by the definition, there exists the inverse matrix $T^{-1}(\theta)$ for every $\theta \in \mathbb{R}_+$ if $V(\tilde{A})$ is non-singular. The non-singularity of $V(\tilde{A})$ will be remarked later in this section.

Then, by letting $\hat{x}_{c\ell}(t) := T^{-1}(\theta)x_{c\ell}(t)$, (2.2) and (3.15)–(3.22) give

$$\dot{\hat{x}}_{c\ell}(t) = \hat{A}_{c\ell}(f, g, \theta)\hat{x}_{c\ell}(t) \tag{3.23}$$

where

$$\hat{A}_{c\ell}(f, g, \theta) := \left[\begin{array}{c|cc} \Lambda(\tilde{A}) & \frac{\theta}{\sqrt{n}} V^{-1}(\tilde{A})B & \theta U_1(f) \\ \hline 0_{1\times N} & 0 & 0_{1\times(n-1)} \\ \frac{1}{\theta} U_2(f) & \sqrt{n} Q^\top C_{KS} W^{-1} F B & -g\Lambda_{-1}(L) + U_3(f) \end{array}\right] \tag{3.24}$$

for

$$U_1(f) := \frac{1}{|\mathbb{N}_M|} V^{-1}(\tilde{A}) B C_{MK} Q, \tag{3.25}$$

$$U_2(f) := n Q^\top C_{KS} W^{-1} F V(\tilde{A}) \Lambda(\tilde{A}), \tag{3.26}$$

$$U_3(f) := \frac{n}{|\mathbb{N}_M|} Q^\top C_{KS} W^{-1} F B C_{MK} Q. \tag{3.27}$$

Based on this transformed system, we obtain a result on the poles of the feedback system Σ.

Lemma 3.1 For the feedback system Σ, assume (A1) and (A2.1)–(A2.3). Suppose also that $S_1, S_2, \ldots, S_m, K_1, K_2, \ldots, K_n$, and M be given by (3.2), (3.3), (3.5), and (3.9)–(3.12). If

(C1) $V(\tilde{A})$ is non-singular,

then the following statements hold.

(a) The feedback system Σ has a pole at the origin of the complex plane.

(b) The other $N + n - 1$ poles are located in the sets

$$\mathbb{D}_1(f, \theta) := \bigcup_{i=1}^{N} \left\{ s \in \mathbb{C} \,\middle|\, \left|s - \lambda_i(\tilde{A})\right| \le \theta \sum_{j=1}^{n-1} \left|[U_1(f)]_{ij}\right| \right\}, \tag{3.28}$$

$$\begin{aligned} \mathbb{D}_2(f, g, \theta) := \bigcup_{i=1}^{n-1} \Bigg\{ s \in \mathbb{C} \,\Bigg|\, & \left|s + g\,\lambda_{i+1}(L) - [U_3(f)]_{ii}\right| \\ & \le \sum_{j=1, j\neq i}^{n-1} \left|[U_3(f)]_{ij}\right| + \frac{1}{\theta} \sum_{j=1}^{N} \left|[U_2(f)]_{ij}\right| \Bigg\}. \end{aligned} \tag{3.29}$$

■

Proof From (3.24), $\hat{A}_{c\ell}(f, g, \theta)$ has a row whose elements are zero and thus has a zero eigenvalue, which implies (a). In addition, by calculating the characteristic polynomial, it can be shown that the other eigenvalues are equivalent to those of the matrix

$$\begin{bmatrix} \Lambda(\tilde{A}) & \theta U_1(f) \\ \frac{1}{\theta} U_2(f) & -g\Lambda_{-1}(L) + U_3(f) \end{bmatrix}.$$

By applying Gershgorin theorem (see Appendix A.1) to this matrix, it follows that the eigenvalues are located in $\mathbb{D}_1(f, \theta)$ and $\mathbb{D}_2(f, g, \theta)$. Hence, (b) holds. ■

Lemma 3.1 gives a region where there are $N + n - 1$ poles of the feedback system Σ. With this result, we can derive conditions on f, g, and θ such that all the poles (except for that at the origin) are located in the open left-half of the complex plane, which gives gain conditions to stabilize the system Σ.

Stability Conditions

From the above discussion, we get the following result.

Theorem 3.1 For the feedback system Σ, suppose that the network topology G is unknown but is known to be an element of a given set $\mathbb{G}$ and assume (A1) and (A2). Let $S_1, S_2, \ldots, S_m$, $K_1, K_2, \ldots, K_n$, and M be given by (3.2), (3.3), (3.5), and (3.9)–(3.12). If (C1) and the following two conditions hold, then (3.6) and (3.7) hold for every $x_0 \in \mathbb{R}^N$.

(C2) All the eigenvalues of the matrix $\tilde{A}$ have negative real-parts.

(C3)

$$g > \max_{G \in \mathbb{G}} \max_{i \in \{1,2,\ldots,n-1\}} \frac{1}{\lambda_{i+1}(L)} \left([U_3(f)]_{ii} + \sum_{j=1, j \neq i}^{n-1} \left| [U_3(f)]_{ij} \right| + \left(\min_{j \in \{1,2,\ldots,N\}} \frac{-\mathrm{Re}(\lambda_j(\tilde{A}))}{\sum_{k=1}^{n-1} \left| [U_1(f)]_{jk} \right|} \right)^{-1} \sum_{j=1}^{N} \left| [U_2(f)]_{ij} \right| \right). \tag{3.30}$$

■

Proof This theorem is a straightforward consequence of Lemma 3.1 and the following two facts.

(i) The state whose behavior is governed by the pole at the origin, is identical to zero.

(ii) If (C2) and (C3) hold, for each $G \in \mathbb{G}$, there exists a $\theta \in \mathbb{R}_+$ such that $\mathbb{D}_1(f, \theta)$ and $\mathbb{D}_2(f, g, \theta)$ are in the open left-half of the complex plane.

The proofs of (i) and (ii) are given in Appendix 3.A. ■

Finally, we comment on the stability conditions. Condition (C1) guarantees the existence of the inverse of $V(\tilde{A})$. Condition (C2) implies that $\tilde{A}$ is Hurwitz. These are satisfied if the gain f is appropriately chosen. It is always possible to choose such a f when the pair (A, B) is controllable. On the other hand, (C3) is imposed for the gain g, and we only have to design it according to this condition. When a f satisfying (C1) and (C2) is given, there exists a $g \in \mathbb{R}_+$ satisfying (3.30) from the following three facts:

- $\lambda_{i+1}(L)$ $(i = 1, 2, \ldots, n-1)$ are non-zero real numbers;
- $[U_3(f)]_{ii}$ is a real number for every $i \in \{1, 2, \ldots, n-1\}$;
- $\mathrm{Re}(\lambda_i(\tilde{A})) \neq 0$ for every $i \in \{1, 2, \ldots, N\}$.

The first one is proven by (L2), (L3), (A2.3), and (A2.4). The second one is shown by the definition of $U_3(f)$. The third one follows from (C2).

3.2.3 Example

Consider the feedback system Σ with $m := 4$ and $n := 6$. The plant P is given by

$$P : \begin{cases} \dot{x}(t) = \begin{bmatrix} 0 & 1 & 0 & 0 \\ 0 & 0 & 1 & 0 \\ 0 & 0 & 0 & 1 \\ 1 & 2 & -3 & 4 \end{bmatrix} x(t) + \begin{bmatrix} 0 \\ 0 \\ 0 \\ 1 \end{bmatrix} u(t), \\ y(t) = x(t). \end{cases}$$

Since the poles of P are -0.3028, $0.5 \pm 0.8660\mathrm{i}$, and 3.3028, P is unstable. The set of the network topologies is $\mathbb{G} := \{G_1, G_2, \ldots, G_8\}$ for $G_1, G_2, \ldots, G_8$ in Figure 3.2. Then, (A1) and (A2) hold.

We employ the sensor nodes S_i $(i = 1, 2, \ldots, 4)$, the controller nodes K_i $(i = 1, 2, \ldots, 6)$, and the actuator node M given by (3.2), (3.3), (3.5), and (3.9)–(3.12). The gain f is set as $f := [-21 \ -36 \ -15 \ -9]$ for which the eigenvalues of $\tilde{A}$ are -1, -2, and $-1 \pm 3\mathrm{i}$. All the eigenvalues of $\tilde{A}$ are distinct and have negative real-parts, and thus (C1) and (C2) hold. Furthermore, g is set as $g := 340$, which satisfies (C3).

Figure 3.3 shows the time responses of Σ for G_1, where $x_0 := [-5 \ -1 \ 2 \ 6]^\top$. The first and second figures illustrate the time trajectories of $x(t)$ and $\xi(t)$ respectively, where each line corresponds to each element of those. Note here that the several lines in the graph of $\xi(t)$ almost overlap with each other. We see that the proposed nodes stabilize Σ though those are designed without knowing that the network topology is G_1.

Also for the other network topologies $G_2, G_3, \ldots, G_8$, similar results are obtained. As an example, Figure 3.4 shows the time responses of Σ for G_8 in the same fashion. Note again that the several lines in the graph of $\xi(t)$ almost overlap with each other. It turns out that Σ is stable also for another network topology. This means that our controller network is robust against changes in the network topology.

In addition, Figure 3.5 depicts the time response of P by the state feedback controller (3.8). Since the time trajectories of $x(t)$ in Figures 3.3 and 3.4 agree

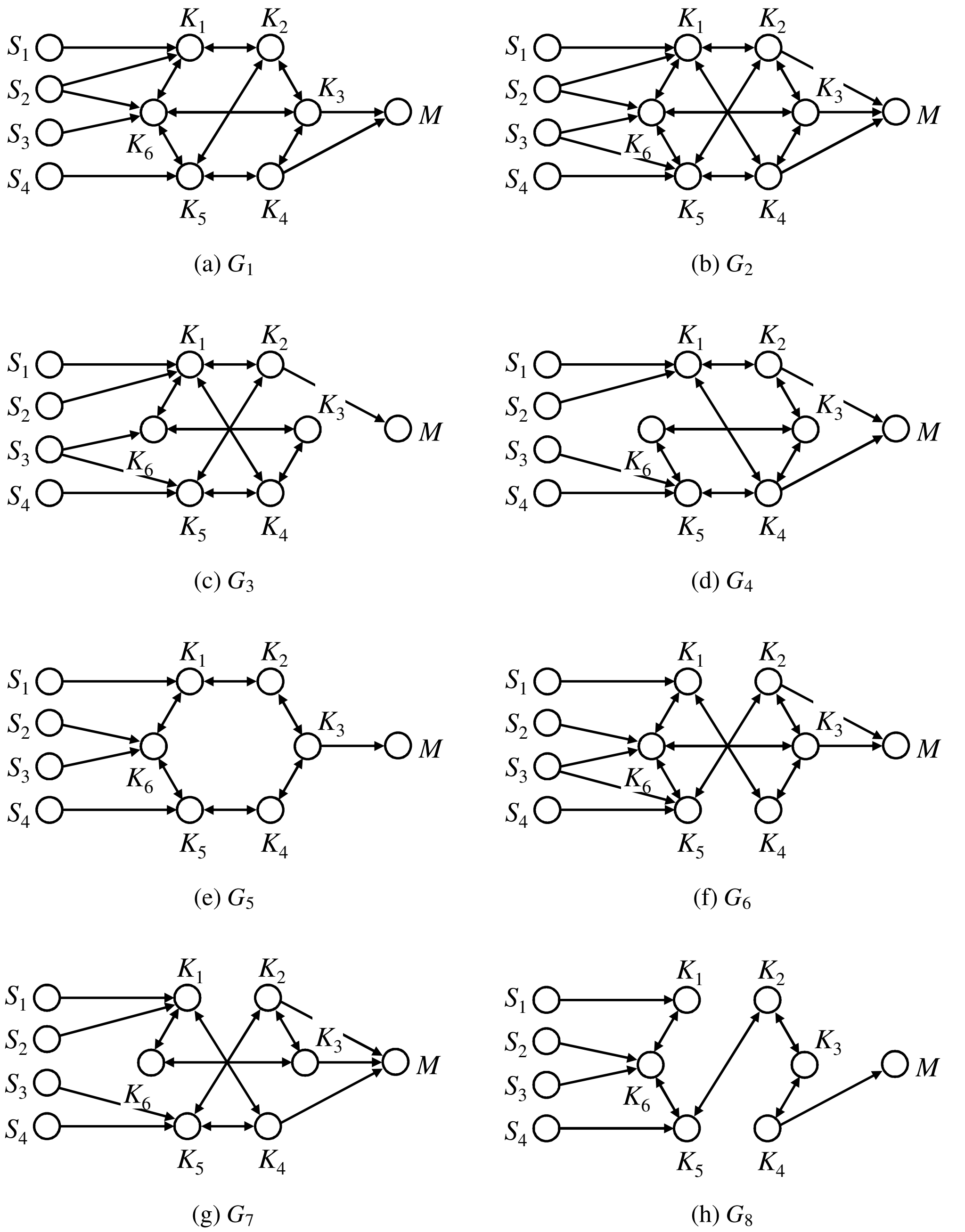

Figure 3.2: Network topologies.

with it in Figure 3.5, we can conclude that our controller network acts as the state feedback controller.

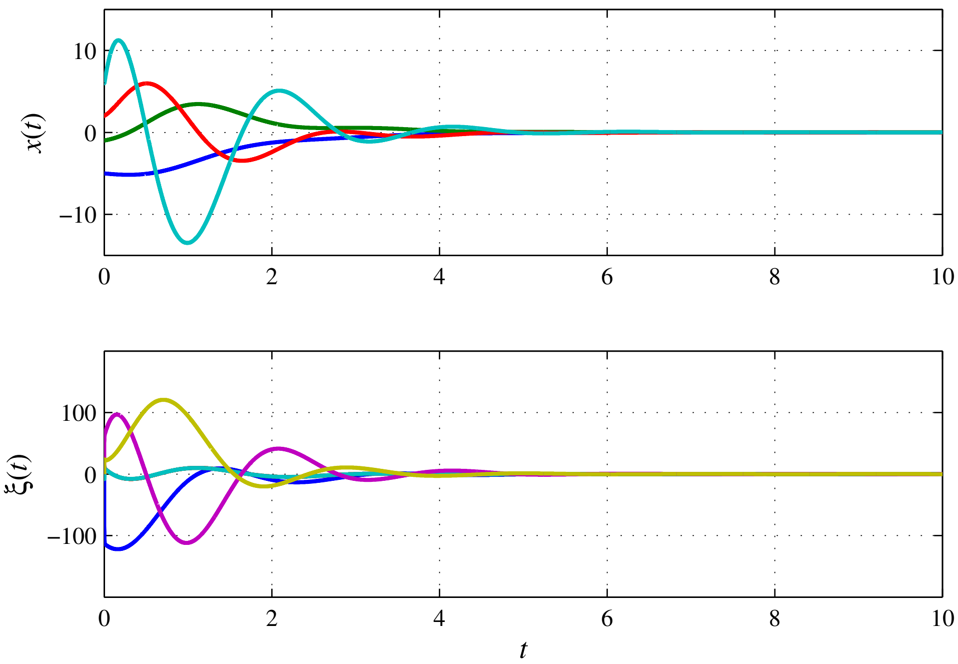

Figure 3.3: Time responses of Σ for G_1.

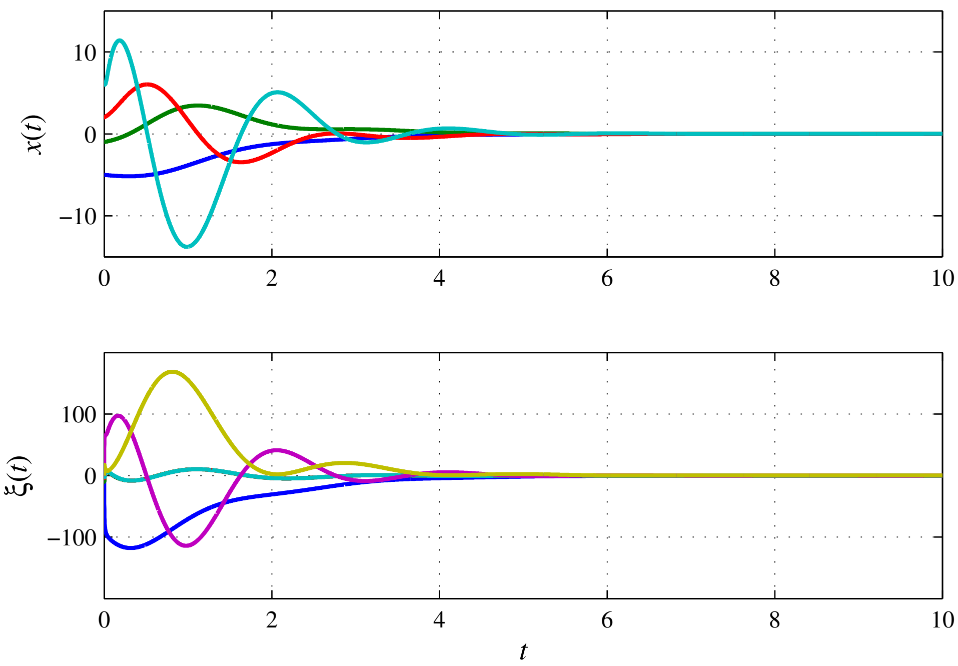

Figure 3.4: Time responses of Σ for G_8.

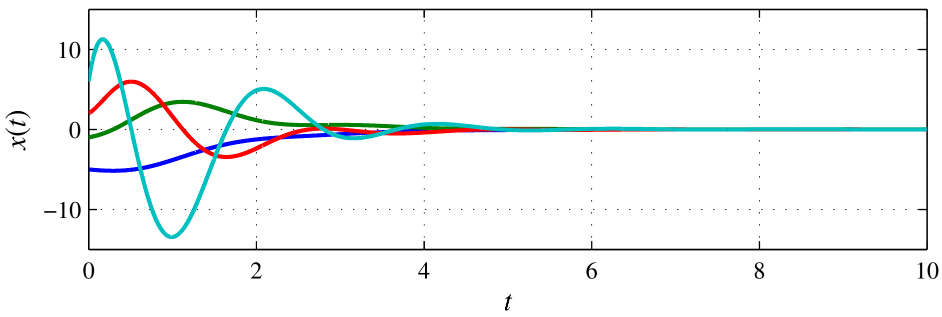

Figure 3.5: Time response of P by the state feedback controller (3.8).

3.3 Relation between Stabilizing Gain and Network Topology

Theorem 3.1 shows that the stabilizing gain g depends on the network topology G. In this section, we clarify the relation between them.

We first provide the following result.

Lemma 3.2 For the matrices $U_1(f)$, $U_2(f)$, and $U_3(f)$ in (3.25)–(3.27), the following relations hold:

$$||U_1(f)||_\infty \leq \sqrt{n-1}||V^{-1}(\tilde{A})B||_\infty, \tag{3.31}$$

$$||U_2(f)||_\infty \leq mn||FV(\tilde{A})\Lambda(\tilde{A})||_\infty, \tag{3.32}$$

$$||U_3(f)||_\infty \leq mn\sqrt{n-1}||FB||_\infty. \tag{3.33}$$

■

Proof See Appendix 3.B. ■

By using Lemma 3.2, the following result is obtained.

Theorem 3.2 For the feedback system Σ, assume (A1) and (A2.1)–(A2.4). Let $S_1, S_2, \ldots, S_m, K_1, K_2, \ldots, K_n$, and M be given by (3.2), (3.3), (3.5), and (3.9)–(3.12). If (C1), (C2), and

(C4)

$$g \geq \frac{mn\sqrt{n-1}}{\lambda_2(L)}\left(||FB||_\infty + \frac{||FV(\tilde{A})\Lambda(\tilde{A})||_\infty||V^{-1}(\tilde{A})B||_\infty}{\min_{i\in\{1,2,\ldots,n\}} -\mathrm{Re}(\lambda_i(\tilde{A}))}\right) \tag{3.34}$$

hold, then (3.6) and (3.7) hold for every $x_0 \in \mathbb{R}^N$. ■

Proof Consider the gain condition (3.42) to stabilize the system Σ for a network topology G. By letting $g_{\min} \in \mathbb{R}$ be the right-hand side of (3.42), we have

$$
\begin{aligned}
g_{\min} &\leq \max_{i\in\{1,2,\ldots,n-1\}} \frac{1}{\lambda_{i+1}(L)} \left(\sum_{j=1}^{n-1} \left| [U_3(f)]_{ij} \right| \right. \\
&\qquad \left. + \left(\min_{j\in\{1,2,\ldots,N\}} \frac{-\mathrm{Re}(\lambda_j(\tilde{A}))}{\sum_{k=1}^{n-1} \left| [U_1(f)]_{jk} \right|} \right)^{-1} \sum_{j=1}^{N} \left| [U_2(f)]_{ij} \right| \right) \\
&\leq \max_{i\in\{1,2,\ldots,n-1\}} \frac{1}{\lambda_{i+1}(L)} \max_{i\in\{1,2,\ldots,n-1\}} \left(\sum_{j=1}^{n-1} \left| [U_3(f)]_{ij} \right| \right. \\
&\qquad \left. + \left(\min_{j\in\{1,2,\ldots,N\}} \frac{-\mathrm{Re}(\lambda_j(\tilde{A}))}{\sum_{k=1}^{n-1} \left| [U_1(f)]_{jk} \right|} \right)^{-1} \sum_{j=1}^{N} \left| [U_2(f)]_{ij} \right| \right) \\
&\leq \frac{1}{\lambda_2(L)} \left(\max_{i\in\{1,2,\ldots,n-1\}} \sum_{j=1}^{n-1} \left| [U_3(f)]_{ij} \right| \right. \\
&\qquad \left. + \left(\min_{j\in\{1,2,\ldots,N\}} \frac{-\mathrm{Re}(\lambda_j(\tilde{A}))}{\sum_{k=1}^{n-1} \left| [U_1(f)]_{jk} \right|} \right)^{-1} \max_{i\in\{1,2,\ldots,n-1\}} \sum_{j=1}^{N} \left| [U_2(f)]_{ij} \right| \right) \\
&\leq \frac{1}{\lambda_2(L)} \left(\max_{i\in\{1,2,\ldots,n-1\}} \sum_{j=1}^{n-1} \left| [U_3(f)]_{ij} \right| \right. \\
&\qquad \left. + \left(\frac{\min_{j\in\{1,2,\ldots,N\}} -\mathrm{Re}(\lambda_j(\tilde{A}))}{\max_{j\in\{1,2,\ldots,N\}} \sum_{k=1}^{n-1} \left| [U_1(f)]_{jk} \right|} \right)^{-1} \max_{i\in\{1,2,\ldots,n-1\}} \sum_{j=1}^{N} \left| [U_2(f)]_{ij} \right| \right) \qquad (3.35)
\end{aligned}
$$

where the first relation is given by

$$
[U_3(f)]_{ii} + \sum_{j=1, j\neq i}^{n-1} \left| [U_3(f)]_{ij} \right| \leq \sum_{j=1}^{n-1} \left| [U_3(f)]_{ij} \right|
$$

for every $i \in \{1, 2, \ldots, n-1\}$, and the others are derived by the definitions of the maximum and minimum functions. So, it follows that

$$
g_{\min} \leq \frac{1}{\lambda_2(L)} \left(\|U_3(f)\|_\infty + \frac{\|U_1(f)\|_\infty \|U_2(f)\|_\infty}{\min_{i\in\{1,2,\ldots,N\}} -\mathrm{Re}(\lambda_i(\tilde{A}))} \right). \qquad (3.37)
$$

Applying Lemma 3.2 to (3.37) implies that an upper bound of the right-hand side of (3.42) is given by that of (3.34). Thus, (3.42) holds under (3.34), which proves the theorem. ■

Theorem 3.2 shows that the second smallest eigenvalue of the graph Laplacian L characterizes the magnitude of the stabilizing gain g, which is consistent with the well-known result [17] in the consensus problem. More precisely, the stabilizing gain g becomes smaller as the eigenvalue increases because the right-hand side of (3.34) goes to zero as $\lambda_2(L) \to \infty$. In general, the graph Laplacian of a sparse graph has small eigenvalues, and so this result implies that the large gain will be needed for the stabilization when the network among the controller nodes is sparse.

With Theorem 3.2, we can easily obtain the stabilizing gain g. More precisely, we design g by using (3.34) for G whose subgraph G_K is sparsest in the given $\mathbb{G}$ in the sense of $\lambda_2(L)$. Then, the resulting g satisfies (3.34) for every $G \in \mathbb{G}$, and thus the feedback system Σ is stable for every $G \in \mathbb{G}$ from Theorem 3.2. In this procedure, it is unnecessary to calculate the right-hand side of (3.30). In other words, we do not have to check the gain condition (3.42) for all $G \in \mathbb{G}$.

3.4 Summary

This chapter has addressed a controller network design problem for stabilization under the constraints that the network topology is unknown and all the controller nodes are the same. For solving this, we have proposed a method to calculate a state feedback control law in a distributed manner. By introducing a parameterized coordinate transformation and reducing the stabilization problem to finding a range of the parameter, we have given gain conditions for the stability of the resulting feedback system. Moreover, the relation between the stabilizing gain and the network topology has been presented, which enables us to easily design the stabilizing gain. These results will be useful to design a controller network which is scalable and robust against changes in the network topology.

Appendix 3.A Proofs of Facts (i) and (ii) in Proof of Theorem 3.1

Proof of (i)

Let $\hat{x}_{c\ell N+1}(t) \in \mathbb{C}$ be the $N+1$-th element of $\hat{x}_{c\ell}(t)$. Then, the behavior is governed by the pole at the origin from (3.23) and (3.24). In addition, (3.15), (3.19), and (3.22) provide

$$\hat{x}_{c\ell N+1}(t) = \frac{\sqrt{n}}{\theta} 1_n^\top \xi(t),$$

and thus $\hat{x}_{c\ell N+1}(t) \equiv 0$ because of (3.4). This proves (i).

Proof of (ii)

Equation (3.28) implies that $\mathbb{D}_1(f,\theta)$ is contained in the open left-half plane if

$$\mathrm{Re}(\lambda_i(\tilde{A})) < -\theta \sum_{j=1}^{n-1} \left|[U_1(f)]_{ij}\right| \tag{3.38}$$

for every $i \in \{1, 2, \ldots, N\}$. Equation (3.38) is rewritten as

$$\theta < -\frac{\mathrm{Re}(\lambda_i(\tilde{A}))}{\sum_{j=1}^{n-1} \left|[U_1(f)]_{ij}\right|} \tag{3.39}$$

and thus there exists a $\theta \in \mathbb{R}_+$ satisfying (3.38) if (C2) holds.

Similarly, it follows from (3.29) that $\mathbb{D}_2(f,g,\theta)$ is in the open left-half plane if

$$\mathrm{Re}\left(-g\lambda_{i+1}(L) + [U_3(f)]_{ii}\right) < -\sum_{j=1, j\neq i}^{n-1} \left|[U_3(f)]_{ij}\right| - \frac{1}{\theta}\sum_{j=1}^{N} \left|[U_2(f)]_{ij}\right| \tag{3.40}$$

for every $i \in \{1, 2, \ldots, n-1\}$. Equation (3.40) implies

$$g > \frac{1}{\lambda_{i+1}(L)}\left([U_3(f)]_{ii} + \sum_{j=1, j\neq i}^{n-1} \left|[U_3(f)]_{ij}\right| + \frac{1}{\theta}\sum_{j=1}^{N} \left|[U_2(f)]_{ij}\right|\right) \tag{3.41}$$

because $\lambda_{i+1}(L)$ $(i = 1, 2, \ldots, n-1)$ are positive real numbers from (L2) and (L3), and $[U_3(f)]_{ii}$ $(i = 1, 2, \ldots, n-1)$ are real numbers by the definition.

Combining (3.39) and (3.41), we obtain the condition

$$\begin{aligned} g > \max_{i\in\{1,2,\ldots,n-1\}} \frac{1}{\lambda_{i+1}(L)} \Bigg(& [U_3(f)]_{ii} + \sum_{j=1, j\neq i}^{n-1} \left|[U_3(f)]_{ij}\right| \\ & + \left(\min_{j\in\{1,2,\ldots,N\}} \frac{-\mathrm{Re}(\lambda_j(\tilde{A}))}{\sum_{k=1}^{n-1} \left|[U_1(f)]_{jk}\right|}\right)^{-1} \sum_{j=1}^{N} \left|[U_2(f)]_{ij}\right| \Bigg) \end{aligned} \tag{3.42}$$

under which there exists a $\theta \in \mathbb{R}_+$ such that $\mathbb{D}_1(f,\theta)$ and $\mathbb{D}_2(f,g,\theta)$ are included in the open left-half plane. Hence, if (C3) holds, there exists such a $\theta \in \mathbb{R}_+$ for each $G \in \mathbb{G}$, which completes the proof.

Appendix 3.B Proof of Lemma 3.2

We first prepare the following result [64].

Lemma 3.3 For the matrix $X \in \mathbb{C}^{n\times m}$, the following relations hold:

$$\|X\|_\infty \leq \sqrt{m}\|X\|_2, \tag{3.43}$$

$$\|X\|_2 \leq \sqrt{m}\|X\|_1. \tag{3.44}$$

■

We also prepare the following lemma.

Lemma 3.4 For the matrix Q in (3.19),

$$\|Q\|_2 = 1, \tag{3.45}$$

$$\|Q^\top\|_2 = 1. \tag{3.46}$$

■

Proof Let us recall that O is an orthogonal matrix, which implies $Q^\top Q = I_{n-1}$. Therefore, all the eigenvalues of $Q^\top Q$ are one, and this shows (3.45). On the other hand, (3.46) is proven as follows. From (3.19), we have

$$OO^\top = \frac{1}{n}1_n 1_n^\top + QQ^\top$$

which gives

$$QQ^\top = I_n - \frac{1}{n}1_n 1_n^\top$$

since $OO^\top = I_n$. Then, there exists a matrix $R \in \mathbb{R}^{n\times n}$ such that

$$R^{-1}QQ^\top R = \begin{bmatrix} 0 & 0_{1\times(n-1)} \\ 0_{(n-1)\times 1} & I_{n-1} \end{bmatrix}. \tag{3.47}$$

In fact, by a simple calculation, it can be shown that

$$R = \begin{bmatrix} 1 & 1_{n-1}^\top \\ 1_{n-1} & -I_{n-1} \end{bmatrix}$$

satisfies (3.47). From (3.47), the eigenvalues of $QQ^\top$ are zero and one, and thus (3.46) holds. ■

Now, we prove Lemma 3.2.

Proof of (3.31)

From (3.25), we have

$$\begin{aligned} \|U_1(f)\|_\infty &= \frac{1}{|\mathbb{N}_M|}\|V^{-1}(\tilde{A})BC_{MK}Q\|_\infty \\ &\leq \frac{1}{|\mathbb{N}_M|}\|V^{-1}(\tilde{A})B\|_\infty\|C_{MK}\|_\infty\|Q\|_\infty \\ &= \|V^{-1}(\tilde{A})B\|_\infty\|Q\|_\infty \end{aligned} \tag{3.48}$$

where the first and second relations are given by the definition of the norm, and the third one follows since $||C_{MK}||_\infty = |\mathbb{N}_M|$ from (3.16). Applying (3.43) and (3.45) to (3.48), we obtain (3.31).

Proof of (3.32)

Equation (3.26) implies

$$\begin{aligned}||U_2(f)||_\infty &= n||Q^\top C_{KS} W^{-1} F V(\tilde{A})\Lambda(\tilde{A})||_\infty \\ &\leq n||Q^\top C_{KS} W^{-1}||_\infty ||F V(\tilde{A})\Lambda(\tilde{A})||_\infty \end{aligned} \tag{3.49}$$

In addition, from (3.43), (3.44), and (3.46), we get

$$\begin{aligned}||Q^\top C_{KS} W^{-1}||_\infty &\leq \sqrt{m}||Q^\top C_{KS} W^{-1}||_2 \\ &\leq \sqrt{m}||Q^\top||_2||C_{KS} W^{-1}||_2 \\ &= \sqrt{m}||C_{KS} W^{-1}||_2 \\ &\leq m||C_{KS} W^{-1}||_1.\end{aligned}$$

Therefore,

$$||Q^\top C_{KS} W^{-1}||_\infty \leq m$$

since $||C_{KS} W^{-1}||_1 = 1$ from (3.15). This, together with (3.49), shows (3.32).

Proof of (3.33)

Similarly to the proofs of (3.31) and (3.32), it follows from (3.27) that

$$\begin{aligned}||U_3(f)||_\infty &= \frac{n}{|\mathbb{N}_M|}||Q^\top C_{KS} W^{-1} F B C_{MK} Q||_\infty \\ &\leq \frac{n}{|\mathbb{N}_M|}||Q^\top C_{KS} W^{-1}||_\infty ||FB||_\infty ||C_{MK}||_\infty ||Q||_\infty \\ &\leq \frac{mn}{|\mathbb{N}_M|}||FB||_\infty ||C_{MK}||_\infty ||Q||_\infty \\ &= mn||FB||_\infty ||Q||_\infty \\ &\leq mn\sqrt{n-1}||FB||_\infty.\end{aligned}$$

This completes the proof.

Chapter 4

Reference Tracking by Controller Networks for Real-time Pricing

This chapter presents a tracking controller network for the real-time pricing. First, we explain the motivation for considering the controller network for the real-time pricing. Next, we formulate a design problem of the controller network for the real-time pricing. For the problem, a necessary condition for the solvability is derived. Moreover, we propose a solution to the problem, and prove that it achieves the real-time pricing.

4.1 Real-time Pricing

In smart girds, one of important issues is *demand response*, *i.e.*, to reduce power demand by offering consumers incentive payments. The reason lies in increasing demand for power and growing environmental concerns. In fact, the demand response prevents blackouts caused by excessive power demand. Furthermore, it reduces energy consumption, which results in lower greenhouse gas emissions.

A method to perform the demand response is the real-time pricing [58]. The real-time pricing is to control the total power consumption of consumers by changing power prices in real-time. For instance, the power consumption will be reduced if the prices are set high. The real-time pricing corresponds to feedback control by regarding the power prices and the power consumption as a controlled input and a control output, respectively, and it is illustrated in Figure 4.1. Motivated by this fact, in the control field, a number of studies have been conducted so far, *e.g.*, [65–68].

Meanwhile, it is assumed there that the power price controller can directly get information on the total power consumption. However, the power consumption of each consumer is measured with a smart meter, and thus the controller will have

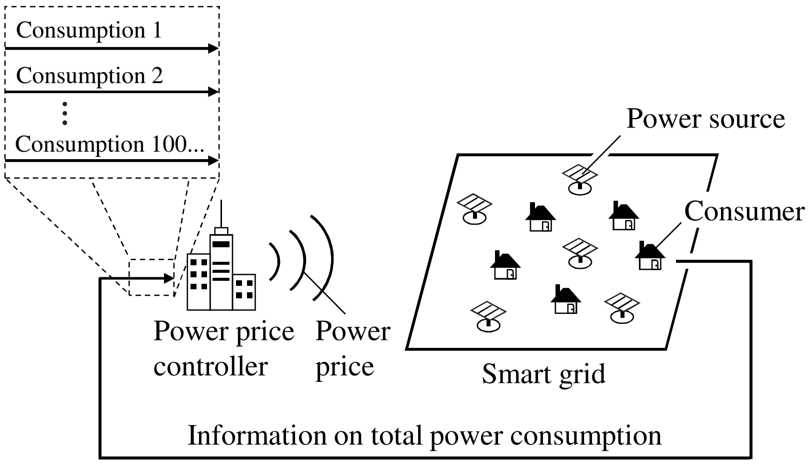

Figure 4.1: Illustration of real-time pricing.

to deal with the numerous data to obtain such information as shown in the upper left of Figure 4.1. For example, in Japan, tens of millions of the data sets may be handled because there are around 52 million houses [69] and the other buildings such as plants and stores. This results in high communication and computational costs, which will be a difficulty in realizing the real-time pricing.

This chapter therefore proposes the real-time pricing system based on the controller network, depicted in Figure 1.7. In this system, each power source has a local controller, and it acts as a distributed estimator for the power consumption. That is, each power source estimates the total power consumption by exchanging information on the required power with its neighbors. The power price controller receives it from the neighbor power sources, and determines the power price. This scheme does not need to collect information from all the consumers, which solves the above issue. In addition, this is based on distributed estimation, and thus is useful to construct distributed energy management systems [70] which have been an important topic in the research field of the smart grids.

With this motivation, we develop a controller network for the real-time pricing in the following sections.

4.2 Problem Formulation

4.2.1 System Description

Consider the real-time pricing system Σ in Figure 4.2, which is composed of m consumers, n power sources, and a power price controller.

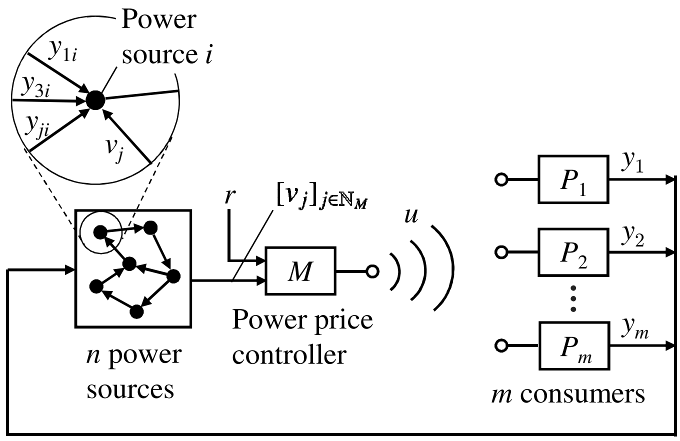

Figure 4.2: Real-time pricing system Σ.

The behavior of consumer i ($i\in\{1,2,\ldots,m\}$) is described by

$$P_i : \begin{cases} \dot{x}_i(t) = a_i(\alpha_i - x_i(t)) + b_i(\beta_i - u(t)), \\ y_i(t) = c_i x_i(t) \end{cases} \tag{4.1}$$

where $x_i(t) \in \mathbb{R}$ is the power consumption, $u(t) \in \mathbb{R}_{0+}$ is the power price, and $y_i(t) \in \mathbb{R}^{p_i}$ denotes how much each of pre-specified p_i power sources supplies the power in order to cover the consumption $x_i(t)$. The numbers $a_i \in \mathbb{R}_+$ and $b_i \in \mathbb{R}_+$ are the sensitivities for the consumption and the price, $\alpha_i \in \mathbb{R}_+$ and $\beta_i \in \mathbb{R}_+$ are the thresholds for them, and $c_i \in (0,1]^{p_i}$ is a vector specifying the rate that the power sources divide the power supply to consumer i. The initial state is given as $x_i(0) = x_{i0} \in \mathbb{R}$.

From the first equation of (4.1), the behavior of consumer i is explained as follows. The first term of the right-hand side represents the change in the power demand based on the current power consumption. The demand decreases if the current power consumption is larger than α_i, and otherwise the demand increases. This represents the property that the consumers do not often use a large amount energy for the reasons of reducing costs and environmental concerns. Meanwhile, the second term expresses the change in the power demand based on the power price. Similarly to the above, the demand decreases if the price is higher than β_i; otherwise it increases. This is quite natural because the real-time pricing does not work well if the consumers do not have such a property.

For power source i ($i \in \{1,2,\ldots,n\}$), we suppose that the local controller

$$K_i : \begin{cases} \dot{\xi}_i(t) = \kappa_1(\xi_i(t), [y_{ji}(t)]_{j\in\mathbb{N}^P_{Ki}}, [v_j(t)]_{j\in\mathbb{N}_{Ki}}), \\ v_i(t) = \kappa_2(\xi_i(t), [y_{ji}(t)]_{j\in\mathbb{N}^P_{Ki}}, [v_j(t)]_{j\in\mathbb{N}_{Ki}}) \end{cases} \tag{4.2}$$

is embedded. Here, $\xi_i(t) \in \mathbb{R}$ is the state, $[y_{ji}(t)]_{j\in\mathbb{N}_{Ki}^P} \in \mathbb{R}^{|\mathbb{N}_{Ki}^P|}$ and $[v_j(t)]_{j\in\mathbb{N}_{Ki}} \in \mathbb{R}^{|\mathbb{N}_{Ki}|}$ are the inputs, $v_i(t) \in \mathbb{R}$ is the output, and $\kappa_1 : \mathbb{R} \times \mathbb{R}^{|\mathbb{N}_{Ki}^P|} \times \mathbb{R}^{|\mathbb{N}_{Ki}|} \to \mathbb{R}$ and $\kappa_2 : \mathbb{R} \times \mathbb{R}^{|\mathbb{N}_{Ki}^P|} \times \mathbb{R}^{|\mathbb{N}_{Ki}|} \to \mathbb{R}$ are functions. The variable $y_{ji}(t) \in \mathbb{R}$ is the power required from consumer j to power source i, and $\mathbb{N}_{Ki}^P \subseteq \{1, 2, \dots, m\}$ and $\mathbb{N}_{Ki} \subseteq \{1, 2, \dots, n\} \setminus \{i\}$ are the index sets of the neighbors, *i.e.,* the consumers and the power sources from which power source i receives information. Similarly to Chapter 3, the functions κ_1 and κ_2 and the initial state $\xi_i(0)$ are assumed to be the same for all the local controllers because of the scalability. In addition, we assume (3.4); namely, the initial state is given as zero.

The power price controller M is of the form

$$M : \begin{cases} \dot{\xi}_M(t) = \mu_1(\xi_M(t), [v_j(t)]_{j\in\mathbb{N}_M}, r(t)), \\ u(t) = \mathrm{sat}_{\bar{u}}(\mu_2(\xi_M(t), [v_j(t)]_{j\in\mathbb{N}_M}, r(t))) \end{cases} \tag{4.3}$$

where $\xi_M(t) \in \mathbb{R}^q$ is the state, $[v_j(t)]_{j\in\mathbb{N}_M} \in \mathbb{R}^{|\mathbb{N}_M|}$ and $r(t) \in \mathbb{R}$ are the inputs, $u(t) \in \mathbb{R}_{0+}$ is the output, *i.e.*, the power price, and $\mu_1 : \mathbb{R}^q \times \mathbb{R}^{|\mathbb{N}_M|} \times \mathbb{R} \to \mathbb{R}^q$ and $\mu_2 : \mathbb{R}^q \times \mathbb{R}^{|\mathbb{N}_M|} \times \mathbb{R} \to \mathbb{R}$ are functions. The set $\mathbb{N}_M \subseteq \{1, 2, \dots, n\}$ is the index set of the neighbors. The saturation function guarantees that the power price $u(t)$ takes a value on $[0, \bar{u}]$ where $\bar{u} \in \mathbb{R}_+$ is the upper bound of the price. We assume that the initial state is given as $\xi_M(0) = 0_{q\times 1}$.

For simplicity of notation, the collective power consumption of the consumers is represented by $x(t) \in \mathbb{R}^m$, *i.e.*, $x(t) := [x_1(t)\ x_2(t)\ \cdots\ x_m(t)]^\top$. The initial state is given as $x_0 := [x_{10}\ x_{20}\ \cdots\ x_{m0}]^\top \in \mathbb{R}^m$. Similarly, $y(t) \in \mathbb{R}^{\sum_{i=1}^m p_i}$ is defined as $y(t) := [y_1^\top(t)\, y_2^\top(t)\ \cdots\ y_m^\top(t)]^\top$. Moreover, let $\xi(t) := [\xi_1(t)\, \xi_2(t)\ \cdots\ \xi_n(t)\ \ \xi_M^\top(t)]^\top \in \mathbb{R}^{n+q}$. This denotes the collective state of the local controllers K_i ($i = 1, 2, \dots, n$) and the power price controller M.

The idea of the real-time pricing system Σ is explained as follows. Information on the power consumption $x_i(t)$ of costumer i is transmitted to the local controller K_j as $y_{ij}(t)$. The local controllers K_i ($i = 1, 2, \dots, n$) estimate the total power consumption $\sum_{i=1}^m x_i(t)$ by sharing the information on the power consumption with their neighbors. The power price controller M sets the power price $u(t)$ based on the estimated total power consumption.

4.2.2 Design Problem of Controller Network for Real-time Pricing

The network topology of the real-time pricing system Σ is denoted by the graph G where the node set corresponds to the consumers, the power sources, and the power price controller, and the edge set corresponds to the connections. Then, the problem considered here is formulated as follows.

Problem 2 For the real-time pricing system Σ, suppose that a step reference input $r \in \mathbb{R}$, an upper bound $\bar{u} \in \mathbb{R}_+$ of the power price, and the network topology G are given. Find local controllers $K_1, K_2, \ldots, K_n$ and a power price controller M (*i.e.,* find functions κ_1, κ_2, μ_1, and μ_2) such that

$$\lim_{t \to \infty} \sum_{i=1}^{m} x_i(t) = r \tag{4.4}$$

for every initial state $x_0 \in \mathbb{R}^m$. ■

Two remarks on Problem 2 are given.

First, in this problem, the power price controller M cannot directly obtain the information on the total power consumption. In fact, since the output $v_i(t)$ of each local controller K_i is assumed to be scalar, it is impossible to send the information of all the power sources, *i.e.,* the vector $y(t) \in \mathbb{R}^{\sum_{i=1}^{m} p_i}$, to the power price controller M. Also, it is difficult to sum up the information of each power source over the network because the same information would be added more than one time. Thus, we cannot obtain a solution to the problem in a direct way. This makes the problem challenging.

Second, we cannot obtain a practical solution to the problem by directly applying the result in Chapter 3. In fact, although we can solve the problem by adding an appropriate offset to the power price and performing stabilization control, the solution requires the exact information on the consumers due to the offset. This is a fatal drawback when the solution is applied to large-scale communities. Also in this sense, Problem 2 is challenging.

4.3 Necessary Condition for Solvability

Problem 2 is not solvable for any reference input $r \in \mathbb{R}$ and upper bound $\bar{u} \in \mathbb{R}_+$ of the power price. This is because the power consumption cannot be substantially reduced if the upper bound of the power price is low.

We provide an example to demonstrate this fact. Consider the following case with 5 consumers. The parameters of consumer i ($i \in \{1, 2, \ldots, 5\}$) are shown in Table 4.1. The reference input and the upper bound of the power price are defined as $r := 2$ and $\bar{u} := 29$. Figure 4.3 illustrates the time evolution of the total power consumption $\sum_{i=1}^{5} x_i(t)$ for $x_0 := [0.5\ \ 0.42\ \ 0.45\ \ 0.47\ \ 0.5]^\top$ and $u(t) \equiv \bar{u}$, where r is expressed by the thin line. We see that the total power consumption is not reduced to the desired level though the maximum price is set. In this case, any local controllers and power price controller cannot be a solution to Problem 2. This implies that we should derive a necessary condition on r and $\bar{u}$ for the solvability of the problem.

Table 4.1: Parameters of each consumer i.

	$i=1$	$i=2$	$i=3$	$i=4$	$i=5$
a_i	0.12	0.12	0.12	0.12	0.12
b_i	14×10^{-4}	12×10^{-4}	7×10^{-4}	9×10^{-4}	5×10^{-4}
α_i	0.37	0.44	0.42	0.33	0.49
β_i	35	25	27	32	30
c_i	$[0.2\ \ 0.8]^\top$	$[0.5\ \ 0.5]^\top$	$[0.3\ \ 0.7]^\top$	$[0.7\ \ 0.3]^\top$	$[0.9\ \ 0.1]^\top$

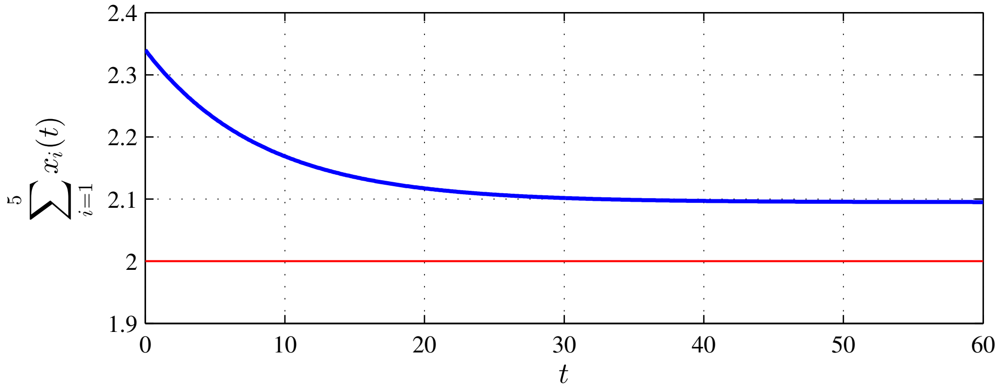

Figure 4.3: Time evolution of total power consumption.

The following result gives a necessary condition for the solvability.

Theorem 4.1 For the real-time pricing system Σ, suppose that $r \in \mathbb{R}$ and $\bar{u} \in \mathbb{R}_+$ are given. If (4.4) holds, then

$$\bar{u} \geq \frac{\displaystyle\sum_{i=1}^{m} \frac{a_i\alpha_i + b_i\beta_i}{a_i} - r}{\displaystyle\sum_{i=1}^{m} \frac{b_i}{a_i}}. \tag{4.5}$$

■

Proof Let $x_e \in \mathbb{R}^m$ and $u_e \in \mathbb{R}$ be the equilibrium state and input of the system Σ, respectively. Then, from (4.1),

$$x_e^i = \frac{a_i\alpha_i + b_i\beta_i}{a_i} - \frac{b_i}{a_i}u_e$$

for every $i \in \{1, 2, \ldots, m\}$, where x_e^i is the i-th element of x_e. Assuming that the total power consumption is equal to r at the equilibrium state, we obtain

$$r = \sum_{i=1}^{m} \frac{a_i\alpha_i + b_i\beta_i}{a_i} - \sum_{i=1}^{m} \frac{b_i}{a_i} u_e$$

because $\sum_{i=1}^{m} x_e^i = r$. This yields

$$u_e = \frac{\displaystyle\sum_{i=1}^{m} \frac{a_i\alpha_i + b_i\beta_i}{a_i} - r}{\displaystyle\sum_{i=1}^{m} \frac{b_i}{a_i}}.$$

So, since (4.5) means $\bar{u} \geq u_e$, it holds under (4.4). This proves the statement. ■

Theorem 4.1 means that Problem 2 cannot be solved if r and $\bar{u}$ do not satisfy (4.5). This enables us to estimate the price needed to track r.

An example for Theorem 4.1 is shown. For the above example, the condition (4.5) is calculated as $\bar{u} \geq 31.4255$. Thus, the condition is not satisfied from $\bar{u} := 29$. This is consistent with Theorem 4.1.

4.4 Controller Network for Real-time Pricing

Now, we present a solution to Problem 2 under the following assumptions:

(A1) For each $i \in \{1, 2, \ldots, m\}$, there exists a $j \in \{1, 2, \ldots, n\}$ satisfying $i \in \mathbb{N}_{Kj}^{P}$.

(A2) $\mathbb{N}_M \neq \emptyset$.

(A3) Consider the subgraph G_K of G, representing the network topology among $K_1, K_2, \ldots, K_n$. There exists an edge from node j to node i if there exists an edge from node i to node j.

(A4) The subgraph G_K is strongly connected.

These assumptions are similar to (A2.1)–(A2.4) in Chapter 3. The first and second ones require that the consumers, the power sources, and the power price controller are connected. The third one implies that the communication links between the power sources are bidirectional. The last one guarantees that every power source is reachable from every other power source on the network. In addition to these, we do not consider the effect of the saturation of the power price in order to focus on the essential issues of the real-time pricing based on the distributed estimation.

4.4.1 Local Controllers and Power Price Controller

For achieving (4.4), we extend the idea in Chapter 3 to integral control. That is, we realize the proportional and integral controller

$$\begin{cases} \dot{\xi}_M(t) = \sum_{i=1}^{m} x_i(t) - r, \\ u(t) = \mathrm{sat}_{\bar{u}}\left(k_P\left(\sum_{i=1}^{m} x_i(t) - r\right) + k_I \xi_M(t)\right) \end{cases} \tag{4.6}$$

in a distributed manner, where $k_P \in \mathbb{R}_+$ is the proportional gain and $k_I \in \mathbb{R}_+$ is the integral gain. For this purpose, we develop local controllers K_i ($i = 1, 2, \ldots, n$) to estimate the total consumption $\sum_{i=1}^{m} x_i(t)$ by communicating with their neighbors.

Based on this idea, we propose the following solution to Problem 2:

$$\kappa_1(\xi_i(t), [y_{ji}(t)]_{j\in\mathbb{N}_{Ki}^P}, [v_j(t)]_{j\in\mathbb{N}_{Ki}}) := \ell \sum_{j\in\mathbb{N}_{Ki}} \left(v_j(t) - \xi_i(t) - \sum_{k\in\mathbb{N}_{Ki}^P} y_{ki}(t)\right), \tag{4.7}$$

$$\kappa_2(\xi_i(t), [y_{ji}(t)]_{j\in\mathbb{N}_{Ki}^P}, [v_j(t)]_{j\in\mathbb{N}_{Ki}}) := \xi_i(t) + \sum_{j\in\mathbb{N}_{Ki}^P} y_{ji}(t), \tag{4.8}$$

$$\mu_1(\xi_M(t), [v_j(t)]_{j\in\mathbb{N}_M}, r(t)) := \frac{n}{|\mathbb{N}_M|} \sum_{j\in\mathbb{N}_M} v_j(t) - r, \tag{4.9}$$

$$\mu_2(\xi_M(t), [v_j(t)]_{j\in\mathbb{N}_M}, r(t)) := k_P\left(\frac{n}{|\mathbb{N}_M|} \sum_{j\in\mathbb{N}_M} v_j(t) - r\right) + k_I \xi_M(t) \tag{4.10}$$

where $\xi_M(t)$ is assumed to be scalar, *i.e.,* $q := 1$, and $\ell \in \mathbb{R}_+$ is the gain of the local controllers. Note that division by zero does not occur in (4.9) and (4.10) because $|\mathbb{N}_M| \neq 0$ from (A2).

The intuitive interpretation of the proposed controllers is as follows. The local controllers K_i ($i = 1, 2, \ldots, n$) given by (4.2), (4.7), and (4.8) are designed in a similar way to that in Chapter 3. That is, these are based on the dynamic consensus protocol proposed in [59]. As the result, $v_i(t)$ ($i = 1, 2, \ldots, n$) track the average of the power required for each power source, *i.e.,* $(1/n)\sum_{j=1}^{n}\sum_{k\in\mathbb{N}_{Kj}^P} y_{kj}(t)$ if (3.4), (A3), and (A4) hold. This means that the local controllers obtain information on the total consumption $\sum_{i=1}^{m} x_i(t)$ because $(1/n)\sum_{j=1}^{n}\sum_{k\in\mathbb{N}_{Kj}^P} y_{kj}(t) = (1/n)\sum_{i=1}^{m} x_i(t)$ from (4.1). On the other hand, the power price controller M given by (4.3), (4.9), and (4.10) works as the controller (4.6) by using the obtained information. In fact, $(n/|\mathbb{N}_M|)\sum_{j\in\mathbb{N}_M} v_j(t) \approx \sum_{j=1}^{m} x_j(t)$ holds in (4.9), and (4.10) because $v_i(t) \approx (1/n)\sum_{j=1}^{m} x_j(t)$ for any $i \in \{1, 2, \ldots, n\}$ as described above.

4.4.2 Convergence Result

Next, we prove that the proposed local controllers and power price controller are a solution to Problem 2.

Let $C_{KP} \in \{0,1\}^{n \times \sum_{i=1}^{m} p_i}$ be the matrix expressing the connections between the local controllers and the consumers, *i.e.,*

$$[C_{KP}]_{ij} := \begin{cases} 1 & \text{if } K_i \text{ receieves the information } y^j, \\ 0 & \text{otherwise} \end{cases} \tag{4.11}$$

where $y^j \in \mathbb{R}$ is the j-th element of y. In a similar way, $C_{MK} \in \{0,1\}^{1\times n}$ is defined as (3.14). Furthermore, the graph Laplacian of the graph G_K is represented by $L \in \mathbb{R}^{n\times n}$. And also, let $A := \mathrm{diag}(a_1, a_2, \ldots, a_m)$, $B := \mathrm{diag}(b_1, b_2, \ldots, b_m)$, $C := \mathrm{diag}(c_1, c_2, \ldots, c_m)$, and $b := [b_1\ b_2\ \cdots\ b_m]^\top$.

Then, the following result is obtained.

Theorem 4.2 For the real-time pricing system Σ, suppose that $r \in \mathbb{R}$, $\bar{u} \in \mathbb{R}_+$, and G are given and assume (A1)–(A4). Let $K_1, K_2, \ldots, K_n$, and M be given by (4.2), (4.3), and (4.7)–(4.10). If

$$k_P > 1 + \frac{\sum_{i=1}^{n-1} |[C_{MK}Q]_{1i}|}{1_m^\top b}, \tag{4.12}$$

$$a_i > |-k_P a_i + k_I| \quad \forall i \in \{1, 2, \ldots, m\}, \tag{4.13}$$

$$\begin{aligned} \ell > \max_{i\in\{1,2,\ldots,n-1\}} \frac{1}{\lambda_{i+1}(L)} \Biggl(\sum_{j=1}^{m} \bigl|[R_1(k_P)]_{ij}\bigr| + [R_2(k_P)]_{ii} \\ + \sum_{j=1, j\neq i}^{n-1} \bigl|[R_2(k_P)]_{ij}\bigr| + |[R_3(k_P,k_I)]_{i1}| \Biggr), \end{aligned} \tag{4.14}$$

then (4.4) holds for every $x_0 \in \mathbb{R}^m$, where $Q \in \mathbb{R}^{n\times(n-1)}$ is given in (3.19),

$$R_1(k_P) := \frac{n}{|\mathbb{N}_M|} Q^\top C_{KP} C (A + k_P b 1_m^\top) B,$$

$$R_2(k_P) := -\frac{k_P n}{|\mathbb{N}_M|} Q^\top C_{KP} C b C_{MK} Q,$$

$$R_3(k_P, k_I) := \frac{n}{|\mathbb{N}_M|} Q^\top C_{KP} C (k_P (A + k_P b 1_m^\top) b - k_I b).$$

■

Proof See Section 4.5. ■

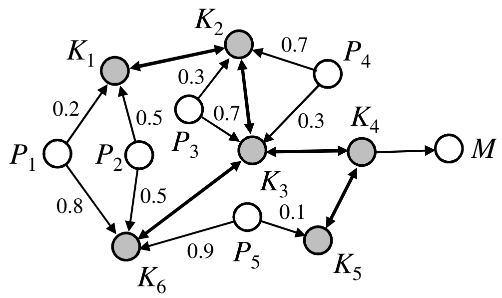

Figure 4.4: Network topology G.

Theorem 4.2 shows that the proposed controllers are a solution to Problem 2 if the gains k_P, k_I, and ℓ are chosen so as to satisfy (4.12)–(4.14). Furthermore, this result allows us to obtain the appropriate gains without the exact information on the consumers. In fact, since the gain conditions (4.12)–(4.14) do not involve the thresholds α_i, β_i $(i = 1, 2, \ldots, m)$ for the power consumption and the power price, we do not have to know the information on them.

Finally, we note that the existence of a $\ell \in \mathbb{R}_+$ satisfying (4.14) is guaranteed when k_P and k_I are given. This follows from the fact that $\lambda_{i+1}(L)$ $(i = 1, 2, \ldots, n-1)$ are positive real numbers because of (2.3) and (L3).

4.4.3 Example

Consider the real-time pricing system Σ with $m := 5$ and $n := 6$. The parameters of consumer i $(i \in \{1, 2, \ldots, 5\})$ are shown in Table 4.1. The reference input and the upper bound of the power price are given by $r := 2$ and $\bar{u} := 50$ satisfying (4.5). The network topology G is given in Figure 4.4 where the label of each edge denotes each element of c_i $(i = 1, 2, \ldots, 5)$. Then, (A1)–(A4) are satisfied. We use the local controllers K_i $(i = 1, 2, \ldots, 6)$ and the power price controller M given by (4.2), (4.3), and (4.7)–(4.10). The gains are set as $k_P := 410$, $k_I := 49.2$, and $\ell := 20$ satisfying (4.12)–(4.14).

Figure 4.5 shows the time responses of Σ for $x_0 := [0.43\ 0.4\ 0.45\ 0.35\ 0.47]^\top$. The first and second figures show the time evolution of the power price $u(t)$ and the total power consumption $\sum_{i=1}^{5} x_i(t)$, respectively. The thin line and the dotted line in the second figure express r and the time evolution of the total power consumption estimated by K_4, *i.e.,* $nv_4(t)$, respectively. It turns out that the total power consumption tracks the reference input. Furthermore, the thick and dotted lines in the second figure almost overlap with each other, and so we can conclude that the proposed local controllers work well as estimators.

Next, an example for a large-scale system is provided. Consider the real-time pricing system Σ with $m := 500$ and $n := 100$. The parameters and the initial state

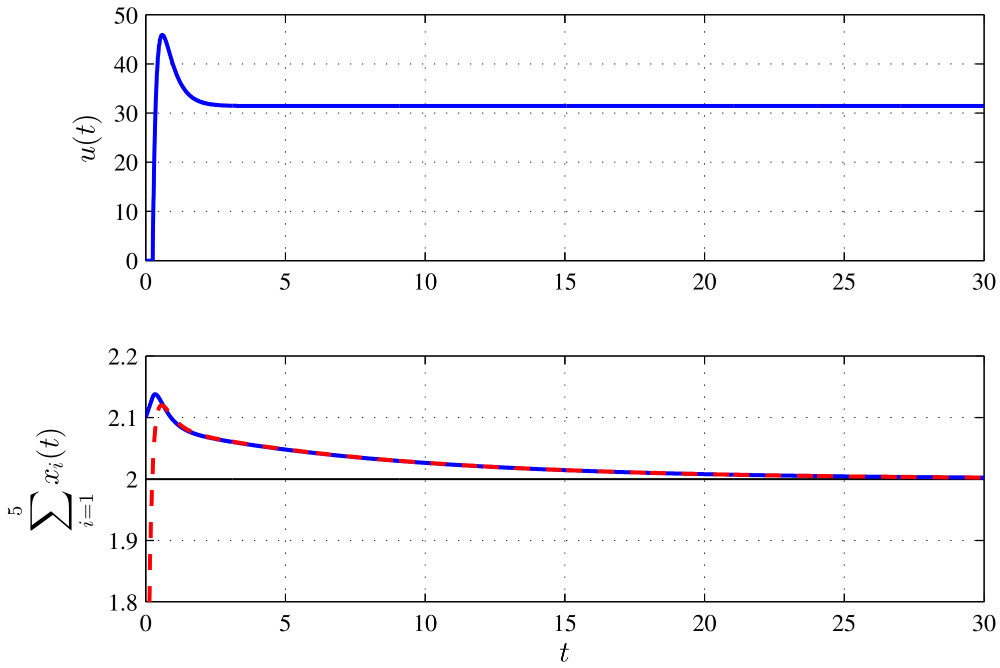

Figure 4.5: Time responses of Σ for $m := 5$ and $n := 6$.

of consumer i ($i \in \{1, 2, \ldots, 500\}$) are given so that $a_i = 0.1$, $5 \times 10^{-4} \le b_i \le 15 \times 10^{-4}$, $0.3 \le \alpha_i \le 0.5$, $25 \le \beta_i \le 35$, $c_i \in (0, 1]^2$, and $0.35 \le x_{i0} \le 0.45$. These (except for a_i) are randomly chosen from the uniform probability distributions on the corresponding intervals. The reference input and the upper bound of the power price are defined as $r := 200$ and $\bar{u} := 50$ satisfying (4.5). The network topology G is given so that (A1)–(A4) hold. We use the local controllers K_i ($i = 1, 2, \ldots, 100$) and the power price controller M given by (4.2), (4.3), and (4.7)–(4.10) with $k_P := 50$, $k_I := 5$, and $\ell := 30$, for which (4.12)–(4.14) hold.

Figure 4.6 depicts the time responses of Σ in the same fashion. It turns out that the total power consumption $\sum_{i=1}^{500} x_i(t)$ tracks the reference input r. This shows that the proposed controllers achieve the real-time pricing even for a large-scale system.

4.5 Proof of Theorem 4.2

In this section, the proof of Theorem 4.2 is provided.

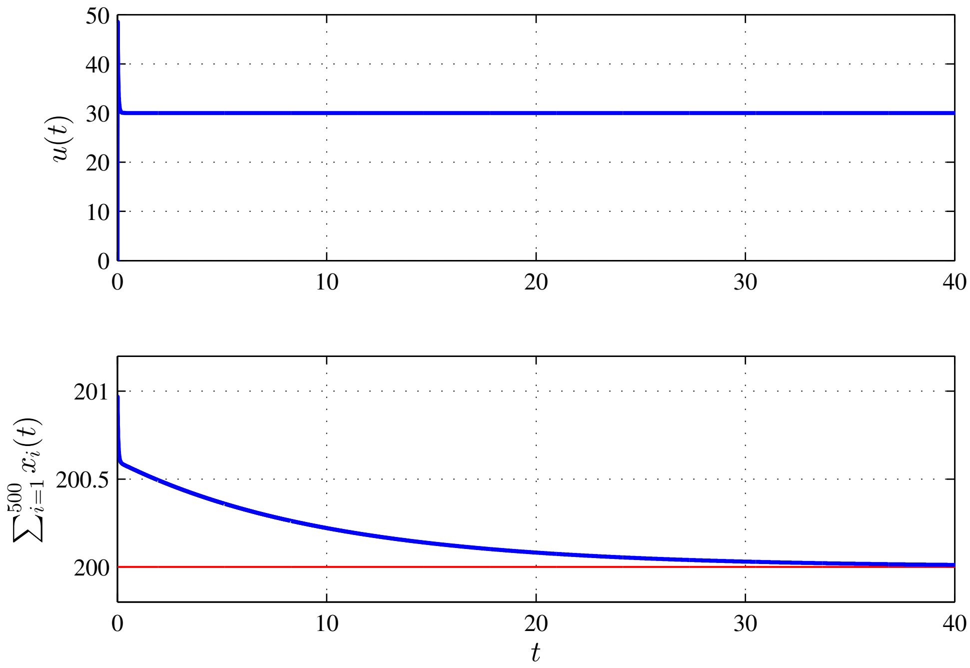

Figure 4.6: Time responses of Σ for $m := 500$ and $n := 100$.

4.5.1 Preliminary

Dynamics of Real-time Pricing System

We prepare the following result.

Lemma 4.1 For the real-time pricing system Σ, suppose that $r \in \mathbb{R}$, $\bar{u} \in \mathbb{R}_+$, and G are given and assume (A1)–(A4). Let $K_1, K_2, \ldots, K_n$, and M be given by (4.2), (4.3), and (4.7)–(4.10). Then

$$1_m^\top x_e = r, \tag{4.15}$$
$$[1_n^\top \quad 0]\xi_e = 0 \tag{4.16}$$

where $\xi_e \in \mathbb{R}^{n+1}$ is the equilibrium state of Σ. ■

Proof See Appendix 4.A. ■

This lemma gives the sum of x_i $(i = 1, 2, \ldots, m)$ and ξ_i $(i = 1, 2, \ldots, n)$ at the equilibrium state. In particular, (4.15) implies that the total power consumption tracks the reference input r if the system Σ converges to the equilibrium state.

We so introduce $e(t) := [x^\top(t) - x_e^\top \quad \xi^\top(t) - \xi_e^\top]^\top \in \mathbb{R}^{m+n+1}$. This corresponds to the deviation from the equilibrium state, which implies that (4.4) holds if $e(t)$

goes to zero as $t \to \infty$. Then, from (3.14), (4.1)–(4.3), and (4.7)–(4.11), the system Σ is expressed as

$$\dot{e}(t) = A_e(k_P, k_I, \ell)e(t) \tag{4.17}$$

where

$$A_e(k_P, k_I, \ell) := \left[\begin{array}{c|cc} -A - \dfrac{k_P n}{|\mathbb{N}_M|} bC_{MK}C_{KP}C & -\dfrac{k_P n}{|\mathbb{N}_M|} bC_{MK} & -k_I b \\ \hline -\ell L C_{KP} C & -\ell L & 0_{n\times 1} \\ \dfrac{n}{|\mathbb{N}_M|} C_{MK}C_{KP}C & \dfrac{n}{|\mathbb{N}_M|} C_{MK} & 0 \end{array}\right]. \tag{4.18}$$

Hence, if the matrix $A_e(k_P, k_I, \ell)$ is Hurwitz, (4.4) holds.

Coordinate Transformation

However, $A_e(k_P, k_I, \ell)$ has a complicated structure, and so it is difficult to immediately determine its stability. Therefore, we propose a coordinate transformation, and then the stability is considered based on the transformed system.

For this purpose, let us consider the transformation matrix

$$T := \left[\begin{array}{c|cc} -B^{-1} & 0_{m\times n} & -k_P 1_m \\ \hline \dfrac{1}{n}(1_n 1_m^\top - nC_{KP}C)B^{-1} & \dfrac{n}{|\mathbb{N}_M|} O & \dfrac{k_P}{n}(1_n 1_m^\top - nC_{KP}C)1_m \\ 0_{1\times m} & 0_{1\times n} & 1 \end{array}\right] \tag{4.19}$$

where $O \in \mathbb{R}^{n\times n}$ is the orthogonal matrix defined as (3.19). Note that the existence of a Q satisfying (3.20) is guaranteed because (L1) and (L2) hold under (A3). Since the matrices B and O are non-singular by the definitions, it can be shown by a simple calculation that T is non-singular.

By letting $\hat{e}(t) := T^{-1}e(t)$, (2.2) and (3.19)–(3.21), and (4.17)–(4.19) provide

$$\dot{\hat{e}}(t) = \hat{A}_e(k_P, k_I, \ell)\hat{e}(t) \tag{4.20}$$

for

$$
\hat{A}_e(k_P, k_I, \ell) :=
$$

$$
\left[\begin{array}{c|cccc}
-A & 0_{m\times 1} & 0_{m\times(n-1)} & -k_P A 1_m + k_I 1_m \\
\hline
0_{1\times m} & 0 & 0_{1\times(n-1)} & 0 \\
R_1(k_P) & -k_P\sqrt{n}Q^\top C_{KP}Cb & R_2(k_P) - \ell\Lambda_{-1}(L) & R_3(k_P, k_I) \\
-b^\top & \dfrac{|\mathbb{N}_M|}{\sqrt{n}} & C_{MK}Q & -k_P 1_m^\top b
\end{array}\right] \tag{4.21}
$$

where (3.16) and the following relation are used:

$$
1_n^\top C_{KP} C = 1_m^\top. \tag{4.22}
$$

Consequently, the stability of $A_e(k_P, k_I, \ell)$ is equivalent to it of $\hat{A}_e(k_P, k_I, \ell)$.

4.5.2 Main Part

Using the above result, we prove Theorem 4.2.

Eigenvalues of $\hat{A}_e$

From (4.21), the following result is obtained.

Lemma 4.2 For the matrix $\hat{A}_e(k_P, k_I, \ell)$, the following statements hold.

(a) The matrix $\hat{A}_e(k_P, k_I, \ell)$ has a zero eigenvalue.

(b) The other $m + n$ eigenvalues are in the sets

$$
\mathbb{D}_1(k_P, k_I) := \bigcup_{i=1}^{m} \left\{ s \in \mathbb{C} \,\middle|\, \left|s + a_i\right| \le |-k_P a_i + k_I| \right\}, \tag{4.23}
$$

$$
\begin{aligned}
\mathbb{D}_2(k_P, k_I, \ell) := \bigcup_{i=1}^{n-1} \Bigg\{ s \in \mathbb{C} \,\Bigg|\, & \left|s + \ell\,\lambda_{i+1}(L) - [R_2(k_P)]_{ii}\right| \\
& \le \sum_{j=1}^{m} \left|[R_1(k_P)]_{ij}\right| + \sum_{j=1, j\ne i}^{n-1} \left|[R_2(k_P)]_{ij}\right| + |[R_3(k_P, k_I)]_{i1}| \Bigg\},
\end{aligned} \tag{4.24}
$$

$$
\mathbb{D}_3(k_P) := \left\{ s \in \mathbb{C} \,\middle|\, \left|s + k_P 1_m^\top b\right| \le 1_m^\top b + \sum_{i=1}^{n-1} |[C_{MK}Q]_{1i}| \right\}. \tag{4.25}
$$

■

Proof See Appendix 4.B. ■

Lemma 4.2 gives a region where the eigenvalues of $\hat{A}_e(k_P, k_I, \ell)$ lie, from which (4.4) holds if

(i) the state whose behavior is characterized by the zero eigenvalue, is identical to zero,

(ii) the sets $\mathbb{D}_1(k_P, k_I)$, $\mathbb{D}_2(k_P, k_I, \ell)$, and $\mathbb{D}_3(k_P)$ are included in the open left-half of the complex plane.

Therefore, we prove (i) and (ii).

Proof of (i)

Equations (4.20) and (4.21) imply that the behavior of $\hat{e}^{m+1}(t)$ is characterized by the zero eigenvalue, where $\hat{e}^{m+1}(t)$ is the $m+1$-th element of $\hat{e}(t)$. From (3.19) and (4.19), we have

$$\hat{e}^{m+1}(t) = \frac{|\mathbb{N}_M|}{n\sqrt{n}} \begin{bmatrix} 1_n^\top & 0 \end{bmatrix} (\xi(t) - \xi_e).$$

Thus, it follows from (3.4) and (4.16) that $\hat{e}^{m+1}(t) \equiv 0$, which proves (i).

Proof of (ii)

From (4.23), the set $\mathbb{D}_1(k_P, k_I)$ is included in the open left-half plane if

$$-a_i < -|-k_P a_i + k_I| \quad \forall i \in \{1, 2, \ldots, m\}. \tag{4.26}$$

The condition (4.26) can be rewritten as (4.13).

Similarly, from (4.24) and (4.25), we obtain the following two conditions:

$$-\ell\lambda_{i+1}(L) + [R_2(k_P)]_{ii} < -\sum_{j=1}^{m} \left|[R_1(k_P)]_{ij}\right| - \sum_{j=1, j\neq i}^{n-1} \left|[R_2(k_P)]_{ij}\right| - |[R_3(k_P, k_I)]_{i1}|$$

for every $i \in \{1, 2, \ldots, n-1\}$, and

$$-k_P 1_m^\top b < -1_m^\top b - \sum_{i=1}^{n-1} |[C_{MK} Q]_{1i}|.$$

Here, we use the fact that $\lambda_{i+1}(L)$ $(i = 1, 2, \ldots, n-1)$ are real numbers from (2.3) in order to get the first condition. The first condition is equivalent to (4.14) since $\lambda_{i+1}(L)$ is positive for every $i \in \{1, 2, \ldots, n-1\}$ from (2.3) and (L3). In addition, the second one can be expressed as (4.12) because the scalar $1_m^\top b$ is positive.

Hence, (ii) holds subject to (4.12)–(4.14), which completes the proof.

4.6 Summary

This chapter has addressed a design problem of a controller network for the real-time pricing. For this problem, a necessary condition for the solvability has been derived. This clarifies the relation between the upper bound of the power price and the reference input which the total power consumption can track. Furthermore, by extending the idea in Chapter 3 to integral control, we have obtained a solution to the design problem. With this result, we can achieve the real-time pricing without collecting information on power consumption from all consumers.

Appendix 4.A Proof of Lemma 4.1

Let $\xi_{-M}(t) \in \mathbb{R}^n$ denote the collective state of the local controllers, *i.e.*, $\xi_{-M}(t) := [\xi_1(t)\ \xi_2(t)\ \cdots\ \xi_n(t)]^\top$. The value at the equilibrium state of the system Σ is represented by $\xi_{-Me} \in \mathbb{R}^n$.

We first prove (4.16). From (4.1), (4.2), (4.7), (4.8), and (4.11), the collective dynamics of the local controllers is given by

$$\dot{\xi}_{-M}(t) = -\ell L \xi_{-M}(t) - \ell L C_{KP} C x(t). \tag{4.27}$$

Multiplying (4.27) on the left by $1_n^\top$ and using (2.4) provide

$$1_n^\top \dot{\xi}_{-M}(t) = 0.$$

This means that $1_n^\top \xi_{-M}(t)$ is an invariant quantity. Thus, it follows from (3.4) that

$$1_n^\top \xi_{-M}(t) \equiv 0,$$

which implies (4.16).

Next, (4.15) is proven as follows. From (4.27), the equation

$$\begin{aligned} 0_{n\times 1} &= -\ell L \xi_{-Me} - \ell L C_{KP} C x_e \\ &= -\ell L(\xi_{-Me} + C_{KP} C x_e) \end{aligned}$$

holds at the equilibrium state of Σ. This yields

$$\xi_{-Me} + C_{KP} C x_e = \gamma 1_n \tag{4.28}$$

for some $\gamma \in \mathbb{R}$ due to (2.2). On the other hand, considering the dynamics of the power price controller, we have

$$\begin{aligned} 0 &= \frac{n}{|\mathbb{N}_M|} C_{MK} \xi_{-Me} + \frac{n}{|\mathbb{N}_M|} C_{MK} C_{KP} C x_e - r \\ &= \frac{n}{|\mathbb{N}_M|} C_{MK} (\xi_{-Me} + C_{KP} C x_e) - r \\ &= \gamma \frac{n}{|\mathbb{N}_M|} C_{MK} 1_n - r. \end{aligned} \tag{4.29}$$

The first equality is given by (3.14), (4.1)–(4.3), (4.8), (4.9), and (4.11), the second one is trivial, and the last one is obtained from (4.28). Equation (4.29) provides

$$\gamma = \frac{r}{n} \tag{4.30}$$

because of (3.16). By substituting (4.30) for (4.28), it follows that

$$\xi_{-Me} + C_{KP} C x_e = \frac{r}{n} 1_n. \tag{4.31}$$

By multiplying (4.31) on the left by $1_n^\top$ and using (4.16) and (4.22), we get (4.15). This completes the proof.

Appendix 4.B Proof of Lemma 4.2

Equation (4.21) shows that $\hat{A}_e(k_P, k_I, \ell)$ has a zero vector in its row. Therefore, one of the eigenvalues is zero, which proves (a). Furthermore, by calculating the characteristic polynomial, it can be shown that the other eigenvalues are equivalent to those of the matrix

$$\left[\begin{array}{c|cc} -A & 0_{m\times(n-1)} & -k_P A 1_m + k_I 1_m \\ \hline R_1(k_P) & R_2(k_P) - \ell\Lambda_{-1}(L) & R_3(k_P, k_I) \\ -b^\top & C_{MK} Q & -k_P 1_m^\top b \end{array}\right].$$

By applying Gershgorin theorem to this matrix and utilizing the fact that b_i ($i = 1, 2, \ldots, m$) are positive, it follows that the eigenvalues are in the sets $\mathbb{D}_1(k_P, k_I)$, $\mathbb{D}_2(k_P, k_I, \ell)$, and $\mathbb{D}_3(k_P)$. This shows (b).

Chapter 5

Motion Coordination by Controller Networks: Robotic Mass Games

This chapter provides a controller network for the robotic mass games, *i.e.,* to let robots organize themselves into a formation displaying a given grayscale image. First, we describe a design problem of the controller network for the mass games. Next, as elemental techniques, we introduce the coverage control and the halftone image processing. Based on these, we develop a controller network for the mass games. The performance is demonstrated by numerical experiments with the standard images. In addition to this, two extensions are provided for practical use and performance improvement.

5.1 Problem Setting

5.1.1 Notation

For the convex set $\mathbb{Q} \subset \mathbb{R}^2$ and the vector $x := [x_1^\top \; x_2^\top \; \cdots \; x_n^\top]^\top \in \mathbb{Q}^n$ composed of distinct 2-dimensional vectors, let $\mathbb{V}_i(x)$ be the *Voronoi cell* for x_i, *i.e.,*

$$\mathbb{V}_i(x) := \left\{ q \in \mathbb{Q} \,\middle|\, \|q - x_i\| \le \|q - x_j\| \; \forall j \in \{1, 2, \ldots, n\} \right\}.$$

The *Delaunay graph* for $x_1, x_2, \ldots, x_n$ is represented by $G(x)$. That is, $G(x)$ is the graph with the node set $\{1, 2, \ldots, n\}$ and the edge set

$$\left\{ (i, j) \in \{1, 2, \ldots, n\}^2 \,\middle|\, \mathbb{V}_i(x) \cap \mathbb{V}_j(x) \neq \emptyset \right\}.$$

Figure 5.1 illustrates an example of Voronoi cells and a Delaunay graph for $n := 5$.

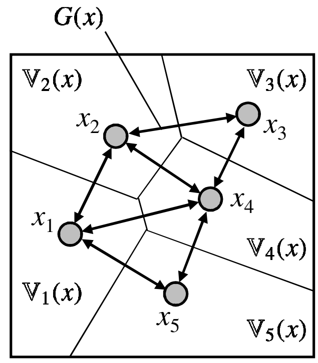

Figure 5.1: Example of Voronoi cells and Delaunay graph

5.1.2 Multi-robot System

Consider the multi-robot system Σ in Figure 5.2, which is composed of n robots.

The dynamics of robot i ($i \in \{1, 2, \ldots, n\}$) is given by

$$P_i : \dot{x}_i(t) = u_i(t) \tag{5.1}$$

where $x_i(t) \in \mathbb{R}^2$ and $u_i(t) \in \mathbb{R}^2$ are the position and the control input. The collective position of the robots is expressed by $x(t) := [x_1^\top(t) \ x_2^\top(t) \ \cdots \ x_n^\top(t)]^\top \in \mathbb{R}^{2n}$, and $x(t)$ is called the *formation* at time t. The initial formation is given as $x(0) = x_0 \in \mathbb{R}^{2n}$.

We suppose that a local controller is embedded in each robot. The local controller for robot i is of the form

$$K_i : u_i(t) = \kappa([x_j(t)]_{j \in \mathbb{N}_i(t)}) \tag{5.2}$$

where $[x_j(t)]_{j \in \mathbb{N}_i(t)} \in \mathbb{R}^{2|\mathbb{N}_i(t)|}$ is the input, $u_i(t) \in \mathbb{R}^2$ is the output, and $\kappa : \mathbb{R}^{2|\mathbb{N}_i(t)|} \to \mathbb{R}^2$ is a function. The set $\mathbb{N}_i(t) \subset \{1, 2, \ldots, n\}$ is the index set of the neighbors, *i.e.,* the robots whose information is available to robot i. As in the previous chapters, the function κ is assumed to be the same for all the robots for the scalability.

If all the robots exist in a bounded convex set $\mathbb{Q} \subset \mathbb{R}^2$, we use $\mathbb{V}_i(x(t))$ to denote the Voronoi cell for $x_i(t)$ (for robot i) and use $G(x(t))$ to denote the corresponding Delaunay graph. Then, we impose the following assumptions for the multi-robot system Σ:

(A1) Each robot has the information on its own position in the world coordinate frame.

(A2) Each robot can obtain the information on the relative positions of the robots connected to itself on the Delaunay graph $G(x(t))$.

These assumptions are satisfied if each robot has, for example, a GPS receiver and stereo cameras.

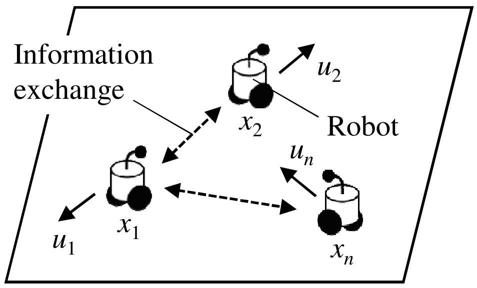

Figure 5.2: Multi-robot system Σ.

5.1.3 Mass Game Problem

Let us consider making the multi-robot system Σ achieve a formation on the field $\mathbb{Q}$. The desired formation is a formation displaying a given grayscale image. The image is represented as an integrable function $\varphi : \mathbb{Q} \to [0, 1]$. The function φ expresses the pixel values on $\mathbb{Q}$, and the values $\varphi(q) = 0$, $\varphi(q) = 1$, and $\varphi(q) \in (0, 1)$ correspond to black, white, and gray, respectively. Then, the problem considered here is stated as follows.

Problem 3 For the multi-robot system Σ, suppose that a grayscale image $\varphi : \mathbb{Q} \to [0, 1]$ is given. Find local controllers $K_1, K_2, \ldots, K_n$ (*i.e.,* find a function κ) such that, for every initial formation $x_0 \in \mathbb{Q}^n$, the final formation $x(\infty)$ displays the image φ on the field $\mathbb{Q}$, as shown in Figure 1.8. ■

Several remarks on Problem 3 are given. First, this problem is different from the generalized problem in Chapter 2 in the respect that the network topology of the system Σ is not given but specified by assumptions (A1) and (A2). The reason is that since the robots, which correspond to the controller nodes, move, it is difficult to realize any network structure. Second, the problem is stated without introducing any mathematical performance indices. This is because the problem contains a specification on human perception (visual perception) and it is in general difficult to quantify it by a mathematical function. Third, we cannot solve the problem by giving the desired position of each robot to the corresponding local controller in advance. In fact, since the local controllers K_i ($i = 1, 2, \ldots, n$) are assumed to be the same for the scalability, it is not possible to give different information to each local controller K_i. Fourth, it is assumed here that all the robots share the information on the grayscale image φ. Thus, the solution will depend on φ. Finally, in order to focus on the essential issues of the mass game, we do not consider the inconvenience caused by collisions among robots.

5.2 Controller Network for Mass Games

In this section, a solution to the mass game problem is presented. First, we introduce two elemental techniques: the coverage control [23] and the halftone image processing [60]. Based on these, we develop mass game controllers.

5.2.1 Elemental Techniques

Coverage Control

The coverage means steering robots arbitrarily placed in an environment so that the sizes of the robots' occupied areas are equal in a certain sense. It is one of the fundamental coordination tasks in various multi-robot problems including mobile sensor networks.

A theoretical framework for coverage control has been developed in [23], and it is summarized as follows. Consider the multi-robot system Σ. For the formation $x := [x_1^\top \ x_2^\top \ \cdots \ x_n^\top]^\top \in \mathbb{R}^{2n}$, we use the performance index

$$J(x) := \int_{\mathbb{Q}} \min_{i \in \{1,2,\ldots,n\}} \|q - x_i\|^2 \phi(q)\, dq \tag{5.3}$$

where $\mathbb{Q}$ is a bounded set representing the coverage field and $\phi : \mathbb{Q} \to \mathbb{R}_{0+}$ is an integrable function which corresponds to the weighting function quantifying the relative importance of each point in $\mathbb{Q}$. By noting that $\min_{i\in\{1,2,\ldots,n\}} \|q - x_i\|^2$ denotes the distance between the point q and the nearest robot's position, the formation x minimizing $J(x)$ under $\phi(q) \equiv 1$ is a configuration that x_i exists near at any point in $\mathbb{Q}$. If $\phi(q) \not\equiv 1$, meanwhile, a similar interpretation holds for the space $\mathbb{Q}$ weighted by ϕ; namely, in the formation x minimizing $J(x)$, more robots are allocated to the points having the large value of ϕ.

It has been proven in [23] that there exist local controllers such that

(i) the time derivative of the resulting $J(x(t))$ is negative semi-definite,

(ii) the set of solutions to $\partial J(x)/\partial x = 0$ is the largest invariant set of the resulting closed-loop system.

From (i), (ii), and LaSalle's principle (see Appendix A.2), the controllers move the robots to a stationary point of $J(x)$, and in this sense, the coverage is completed. It has been shown there that such controllers are given by

$$u_i(t) = k\left(\mathrm{cent}(\mathbb{V}_i(x(t)), \phi) - x_i(t)\right) \tag{5.4}$$

where $k \in \mathbb{R}_+$ is the gain and $\mathrm{cent}(\mathbb{V}_i(x(t)), \phi) \in \mathbb{R}^2$ is the weighted centroid of $\mathbb{V}_i(x(t))$. The controller (5.4) is of the form (5.2) under assumptions (A1) and (A2). This is because the Voronoi cell $\mathbb{V}_i(x(t))$ depends on the positions of robot i and the robots connected to it on the Delaunay graph $G(x(t))$.

Halftone Image Processing

The halftone image processing is to transform grayscale images into binary images with preserving the visual quality as much as possible. This processing is typically performed to output grayscale images by print or display devices whose output is restricted to few colors.

The basic idea is that more black pixels are placed at the parts corresponding to the dark parts of the original grayscale image. More precisely, black pixels are allocated in the binary image so that, for any part of the binary image, the density of the black pixels is nearly equal to the average pixel values of the corresponding part of the grayscale image. As the result, the allocated black and white pixels are blended into smooth tones by the spatial lowpass filtering property of the human eye. An example is depicted in Figure 5.3 where a grayscale image and the binary image given by a halftone image processing technique are illustrated.

5.2.2 Proposed Controllers

Now, we propose mass game controllers.

The idea of the proposed controllers is outlined as follows. As seen in Section 5.2.1, the coverage controllers given by (5.4) enable us to place the robots so that the distribution of the robots becomes a desirable one specified by the weighting function ϕ. The halftone image processing, on the other hand, allows us to obtain a similar binary image to a given grayscale image by placing black pixels so that the distribution of the black pixels corresponds to the pixel values of the original grayscale image. These facts imply that the mass games would be achieved by

- letting the robots play the role of the black pixels,
- placing the robots (by the coverage control) so that the distribution of the robots corresponds to the reference image φ.

Based on this idea, we propose the mass game controllers given by (5.4) with

$$\phi(q) := e^{-10\varphi(q)}. \tag{5.5}$$

The weighting function (5.5) has a large value if the pixel value $\varphi(q)$ at the point q is small, and has a small value if the pixel value $\varphi(q)$ at the point q is large. Therefore, the proposed controllers generate a formation where more robots are allocated to areas corresponding to darker parts of the reference image φ, which would complete the mass game. The weighting function $\phi(q)$ is given as an exponential function of the reference image φ for accentuating the darkness of φ. The coefficient is set to 10 by calibration for a test pattern. The result of the calibration is given in Appendix 5.A.

(a) Original grayscale image

(b) Resulting binary image

Figure 5.3: Halftone image processing.

5.2.3 Numerical Experiments

The resulting controller network is verified by the standard method in the image processing area, *i.e.,* by numerical experiments with the standard images in [61].

Consider the multi-robot system Σ where $n := 5000$ and $\mathbb{Q} := [0, 100]^2$. The reference image φ is *Lenna* in Figure 5.3 (a), which is one of the standard images. This is an eight-bit grayscale image, and thus $\varphi(q) \in \{0, 1/255, 2/255, \ldots, 1\}$. The initial formation x_0 is given randomly from the uniform probability distribution on $\mathbb{Q}^{5000}$. We use the local controllers K_i ($i = 1, 2, \ldots, 5000$) given by (5.4) and (5.5) with $k := 2$.

Figure 5.4 depicts the time series of the resulting formations, where the solid squares represent the robots. We can see that the robots organize themselves into a formation displaying the grayscale image as time goes on. Also for other standard images, similar results are obtained. Figures 5.5–5.7 illustrate the results for the standard images *Barbara*, *Mandrill*, and *Pepper*, where (a), (b), and (c) represent the reference image, the initial formation, and the final formation (at $t = 20$), respectively. These show that our controller network achieves the mass games for various images.

Remark 5.1 The proposed controllers may not achieve the mass games for the non-uniform initial distribution. This is because if the initial distribution is biased toward an area in $\mathbb{Q}$, the resulting distribution is also biased toward there. In this case, we first make the uniform distribution by letting the robots perform a random walk for a while. Then, the proposed controllers are applied to the robots, and a similar result to Figures 5.4–5.7 is obtained. ■

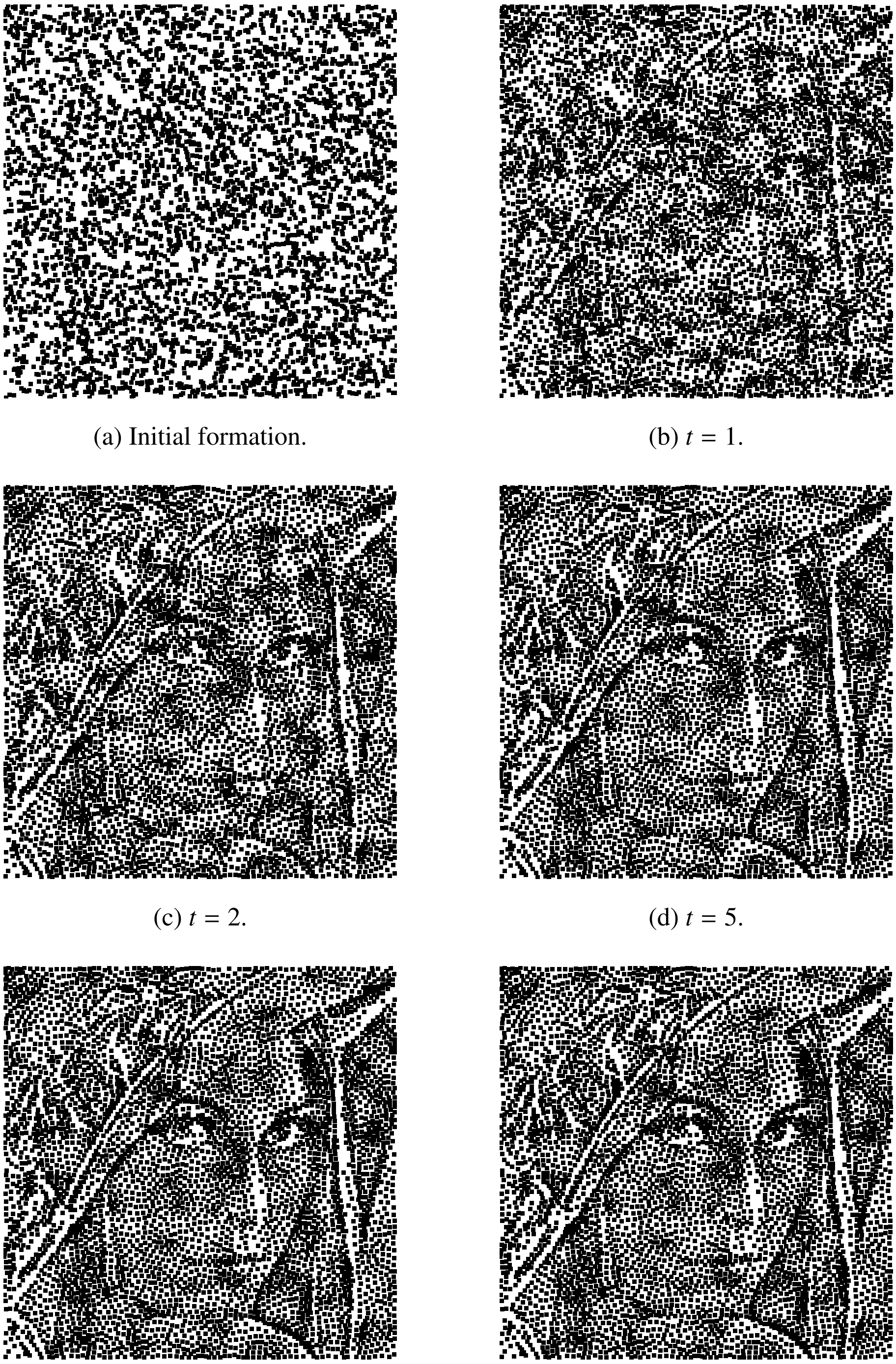

(a) Initial formation.

(b) $t = 1$.

(c) $t = 2$.

(d) $t = 5$.

(e) $t = 10$.

(f) $t = 20$.

Figure 5.4: Simulation result for Lenna.

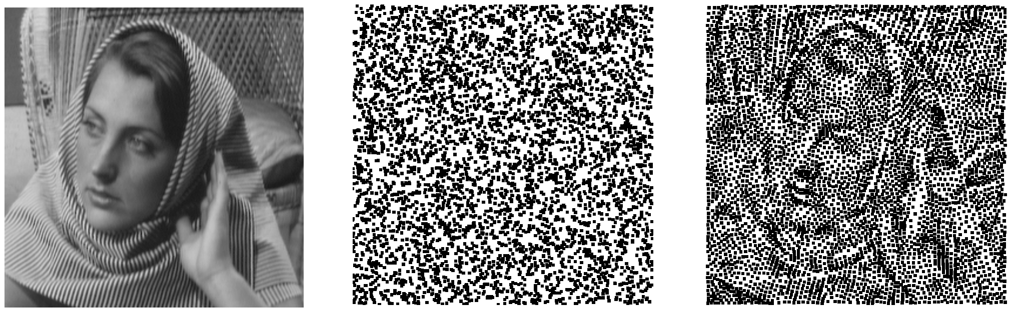

(a) Reference image. (b) Initial formation. (c) Final formation.

Figure 5.5: Simulation result for Barbara.

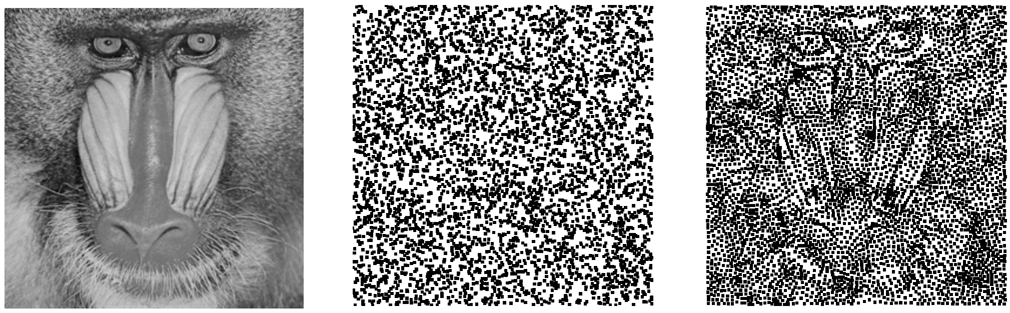

(a) Reference image. (b) Initial formation. (c) Final formation.

Figure 5.6: Simulation result for Mandrill.

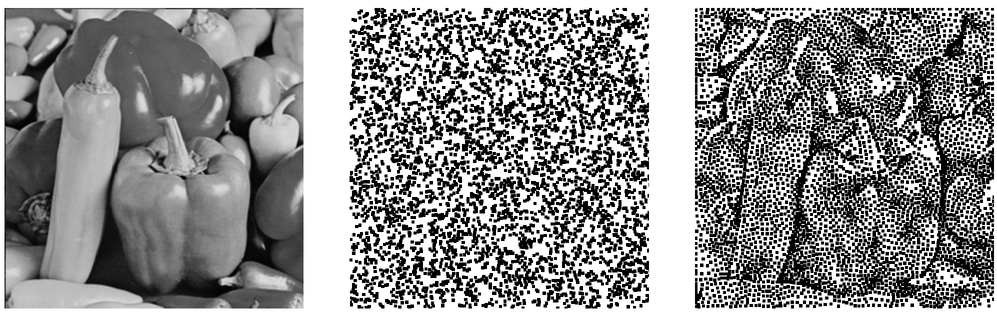

(a) Reference image. (b) Initial formation. (c) Final formation.

Figure 5.7: Simulation result for Pepper.

5.3 Extension to Case of r-Disk Proximity Networks

While the proposed controllers achieve the mass games, the communication structure based on the Delaunay graph is required. This implies that each robot can communicate with distant robots. An example is depicted in Figure 5.8 where the circles, the arrows, and the areas separated by the thin lines express the robots, the communication links, and the Voronoi cells, respectively. We see that Robot 4 is far away from robot 1, but communicates with it. However, since communication range constraints are imposed for robots in practical cases, such communication may be impossible. This is a difficulty in applying the proposed controllers to real robots. Therefore, in this section, we extend the proposed controllers to the case of *r-disk proximity networks* where each robot only communicates with the robots within radius r.

5.3.1 Proposed Controllers

Consider the multi-robot system Σ. For this system, we assume here that (A1) and

(A3) each robot can obtain the information on the relative positions of the robots within radius r.

Under these assumptions, a solution to the mass game problem is provided.

The idea of our solution is explained as follows. From the discussion in the previous section, the mass games can be achieved by minimizing the performance index $J(x)$ in (5.3) with (5.5). However, the controller (5.4) with (5.5) to generate a formation minimizing $J(x)$ cannot be implemented as the controller (5.2) subject to (A3). Therefore, we extend the performance index $J(x)$ by taking into the communication range constraint, and derive local controllers to achieve a formation minimizing the resulting performance index.

Based on this idea, the performance index $J(x)$ in (5.3) with (5.5) is extended as follows:

$$\hat{J}(x) := \int_{\mathbb{Q}} \min_{i\in\{1,2,\ldots,n\}} \gamma(\|q-x_i\|)e^{-10\varphi(q)}\,dq \tag{5.6}$$

where

$$\gamma(\|q-x_i\|) := \begin{cases} \|q-x_i\|^2 & \text{if } \|q-x_i\| < \dfrac{r}{2}, \\ \dfrac{r^2}{4} & \text{otherwise.} \end{cases} \tag{5.7}$$

The performance index $\hat{J}(x)$ is given by replacing $\|q-x_i\|^2$ in $J(x)$ with $\gamma(\|q-x_i\|)$. The function $\gamma(\|q-x_i\|)$ is the same as $\|q-x_i\|^2$ if $\|q-x_i\| < r/2$; otherwise, it has

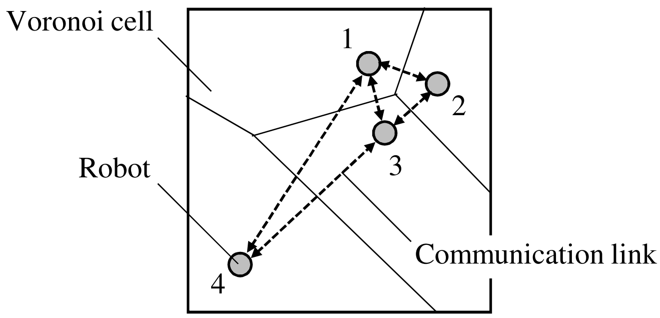

Figure 5.8: Communication structure based on Delaunay graph.

the value $r^2/4$, *i.e.,* the value of $\|q - x_i\|^2$ at $\|q - x_i\| = r/2$. So, in $\hat{J}(x)$, the value of $\|q - x_i\|$ is restricted to the range of 0 to $r/2$.

For such a performance index, our mass game controllers are given by

$$u_i(t) = k\big(\mathrm{cent}(\mathbb{V}_i(x(t)) \cap \mathbb{B}(x_i(t), r/2), e^{-10\varphi(q)}) - x_i(t)\big). \tag{5.8}$$

The controller (5.8) is of the form (5.2) under assumptions (A1) and (A3) because the set $\mathbb{V}_i(x(t)) \cap \mathbb{B}(x_i(t), r/2)$ depends on the positions of robot i and the robots within radius r.

For the proposed controllers, we obtain the following result.

Theorem 5.1 For the multi-robot system Σ, suppose that $\varphi : \mathbb{Q} \to [0, 1]$ is given and assume (A1) and (A3). Let $K_1, K_2, \ldots, K_n$ be given by (5.8). Then, $x(t)$ converges to a solution to $\partial\hat{J}(x)/\partial x = 0$ for every $x_0 \in \mathbb{R}^{2n}$. ■

Proof This theorem is proven by the following two facts and LaSalle's principle.

(i) The time derivative of $\hat{J}(x(t))$ is negative semi-definite.

(ii) The largest invariant set contained in the set $\{x \in \mathbb{R}^{2n} \mid \dot{\hat{J}}(x) = 0\}$ is the set of solutions to $\partial\hat{J}(x)/\partial x = 0$.

The proofs of (i) and (ii) are given in Appendix 5.B. ■

Theorem 5.1 means that the proposed controllers steer the robots to a stationary point of the performance index $\hat{J}(x)$. Therefore, the mass games are achieved if r is sufficiently large, because $\gamma(\|q - x_i\|) \equiv \|q - x_i\|^2$ as $r \to \infty$,

An example is given. Consider the multi-robot system Σ over a r-disk proximity network, where $n := 5000$, $\mathbb{Q} := [0, 100]^2$, and $r := 5$. The reference image φ is *Pepper* in Figure 5.7 (a). The initial formation x_0 is chosen randomly from the uniform probability distribution on $\mathbb{Q}^{5000}$. We employ the local controllers

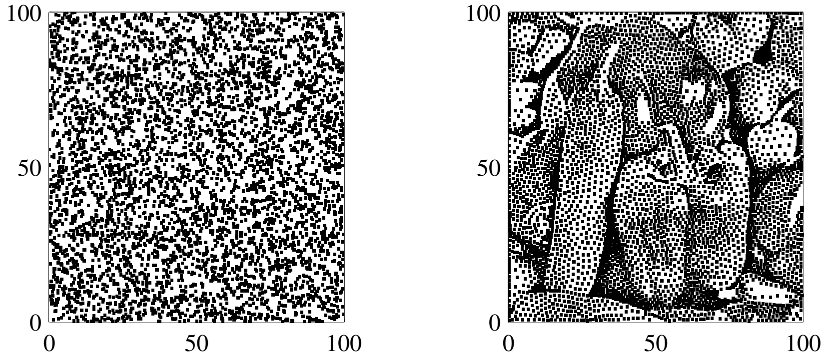

(a) Initial formation. (b) Final formation.

Figure 5.9: Simulation result for $r := 5$.

K_i ($i = 1, 2, \ldots, 5000$) given by (5.8) with $k := 2$. Figure 5.9 illustrates the initial formation and the resulting formation (at $t = 100$) in the same fashion. This shows that the mass game is achieved though the communication range constraint is imposed for the robots. Furthermore, by comparing with Figure 5.7 (c), we can conclude that the performance of the proposed controllers is comparable to that of the controllers given in the previous section.

5.3.2 Condition on Communication Range for Mass Games

According to the above result, the proposed controllers achieve the mass games if the communication range r is sufficiently large. Now, how do we choose the r?

An answer to this question is given by the following result.

Theorem 5.2 For the performance indices $J(x)$ given by (5.3) and (5.5) and $\hat{J}(x)$ in (5.6), the following relation holds:

$$\hat{J}(x) \leq J(x) \leq \hat{J}(x) + \Delta(x, r) \tag{5.9}$$

where

$$\Delta(x, r) := \left(\mathrm{diam}(\mathbb{Q})^2 - \frac{r^2}{4}\right) \int_{\mathbb{Q} \setminus \cup_{i=1}^{n} \mathbb{B}(x_i, r/2)} e^{-10\varphi(q)}\, dq. \tag{5.10}$$

■

Proof The proof is provided in a similar way to that in [71].

From (5.7), $\gamma(\|q - x_i\|) \leq \|q - x_i\|^2$ holds for every $q, x_i \in \mathbb{Q}$, which gives the fist inequality.

Meanwhile, the second inequality is shown as follows. By the definition of the Voronoi cell $\mathbb{V}_i(x)$, the performance index $J(x)$ can be rewritten as

$$J(x) = \sum_{i=1}^{n} \int_{\mathbb{V}_i(x)} \|q - x_i\|^2 e^{-10\varphi(q)}\, dq. \tag{5.11}$$

Similarly, $\hat{J}(x)$ can be rewritten as

$$\begin{aligned}\hat{J}(x) &= \sum_{i=1}^{n} \int_{\mathbb{V}_i(x)} \gamma(\|q - x_i\|) e^{-10\varphi(q)}\, dq \\ &= \sum_{i=1}^{n} \int_{\mathbb{V}_i(x)\cap\mathbb{B}(x_i,r/2)} \|q - x_i\|^2 e^{-10\varphi(q)}\, dq + \int_{\mathbb{V}_i(x)\setminus\mathbb{B}(x_i,r/2)} \frac{r^2}{4} e^{-10\varphi(q)}\, dq \end{aligned}\tag{5.12}$$

where the first equality follows from the definition of the Voronoi cell $\mathbb{V}_i(x)$ and the monotonically non-decreasing property of $\gamma(\|q - x_i\|)$, the second one is given by (5.7). From (5.11) and (5.12), we have

$$\begin{aligned} J(x) - \hat{J}(x) &= \sum_{i=1}^{n} \int_{\mathbb{V}_i(x)\setminus\mathbb{B}(x_i,r/2)} \left(\|q - x_i\|^2 - \frac{r^2}{4}\right) e^{-10\varphi(q)}\, dq \\ &\le \sum_{i=1}^{n} \int_{\mathbb{V}_i(x)\setminus\mathbb{B}(x_i,r/2)} \left(\mathrm{diam}(\mathbb{Q})^2 - \frac{r^2}{4}\right) e^{-10\varphi(q)}\, dq \\ &= \left(\mathrm{diam}(\mathbb{Q})^2 - \frac{r^2}{4}\right) \int_{\mathbb{Q}\setminus\cup_{i=1}^{n}\mathbb{B}(x_i,r/2)} e^{-10\varphi(q)}\, dq. \end{aligned}\tag{5.13}$$

This shows the second inequality, which completes the proof. ■

Theorem 5.2 gives the relation between the performance indices $J(x)$ and $\hat{J}(x)$ and the communication range r. From (5.10), $\Delta(x, r) = 0$ if $\mathbb{Q} \setminus \cup_{i=1}^{n} \mathbb{B}(x_i, r/2) = \emptyset$, which gives $J(x) = \hat{J}(x)$ because of (5.9). Therefore, if the gap between $J(x)$ and $\hat{J}(x)$ is small, there exists a formation satisfying $\mathbb{Q} \subset \cup_{i=1}^{n} \mathbb{B}(x_i, r/2)$. This is useful information to estimate a minimum r for achieving the mass games.

We show an example. Consider the example in Section 5.3.1. Since $n := 5000$ and $\mathbb{Q} := [0, 100]^2$, we choose the communication range as $r := 2$ so that there exists a formation satisfying $\mathbb{Q} \subset \cup_{i=1}^{5000} \mathbb{B}(x_i, r/2)$. Then, the resulting formation is illustrated in Figure 5.10 (a). We see that a formation displaying the reference image is generated. On the other hand, Figure 5.10 (b) shows the resulting formation when $r := 1$ for which $\mathbb{Q} \subset \cup_{i=1}^{5000} \mathbb{B}(x_i, r/2)$ does not hold for every $x \in \mathbb{Q}^{5000}$. It turns out that the resulting formation does not display the reference image. In this way, we can easily obtain a minimum r for achieving the mass game.

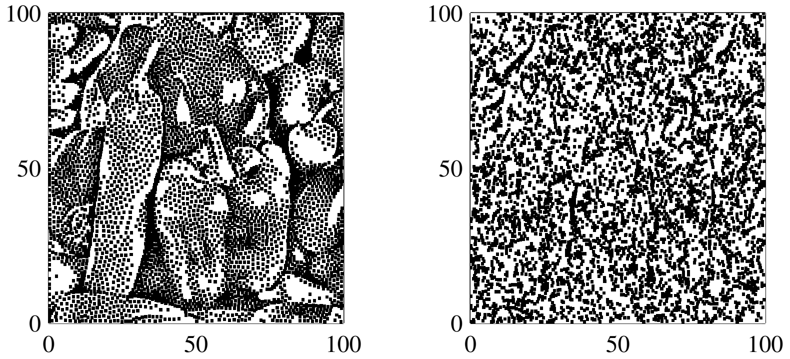

(a) $r = 2$. (b) $r = 1$.

Figure 5.10: Simulation results for several communication range r.

5.4 Extension to Case of a Variable Number of Player Robots

The controllers proposed in the previous sections are for the mass game with a *fixed* number of player robots, and let all the robots participate in the mass game even for a bright image which only needs a few robots. This results in a critical drawback that the brightness of the resulting image does not agree with that of the given image. An example is illustrated in Figure 5.11. We see that there are too many robots and the resulting image is darker than the reference image. We thus extend our result to the case of a *variable* number of player robots, and present controllers classifying the robots into a player group and a nonplayer group in a distributed manner.

5.4.1 Proposed Controllers

Consider the multi-robot system Σ. The local controller K_i ($i \in \{1, 2, \ldots, n\}$) treated here is of the form

$$K_i : \begin{cases} \dot{\xi}_i(t) = \kappa_1(\xi_i(t), [x_j(t)]_{j \in \mathbb{N}_i(t)}, t), \\ u_i(t) = \kappa_2(\xi_i(t), [x_j(t)]_{j \in \mathbb{N}_i(t)}, t) \end{cases} \tag{5.14}$$

where $\xi_i(t) \in \mathbb{R}^p$ is the state, $[x_j(t)]_{j \in \mathbb{N}_i(t)} \in \mathbb{R}^{2|\mathbb{N}_i(t)|}$ is the input, $u_i(t) \in \mathbb{R}^2$ is the output, and $\kappa_1 : \mathbb{R}^p \times \mathbb{R}^{2|\mathbb{N}_i(t)|} \times \mathbb{R}_{0+} \to \mathbb{R}^p$ and $\kappa_2 : \mathbb{R}^p \times \mathbb{R}^{2|\mathbb{N}_i(t)|} \times \mathbb{R}_{0+} \to \mathbb{R}^2$ are functions. The functions κ_1 and κ_2 and the initial state $\xi_i(0)$ are assumed to be the same for the scalability. The initial state is given as zero, *i.e.*, $\xi_i(0) = 0_{p \times 1}$.

For this system, suppose that a set $\hat{\mathbb{Q}} \supset \mathbb{Q}$ is given. This provides the space $\hat{\mathbb{Q}} \setminus \mathbb{Q}$ for evacuating unnecessary robots to display the reference image. Also, we

(a) Reference image. (b) Resulting formation.

Figure 5.11: Simulation result for bright image.

assume (A1) and (A2) for the system Σ. We further assume that the size of each robot is equal, and denote by $a \in \mathbb{R}_+$ the area ratio of one robot to the field $\mathbb{Q}$.

Then, we propose the following solution to the mass game problem with a variable number of player robots:

$$\kappa_1(\xi_i(t), [x_j(t)]_{j\in\mathbb{N}_i(t)}, t) := \begin{cases} 1 & \text{if } x_i(t) \in \mathbb{Q},\ \eta(\mathbb{V}_i(\bar{x}(t)), a) \le 0,\ |\xi_i(t)| \le 1, \\ 0 & \text{otherwise,} \end{cases} \tag{5.15}$$

$$\kappa_2(\xi_i(t), [x_j(t)]_{j\in\mathbb{N}_i(t)}, t) := \begin{cases} k\dfrac{x_i(t) - \mathrm{cent}(\mathbb{Q}, 1)}{\|x_i(t) - \mathrm{cent}(\mathbb{Q}, 1)\|} & \text{if } x_i(t) \in \mathbb{Q},\ \xi_i(t) = 0, \\ k(\mathrm{cent}(\mathbb{V}_i(\bar{x}(t)), \phi) - x_i(t)) & \text{if } x_i(t) \in \mathbb{Q},\ \xi_i(t) \ne 0, \\ \dfrac{k}{(1+t)^c}\dfrac{x_i(t) - \mathrm{cent}(\mathbb{Q}, 1)}{\|x_i(t) - \mathrm{cent}(\mathbb{Q}, 1)\|} & \text{otherwise} \end{cases} \tag{5.16}$$

where $\xi_i(t)$ is assumed to be scalar, *i.e.,* $p := 1$, $c \in \mathbb{R}_+$ is the gain,

$$\eta(\mathbb{V}_i(\bar{x}(t)), a) := \frac{a\displaystyle\int_{\mathbb{Q}} 1\, dq}{\displaystyle\int_{\mathbb{V}_i(\bar{x}(t))} 1\, dq} - \frac{\displaystyle\int_{\mathbb{V}_i(\bar{x}(t))} 1 - \varphi(q)\, dq}{\displaystyle\int_{\mathbb{V}_i(\bar{x}(t))} 1\, dq}, \tag{5.17}$$

$$\bar{x}(t) := [x_j(t)]_{j\in\{\ell\in\{1,2,\ldots,n\}|x_\ell(t)\in\mathbb{Q}\}}. \tag{5.18}$$

The right-hand side of (5.17) is composed of the area ratio of robot i to $\mathbb{V}_i(\bar{x}(t))$, *i.e.,* $a\int_{\mathbb{Q}} 1\, dq / \int_{\mathbb{V}_i(\bar{x}(t))} 1\, dq$, and the darkness of the reference image φ in $\mathbb{V}_i(\bar{x}(t))$, *i.e.,* $\int_{\mathbb{V}_i(\bar{x}(t))} 1 - \varphi(q)\, dq \,/\, \int_{\mathbb{V}_i(\bar{x}(t))} 1\, dq$. Hence, $\eta(\mathbb{V}_i(\bar{x}(t)), a)$ quantifies the difference between the formation and the reference image on the Voronoi cell $\mathbb{V}_i(\bar{x}(t))$. The vector $\bar{x}(t)$ is the collective position of the robots in the field $\mathbb{Q}$.

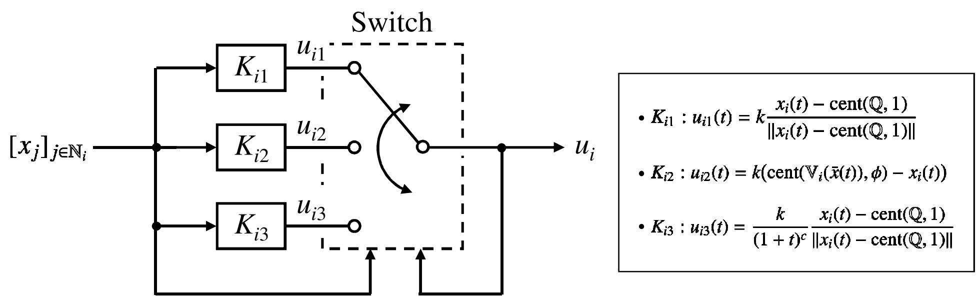

Figure 5.12: Structure of proposed controllers.

The proposed controllers are three-mode switching controllers as illustrated in Figure 5.12 where K_{i1}, K_{i2}, and K_{i3} are the sub-controllers corresponding to the first, second and third equations in (5.16), and $u_{i1}, u_{i2}, u_{i3} \in \mathbb{R}^2$ are the outputs. These sub-controllers and the switching rule are explained as follows.

Considering that $\mathbb{Q}$ is the field to express the reference image φ, we call the robots in $\mathbb{Q}$ the *player* and call the others the *nonplayer*. The sub-controllers K_{i1} and K_{i2} are for the players. The sub-controller K_{i1} moves robot i away from the centroid of $\mathbb{Q}$. Thus, if this is selected for a while, robot i eventually leaves from $\mathbb{Q}$ and becomes a nonplayer. The sub-controller K_{i2} corresponds to the mass game controller given in Section 5.2 by regarding $\bar{x}(t)$ as $x(t)$. As the result, K_{i2} achieves a formation displaying the reference image φ on the field $\mathbb{Q}$. On the other hand, the sub-controller K_{i3} is for the nonplayers. This is similar to K_{i1}, and moves the nonplayers away from the mass game field $\mathbb{Q}$. However, the nonplayers stop after a while because, from $\lim_{t\to\infty} 1/(1+t)^c = 0$ for $c \in \mathbb{R}_+$, the output $u_{i3}(t)$ goes to zero as $t \to \infty$.

Next, let us consider the switching rule. If robot i is a player, the sub-controller K_{i1} or K_{i2} is selected as follows. By definition, $\eta(\mathbb{V}_i(\bar{x}(t)), a) \leq 0$ means that the resulting formation looks brighter than or equal to the reference image φ on the Voronoi cell $\mathbb{V}_i(\bar{x}(t))$. In this case, robot i should stay at the current position and participate in the mass game. Thus, from (5.14)–(5.16) and $\xi_i(0) = 0$, $\dot{\xi}_i(t) = 1$ holds and K_{i2} is selected. The condition $|\xi_i(t)| \leq 1$ guarantees that $\xi_i(t)$ is bounded. The sub-controller K_{i1} is selected as long as $\eta(\mathbb{V}_i(\bar{x}(t)), a) > 0$. This is because $\eta(\mathbb{V}_i(\bar{x}(t)), a) > 0$ implies that the resulting formation looks darker than the reference image φ on the Voronoi cell $\mathbb{V}_i(\bar{x}(t))$, and as the result, extra robots leave from the mass game field $\mathbb{Q}$. On the other hand, when robot i is a nonplayer, the sub-controller K_{i3} is always active.

Finally, two remarks on the proposed controllers are given.

First, when $x_i(t) = \mathrm{cent}(\mathbb{Q}, 1)$, division by zero occurs in the sub-controllers K_{i1} and K_{i3}. However, in the proposed switching controllers, the problem is avoided if $x_i(0) \neq \mathrm{cent}(\mathbb{Q}, 1)$. This is shown by the following three facts.

(i) Let the local controller for robot i be given by K_{i1}. If $x_i(0) \neq \text{cent}(\mathbb{Q}, 1)$, then $x_i(t) \neq \text{cent}(\mathbb{Q}, 1)$ for every $t \in \mathbb{R}_{0+}$.

(ii) Once K_{i2} becomes active, K_{i1} does not become active.

(iii) When $x_i(t) = \text{cent}(\mathbb{Q}, 1)$, K_{i3} is not selected.

Since (i) and (iii) are trivial, (ii) is proven. From (5.14) and (5.15), $\xi_i(t)$ is non-decreasing. Because of this and $\xi_i(0) = 0$, if $\xi_i(t_0) \neq 0$ at a time $t_0 \in (0, \infty)$, $\xi_i(t) \neq 0$ holds for $t \geq t_0$. Therefore, (ii) is shown by (5.14) and (5.16).

Second, the proposed controllers depend only on the positions of the neighbors under assumptions (A1) and (A2). In fact, K_{i1} and K_{i3} are controllers depending on the position of robot i, and K_{i2} is of the form (5.2) under (A1) and (A2) as described in Section 5.2. Furthermore, the switching rule is based on the Voronoi cell $\mathbb{V}_i(\bar{x}(t))$, and so it depends on the positions of the neighbors.

5.4.2 Convergence Result

For the proposed controllers, the following result is obtained.

Theorem 5.3 For the multi-robot system Σ, suppose that $\hat{\mathbb{Q}} \supset \mathbb{Q}$ and $\varphi : \mathbb{Q} \to [0, 1]$ are given, and assume (A1) and (A2). Let $K_1, K_2, \ldots, K_n$ be given by (5.14)–(5.16). Let also $x^* \in \mathbb{R}^{2n}$ be a formation such that the positions of the robots in $\mathbb{Q}$ are a solution to $\partial J(x)/\partial x = 0$. If $x_0 \in (\mathbb{Q} \setminus \text{cent}(\mathbb{Q}, 1))^n$ and

$$c > 1 + \frac{k}{\min\limits_{(q_1,q_2)\in \text{bd}(\hat{\mathbb{Q}})\times\text{bd}(\mathbb{Q})} \|q_1 - q_2\|}, \tag{5.19}$$

then $x(t) \in \hat{\mathbb{Q}}^n$ for every $t \in \mathbb{R}_{0+}$ and $x(t)$ converges to x^*. ■

Proof The following three facts prove the theorem.

(i) There exists a time instant $\tau \in \mathbb{R}_{0+}$ such that the robots are classified into the players with K_{i2} and the nonplayers from τ. The two groups are fixed.

(ii) The sub-controller K_{i2} corresponds to the coverage controller (5.4). So, if all the players are steered by K_{i2}, the configuration converges to a solution of $\partial J(x)/\partial x = 0$.

(iii) If $x_0 \in (\mathbb{Q} \setminus \text{cent}(\mathbb{Q}, 1))^n$ and (5.19) hold, the nonplayers remain in the space $\hat{\mathbb{Q}} \setminus \mathbb{Q}$ and converge to a configuration.

The proofs of (i)–(iii) are given in Appendix 5.C. ■

Theorem 5.3 means that the robots remain in the space $\hat{\mathbb{Q}}$ and converge to a formation x^* if the gains k and c are selected so as to satisfy (5.19).

5.4.3 Numerical Experiments

Consider the multi-robot system Σ in Figure 5.2, where $n := 7500$, $\mathbb{Q} := [50, 350]^2$, $\hat{\mathbb{Q}} := [0, 400]^2$, and $a := 10^{-4}$. The reference image φ is *Airplane* in Figure 5.11 (a). The initial formation x_0 is given randomly from the uniform probability distribution on $(\mathbb{Q} \setminus \mathrm{cent}(\mathbb{Q}, 1))^{7500}$. We use the local controllers K_i ($i = 1, 2, \ldots, 7500$) given by (5.14)–(5.16) with $k := 10$ and $c := 1.3$ satisfying (5.19).

Figure 5.13 depicts the time series of the resulting formations. This shows that the proposed controllers evacuate unnecessary robots for displaying the reference image, and achieve the mass game. Also for other standard images, similar results are obtained. Figures. 5.14–5.16 show the results for the standard images *Elaine*, *House*, and *Clock*, where (a), (b), and (c) represent the reference image, the initial formation, and the final formation (at $t = 100$), respectively. From these results, we conclude that the proposed controllers solve the mass game problem for any reference image.

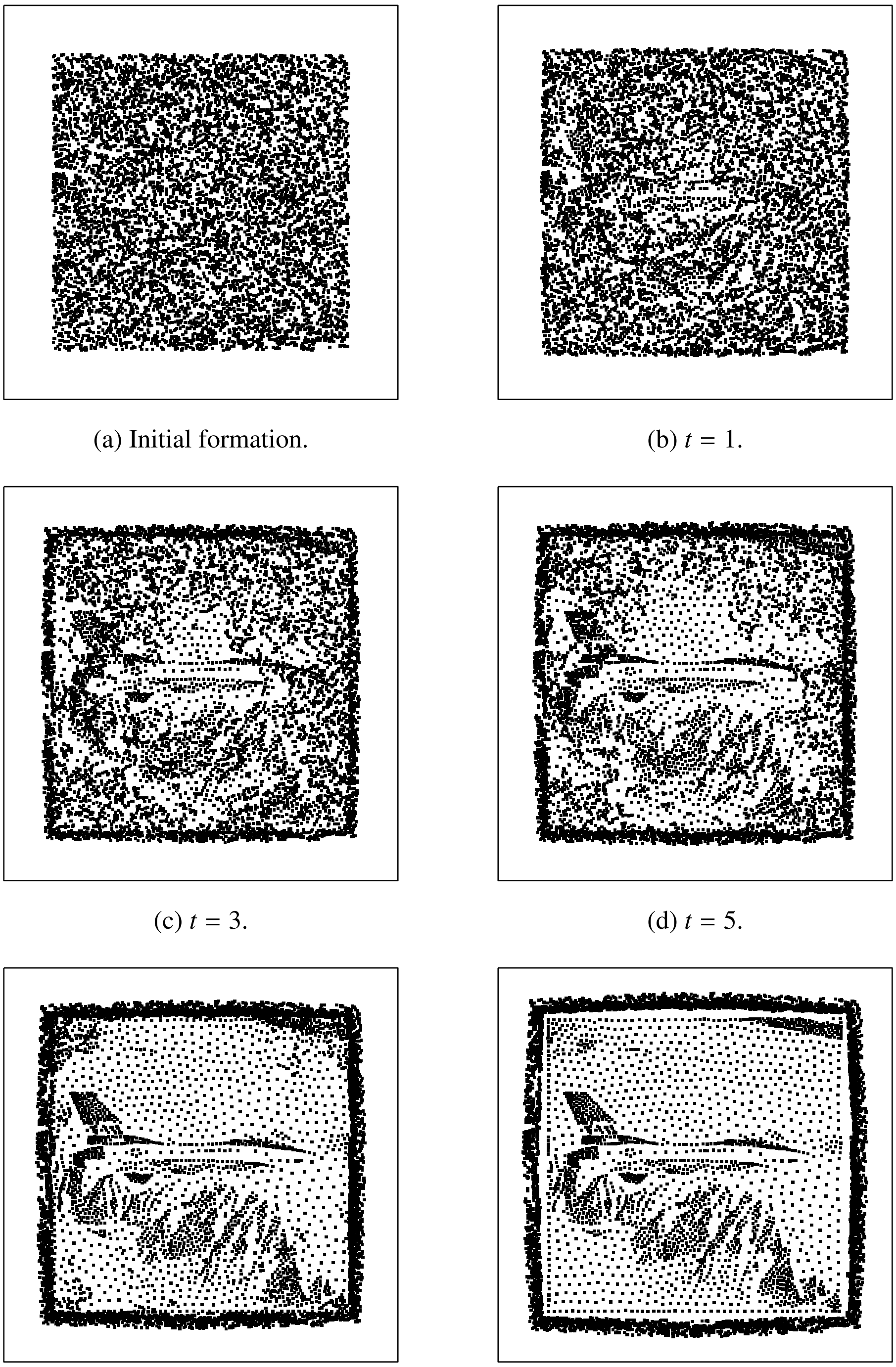

(a) Initial formation. (b) $t = 1$. (c) $t = 3$. (d) $t = 5$. (e) $t = 10$. (f) $t = 100$.

Figure 5.13: Simulation result for Airplane.

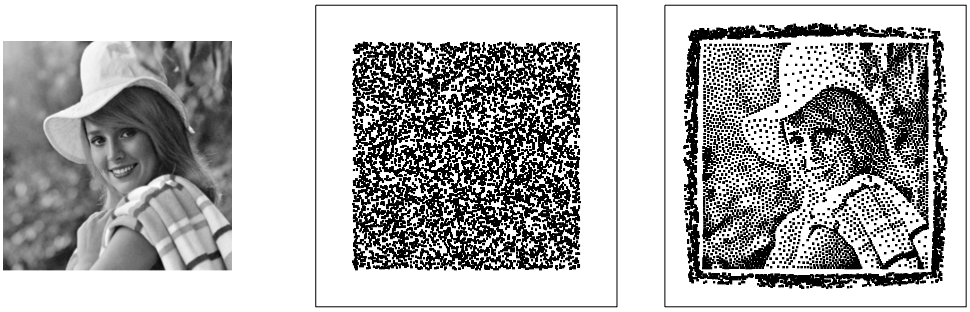

(a) Reference image. (b) Initial formation. (c) Final formation.

Figure 5.14: Simulation result for Elaine.

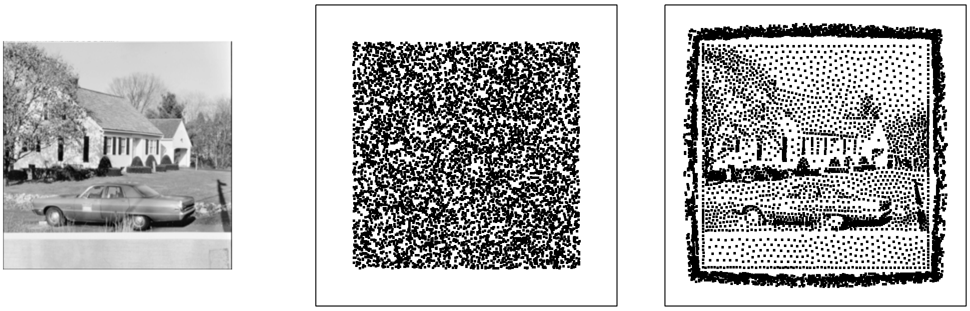

(a) Reference image. (b) Initial formation. (c) Final formation.

Figure 5.15: Simulation result for House.

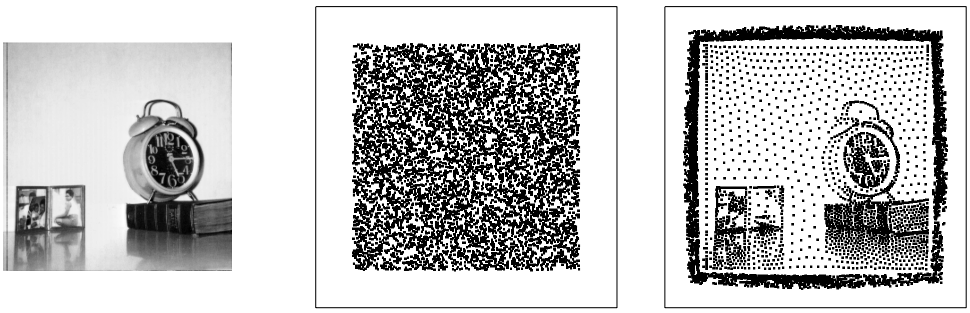

(a) Reference image. (b) Initial formation. (c) Final formation.

Figure 5.16: Simulation result for Clock.

Next, we perform the quantitative evaluation of the proposed controllers. As mentioned in Section 5.1.3, it is in general difficult to quantify the specification on human perception, that is, the visual quality. Therefore, the following method is proposed.

We first introduce the performance index called the *peak signal to noise ratio* (see, *e.g.,* [63]) :

$$\mathrm{PSNR} := 10\log_{10}\left(\frac{\mu \times \nu}{\|V - W\|^2}\right) \tag{5.20}$$

where $V \in \mathbb{R}^{\mu\times\nu}$ and $W \in \mathbb{R}^{\mu\times\nu}$ are the matrices denoting two images. This criterion is typically used to quantify the difference between an original image and a processed image. The higher value implies that the two images are closer.

However, the resulting formation is not a digital image but a formation; that is, the robots can be placed at any locations in $\mathbb{Q}$. So, the PSNR value of the resulting formation is defined as follows. Let $\Phi \in \mathbb{R}^{\mu\times\nu}$ be the matrix whose (i, j)-th element is the (i, j)-th pixel value of the $\mu \times \nu$ discretized image of φ. We divide the mass game field $\mathbb{Q}$ into the $\mu \times \nu$ blocks $\mathbb{Q}_{ij}$ $(i = 1, 2, \ldots, \mu,\ j = 1, 2, \ldots, \nu)$, and let $X \in \mathbb{R}^{\mu\times\nu}$ be the matrix corresponding to the resulting formation, *i.e.,*

$$[X]_{ij} := \begin{cases} 0 & \text{if } a_{ij} \geq 0.5, \\ 1 & \text{otherwise} \end{cases} \tag{5.21}$$

where $a_{ij} \in \mathbb{R}_{0+}$ is the area ratio of the robots over $\mathbb{Q}_{ij}$ to $\mathbb{Q}_{ij}$. Then, V and W in (5.20) are defined as the matrices given by applying a human visual filter (see Appendix 5.D) to Φ and X, which, together with (5.20), gives the PSNR value of the resulting formation. Using this, we perform the quantitative evaluation of the proposed controllers.

Table 5.1 shows the PSNR values of the resulting formations. For comparison, the PSNR values for several halftone images and the formations by the controllers proposed in Section 5.2, which are defined in the same manner as above, are also provided in the table. Here, $\mu := 256$ and $\nu := 256$, and the halftone images are generated by applying the standard method called the *error diffusion* [60] to the downsampled $\mu \times \nu$ original image.

Noting again that the higher PSNR value indicates better performance, we see that the proposed controllers provide formations which are better than the 64×64 pixel halftone images and worse than the 128×128 pixel halftone images, in terms of the visual quality. The number of the robots, which corresponds to the number of black pixels, is 7500, and so we conclude that the proposed controllers generate formations whose visual quality is comparable to that of the halftone images.

Furthermore, by comparing with the formations by the the controllers given in Section 5.2, It turns out that the proposed controllers have much better performance (approximately up to 8.6 dB). The reason is that the proposed controllers

Table 5.1: PSNR performance of proposed controllers

PSNR [dB]	Airplane	Elaine	House	Clock
Resulting formation	13.14	12.38	12.73	13.99
Halftone image (64×64 pixels)	8.65	8.13	8.29	9.39
Halftone image (128×128 pixels)	13.80	13.83	13.89	14.28
Halftone image (256×256 pixels)	25.94	26.33	25.77	25.10
Formation by (5.4) and (5.5)	6.32	9.49	7.68	5.33

evacuate unnecessary robots for displaying the reference images, while the previous controllers do not. In fact, Table 5.2 shows the numbers of the players in the resulting formations, and they are different for each reference image. Moreover, by noting that Airplane and Clock are brighter than House and Elaine, the number of the players is smaller for brighter images which only need fewer robots to express themselves. Meanwhile, in the previous controllers, the number of the players is the same for any reference image, and thus the performance for brighter images is worse. This is shown in Table 5.1.

Finally, we investigate the relation between the performance and the size of the robots. Table 5.3 presents the PSNR values of the resulting formations for several a, where $n := 3000$. We see that the performance for $a := 1.0 \times 10^{-4}$, *i.e.,* medium-sized robots, is best. The reason can be considered as follows. Let us recall that the robots correspond to black pixels. If a is a large value, the resulting formation looks a low-resolution image, and so the visual quality will be bad. Conversely, if a is a small value and the number of the robots is not enough to display reference images, then the proposed controllers provide formations which look brighter than the reference images.

In this way, we have evaluated the performance of the proposed controllers. From the above result, it is concluded that the proposed controllers are a solution to the mass game problem.

5.5 Summary

This chapter has considered a design problem of a controller network for the mass games. Based on ideas from the control theory and the image processing, we have derived a controller network to generate formations displaying grayscale images. The performance has been verified by numerical experiments with the standard images, which has shown that our controller network realizes the mass games. In addition to this, we have presented extensions to the cases of r-disk proximity

Table 5.2: Numbers of players in resulting formations

	Airplane	Elaine	House	Clock
Player	2233	3813	2925	2157

Table 5.3: PSNR performance of proposed controllers for several a

Area ratio a	Airplane	Elaine	House	Clock
3.0×10^{-4}	10.96	9.96	10.29	11.82
1.0×10^{-4}	12.74	10.66	12.11	12.56
0.3×10^{-4}	11.30	7.60	9.67	10.94

networks and a variable number of player robots. The former enables us to achieve the mass games even though the communication range of the robots is limited. The latter drastically improves the visual quality of the resulting formations.

Appendix 5.A Calibration of Weighting Function ϕ

Figure 5.17 shows the resulting formations for several weighting functions, where the setting of the simulation is the same as that in Section 5.2.3. From these results and the reference image shown in Figure 5.3 (a), we have chosen $\phi(q) := e^{-10\varphi(q)}$ as a weighting function. This is because Figure 5.17 (c) well captures the feature that the cheek of the lady in Figure 5.3 (a) is expressed by almost the same darkness.

Appendix 5.B Proofs of Facts (i) and (ii) in Proof of Theorem 5.1

Proof of (i)

It has been shown in [71] that the partial derivative of $\hat{J}(x)$ with respect to x_i is expressed as

$$\frac{\partial \hat{J}(x)}{\partial x_i} = -2 \int_{\mathbb{V}_i(x) \cap \mathbb{B}(x_i, r/2)} e^{-10\varphi(q)} dq \, (\mathrm{cent}(\mathbb{V}_i(x) \cap \mathbb{B}(x_i, r/2), e^{-10\varphi(q)}) - x_i)^\top. \tag{5.22}$$

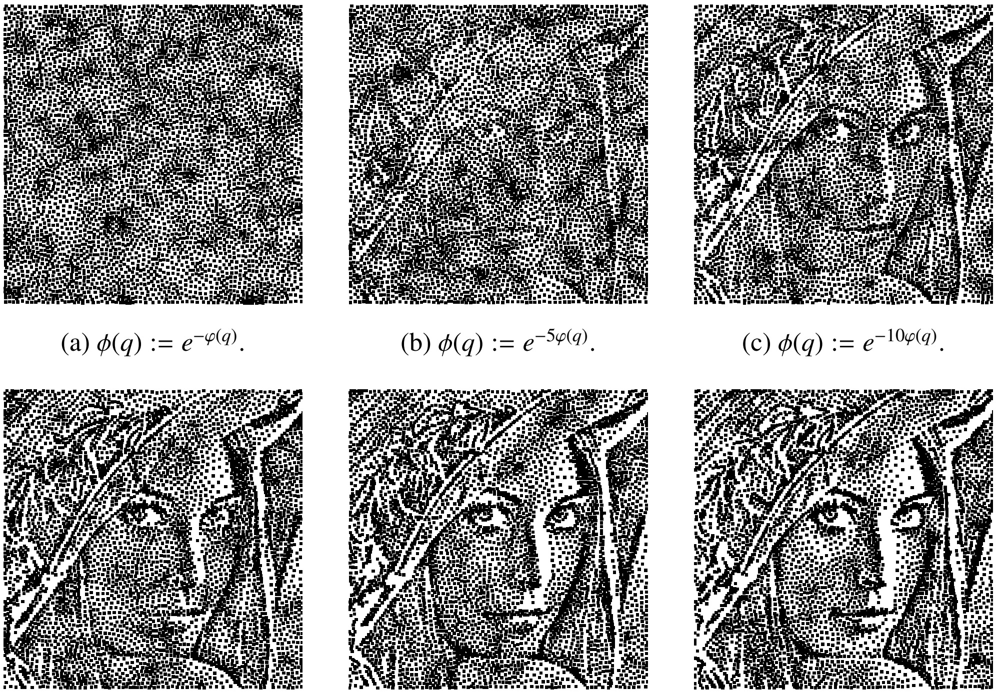

(a) $\phi(q) := e^{-\varphi(q)}$. (b) $\phi(q) := e^{-5\varphi(q)}$. (c) $\phi(q) := e^{-10\varphi(q)}$.

(d) $\phi(q) := e^{-15\varphi(q)}$. (e) $\phi(q) := e^{-20\varphi(q)}$. (f) $\phi(q) := e^{-25\varphi(q)}$.

Figure 5.17: Simulation results for several weighting functions.

From (5.1), (5.8), and (5.22), we have

$$\begin{aligned}\dot{\hat{J}}(x(t)) &= \sum_{i=1}^{n} \frac{\partial \hat{J}(x(t))}{\partial x_i} \dot{x}_i(t) \\ &= -2k \sum_{i=1}^{n} \int_{\mathbb{V}_i(x(t)) \cap \mathbb{B}(x_i(t), r/2)} e^{-10\varphi(q)} dq \\ &\qquad \times \|\mathrm{cent}(\mathbb{V}_i(x(t)) \cap \mathbb{B}(x_i(t), r/2), e^{-10\varphi(q)}) - x_i(t)\|^2. \qquad (5.23)\end{aligned}$$

Thus, since $k > 0$ and $e^{-10\varphi(q)} > 0$ for every $q \in \mathbb{Q}$, $\dot{\hat{J}}(x(t))$ is negative semi-definite, which completes the proof.

Proof of (ii)

From (5.23), the set of the points satisfying $\dot{\hat{J}}(x) = 0$ is given by

$$\left\{ x \in \mathbb{R}^{2n} \,\middle|\, x_i = \mathrm{cent}(\mathbb{V}_i(x) \cap \mathbb{B}(x_i, r/2), e^{-10\varphi(q)}) \ (i = 1, 2, \ldots, n) \right\}. \qquad (5.24)$$

From (5.1) and (5.8), $\dot{x}_i(t) \equiv 0\ \forall i \in \{1, 2, \ldots, n\}$ for any x of the set (5.24). So, the set (5.24) is an invariant set. Moreover, it follows from (5.22) that the set (5.24) is the set of solutions to $\partial \hat{J}(x)/\partial x = 0$. This proves (ii).

Appendix 5.C Proofs of Facts (i)–(iii) in Proof of Theorem 5.3

Proof of (i)

The following three facts show (i).

- If robot i is a player and the controller K_i is switched to K_{i2}, then it is not switched to K_{i1}.
- When the above switching does not occur, robot i becomes a nonplayer in a finite time by the sub-controller K_{i1},
- A nonplayer does not become a player.

The first one follows from fact (ii) in Section 5.4.1. The second one is as described in Section 5.4.1. The third one follows since the sub-controller K_{i3} moves robot i away from the field $\mathbb{Q}$.

Proof of (ii)

From (5.18), $\bar{x}(t)$ denotes the collective position of the players. Thus, by regarding $\bar{x}(t)$ in K_{i2} as $x(t)$ in (5.4), facts (i) and (ii) in Section 5.2.1 and LaSalle's principle prove the statement.

Proof of (iii)

First, we show that the nonplayers remain in the space $\hat{\mathbb{Q}} \setminus \mathbb{Q}$. As aforementioned, a nonplayer does not become a player. Therefore, if robot i becomes a nonplayer at a time $t_1 \in [0, \infty)$, it is a nonplayer and is governed by K_{i3} on the time interval

$[t_1, \infty)$. Then, from (5.1), (5.14), and (5.16), we have

$$\begin{aligned}
\max_{t_2 \in [t_1,\infty)} \|x_i(t_2) - x_i(t_1)\| &= \max_{t_2 \in [t_1,\infty)} \left\| \int_{t_1}^{t_2} \dot{x}_i(t) dt \right\| \\
&\leq \max_{t_2 \in [t_1,\infty)} \int_{t_1}^{t_2} \|\dot{x}_i(t)\| \, dt \\
&< \int_{t_1}^{\infty} \|\dot{x}_i(t)\| \, dt \\
&\leq \int_{t_1}^{\infty} \frac{k}{(1+t)^c} dt + \int_{0}^{t_1} \frac{k}{(1+t)^c} dt \\
&= \begin{cases} \infty & \text{if } c \leq 1, \\ -\dfrac{k}{1-c} & \text{otherwise.} \end{cases}
\end{aligned} \tag{5.25}$$

Moreover, it can be shown by a simple calculation that

$$\max_{t_2 \in [t_1,\infty)} \|x_i(t_2) - x_i(t_1)\| < \min_{(q_1,q_2) \in \mathrm{bd}(\hat{\mathbb{Q}}) \times \mathrm{bd}(\mathbb{Q})} \|q_1 - q_2\| \tag{5.26}$$

under (5.19). So, if $x_i(0) \in \mathbb{Q} \setminus \mathrm{cent}(\mathbb{Q}, 1)$, then $x_i(t) \in \hat{\mathbb{Q}} \setminus \mathbb{Q}$ for every $t \in [t_1, \infty)$. This shows the above statement.

Next, we prove that the nonplayers converge to a configuration. Suppose again that robot i is a nonplayer and is steered by K_{i3} on the time interval $[t_1, \infty)$. Then, from (5.14), (5.16), and the fact that $\lim_{t\to\infty} 1/(1+t)^c = 0$ for $c \in \mathbb{R}_+$, we obtain $\lim_{t\to\infty} u_i(t) = 0$. Hence, $\lim_{t\to\infty} \dot{x}_i(t) = 0$ holds because of (5.1). This implies the statement, and the proof is completed.

Appendix 5.D Human Visual Filter

The human visual filter, proposed in [72] as a model of the human visual system, is shown in Figure 5.18. The matrices U and Y are the input and output images of $\mu \times \nu$ pixels. The map $\mathcal{F}$ is the Fourier transformation with the Nyquist frequency

$$\omega_{xmax} := \frac{\pi \nu \delta}{360 \ell_x}, \qquad \omega_{ymax} := \frac{\pi \mu \delta}{360 \ell_y}$$

where $\delta \in \mathbb{R}_+$ is the viewing distance from the eye and $\ell_x \in \mathbb{R}_+$ and $\ell_y \in \mathbb{R}_+$ are the image sizes in the horizontal and vertical directions. The output is denoted by $\tilde{U}(\omega_x, \omega_y)$ for the horizontal and vertical frequency variables ω_x and ω_y in cycles per degree. The filter H denotes the spatial lowpass filtering property of the human

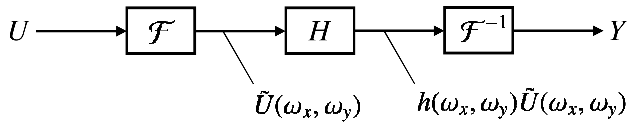

Figure 5.18: Block diagram of human visual filter.

eye, which multiplies

$$h(\omega_x, \omega_y) := \begin{cases} \Big(0.0499 + 0.2964\omega_r(\omega_x, \omega_y)\Big)\exp\Big(-(0.114\omega_r(\omega_x, \omega_y))^{1.1}\Big) \\ \qquad\qquad\qquad\qquad\qquad\qquad\qquad \text{if } \omega_r(\omega_x, \omega_y) \geq 7.8909, \\ 0.9809 \qquad\qquad\qquad\qquad\qquad\qquad \text{otherwise} \end{cases}$$

by $\tilde{U}(\omega_x, \omega_y)$, where

$$\omega_r(\omega_x, \omega_y) := \frac{\sqrt{\omega_x{}^2 + \omega_y{}^2}}{0.15\cos\Big(4\arctan(\omega_y/\omega_x)\Big) + 0.85}.$$

Finally, the map $\mathcal{F}^{-1}$ is the inverse Fourier transformation. In Section 5.4.3, we have used this human visual filter with $d := 500$ [mm], $\ell_x := 30$ [mm], and $\ell_y := 30$ [mm].

Chapter 6

Conclusion

This thesis has addressed several design problems of the controller network. More precisely, we have considered the problems of

1) designing a controller network to stabilize a given plant subject to the constraints that the network topology is unknown and all the controller nodes are the same,

2) designing a controller network for the real-time pricing, such that the total power consumption of consumers tracks a given reference input subject to a constraint on the range of the power price,

3) designing a controller network for the robotic mass games, *i.e.,* to let robots organize themselves into a formation displaying a given grayscale image.

For these three problems, the thesis has made the following contributions.

- In Chapter 3, we have presented a solution to problem 1. It is given as the combination of sensor nodes, controller nodes, and an actuator node, such that the resulting network acts as a state feedback controller. By introducing a parameterized coordinate transformation and reducing the stabilization problem to finding a range of the parameter, we have derived gain conditions for the stability of the resulting feedback system. Furthermore, we have clarified the relation between the stabilizing gain and the network topology, which enables us to easily design the stabilizing gain. These results will be useful to design a controller network which is scalable and robust against changes in the network topology.

- In Chapter 4, we first have derived a necessary for solvability of problem 2. This clarifies the relation between the upper bound of the power price and the reference input which the total power consumption can track. Then, we have presented a controller network for the real-time pricing by extending the result in Chapter 3 to integral control. With this result, we can achieve the real-time pricing without collecting the information on the power consumption from all the consumers.

- In Chapter 5, we have given a solution to problem 3. The key idea behind this result is to fuse ideas from the control theory and the image processing. The solution has been verified by numerical experiments with the standard images, and it has been demonstrated that our controller network generates formations displaying grayscale images. In addition, we have presented extensions to the cases of r-disk proximity networks and a variable number of player robots. The former enables us to achieve the mass games even though the communication range of the robots is limited. The latter drastically improves the visual quality of the resulting formations.

Although such results have been obtained, there are a number of issues to be addressed. We conclude this thesis by showing some of them as follows:

- In all the problems handled here, we should consider unreliability of communication, *e.g.,* noise, delays, and packet dropouts, for practical use.
- Our result for problem 1 should be extended to output-feedback control and multiple-input plants for a wide range of applications.
- For problem 2, we should give a solution considering the effect of the saturation of the power price because it may make the real-time pricing system unstable and as a result social disruption is caused.
- It is necessary from a practical standpoint to introduce a collision avoidance algorithm (*e.g.,* the potential field method [22]) to our controller network for problem 3.

Appendix A

Auxiliary Results for Proofs

We present here results used in some proofs in this thesis.

A.1 Gershgorin Theorem

The following result is known as *Gershgorin theorem*.

Theorem A.1 For the matrix $M \in \mathbb{C}^{n\times n}$, all the eigenvalues of M are in the set

$$\bigcup_{i=1}^{n} \left\{ s \in \mathbb{C} \,\middle|\, \left|s - [M]_{ii}\right| \leq \sum_{j=1, j\neq i}^{n} \left|[M]_{ij}\right| \right\}. \tag{A.1}$$

■

The proof can be found in [73].

Gershgorin theorem gives the relation between the elements of a matrix and the region where the eigenvalues exist. This allows us to obtain information on the eigenvalues of a matrix from its elements.

A.2 LaSalle's Principle

Consider the system

$$\dot{x}(t) = f(x(t)) \tag{A.2}$$

where $x(t) \in \mathbb{R}^n$ is the state and $f : \mathbb{R}^n \to \mathbb{R}^n$ is a Lipschitz function on $\mathbb{R}^n$. For this system, a set $\mathbb{S}$ is said to be an *invariant set* if

$$x(t) \in \mathbb{S} \qquad \forall t \in \mathbb{R}_+$$

for every $x(0) \in \mathbb{S}$.

The following theorem provides a sufficient condition to guarantee that the solution to the system (A.2) converges to an invariant set, which is called *LaSalle's principle*.

Theorem A.2 Consider the system (A.2). Let $\mathbb{M} \subset \mathbb{R}^n$ be a compact set and let $V : \mathbb{R}^n \to \mathbb{R}$ be a continuously differentiable function. Assume that $\mathbb{M}$ is an invariant set for (A.2) and $\dot{V}(x) \leq 0$ for every $x \in \mathbb{M}$. Then, every solution to (A.2) starting in $\mathbb{M}$ converges to the largest invariant set in $\{x \in \mathbb{M} \,|\, \dot{V}(x) = 0\}$. ■

The proof can be found in [74].

Bibliography

[1] M. Pajic, S. Sundaram, G. J. Pappas, and R. Mangharam, “The wireless control network: A new approach for control over networks,” *IEEE Transactions on Automatic Control*, vol. 56, no. 10, pp. 2305–2318, 2011.

[2] J. Broch, D. A. Maltz, D. B. Johnson, Y.-C. Hu, and J. Jetcheva, “A performance comparison of multi-hop wireless ad hoc network routing protocols,” in *Proceedings of the 4th Annual ACM/IEEE International Conference on Mobile Computing and Networking*, pp. 85–97, 1998.

[3] K. Jain, J. Padhye, V. N. Padmanabhan, and L. Qiu, “Impact of interference on multi-hop wireless network performance,” *Wireless Networks*, vol. 11, no. 4, pp. 471–487, 2005.

[4] R. Alur, A. D’Innocenzo, K. H. Johansson, G. J. Pappas, and G. Weiss, “Compositional modeling and analysis of multi-hop control networks,” *IEEE Transactions on Automatic Control*, vol. 56, no. 10, pp. 2345–2357, 2011.

[5] A. D’Innocenzo, M. Di Benedetto, and E. Serra, “Fault tolerant control of multi-hop control networks,” *IEEE Transactions on Automatic Control*, vol. 58, no. 6, pp. 1377–1389, 2013.

[6] W. Ren and R. W. Beard, *Distributed Consensus in Multi-vehicle Cooperative Control*. Springer, 2008.

[7] M. Pajic, R. Mangharam, G. J. Pappas, and S. Sundaram, “Topological conditions for in-network stabilization of dynamical systems,” *IEEE Journal on Selected Areas in Communications*, vol. 31, no. 4, pp. 794–807, 2013.

[8] M. Pajic, S. Sundaram, J. Le Ny, G. J. Pappas, and R. Mangharam, “Closing the loop: A simple distributed method for control over wireless networks,” in *Proceedings of the 11th International Conference on Information Processing in Sensor Networks*, pp. 25–36, 2012.

[9] F. Miao, M. Pajic, R. Mangharam, and G. J. Pappas, “Networked realization of discrete-time controllers,” in *Proceedings of the American Control Conference*, pp. 2996–3001, 2013.

[10] K. J. Hunt, D. Sbarbaro, R. Żbikowski, and P. J. Gawthrop, “Neural networks for control systems-a survey,” *Automatica*, vol. 28, no. 6, pp. 1083–1112, 1992.

[11] W. Ren and B. Xu, “Wireless neural control network for nonlinear systems,” in *Proceedings of the 32nd Chinese Control Conference*, pp. 6537–6542, 2013.

[12] W. Ren and B. Xu, “Distributed wireless networked control for a class of lurie-type nonlinear systems,” *Mathematical Problems in Engineering*, vol. 2014, Article ID 708252, 14 pages, 2014.

[13] H.-D. Wang and H.-N. Wu, “Distributed consensus observers based H_∞ control for continuous systems with sensor and actuator networks,” in *Proceedings of the 33rd Chinese Control Conference*, pp. 4320–4325, 2014.

[14] H. Ando, Y. Oasa, I. Suzuki, and M. Yamashita, “Distributed memoryless point convergence algorithm for mobile robots with limited visibility,” *IEEE Transactions on Robotics and Automation*, vol. 15, no. 5, pp. 818–828, 1999.

[15] J. Lin, A. S. Morse, and B. D. Anderson, “The multi-agent rendezvous problem,” in *Proceedings of the 42nd IEEE Conference on Decision and Control*, vol. 2, pp. 1508–1513, 2003.

[16] J. Cortés, S. Martínez, and F. Bullo, “Robust rendezvous for mobile autonomous agents via proximity graphs in arbitrary dimensions,” *IEEE Transactions on Automatic Control*, vol. 51, no. 8, pp. 1289–1298, 2006.

[17] R. Olfati-Saber, J. A. Fax, and R. M. Murray, “Consensus and cooperation in networked multi-agent systems,” *Proceedings of the IEEE*, vol. 95, no. 1, pp. 215–233, 2007.

[18] A. Kashyap, T. Başar, and R. Srikant, “Quantized consensus,” *Automatica*, vol. 43, no. 7, pp. 1192–1203, 2007.

[19] C. H. Caicedo-Nunez and M. Zefran, “Rendezvous under noisy measurements,” in *Proceedings of the 47th IEEE Conference on Decision and Control*, pp. 1815–1820, 2008.

[20] H. Yu and X. Xia, "Adaptive consensus of multi-agents in networks with jointly connected topologies," *Automatica*, vol. 48, no. 8, pp. 1783–1790, 2012.

[21] H. Du, S. Li, and S. Ding, "Bounded consensus algorithms for multi-agent systems in directed networks," *Asian Journal of Control*, vol. 15, no. 1, pp. 282–291, 2013.

[22] A. Howard, M. J. Matarić, and G. S. Sukhatme, "Mobile sensor network deployment using potential fields: A distributed, scalable solution to the area coverage problem," in *Proceedings of the 6th International Symposium on Distributed Autonomous Robotics Systems*, 2002.

[23] J. Cortes, S. Martinez, T. Karatas, and F. Bullo, "Coverage control for mobile sensing networks," *IEEE Transactions on Robotics and Automation*, vol. 20, no. 2, pp. 243–255, 2004.

[24] W. Li and C. G. Cassandras, "Distributed cooperative coverage control of sensor networks," in *Proceedings of the 44th IEEE Conference on Decision and Control and the European Control Conference*, pp. 2542–2547, 2005.

[25] L. C. Pimenta, V. Kumar, R. C. Mesquita, and G. A. Pereira, "Sensing and coverage for a network of heterogeneous robots," in *Proceedings of the 47th IEEE Conference on Decision and Control*, pp. 3947–3952, 2008.

[26] M. Schwager, D. Rus, and J.-J. Slotine, "Decentralized, adaptive coverage control for networked robots," *The International Journal of Robotics Research*, vol. 28, no. 3, pp. 357–375, 2009.

[27] K. Laventall and J. Cortés, "Coverage control by multi-robot networks with limited-range anisotropic sensory," *International Journal of Control*, vol. 82, no. 6, pp. 1113–1121, 2009.

[28] M. Zhu and S. Martínez, "Distributed coverage games for energy-aware mobile sensor networks," *SIAM Journal on Control and Optimization*, vol. 51, no. 1, pp. 1–27, 2013.

[29] C. W. Reynolds, "Flocks, herds and schools: A distributed behavioral model," *Computer Graphics*, vol. 21, no. 4, pp. 25–34, 1987.

[30] R. Olfati-Saber, "Flocking for multi-agent dynamic systems: Algorithms and theory," *IEEE Transactions on Automatic Control*, vol. 51, no. 3, pp. 401–420, 2006.

[31] H. G. Tanner, A. Jadbabaie, and G. J. Pappas, “Flocking in fixed and switching networks,” *IEEE Transactions on Automatic Control*, vol. 52, no. 5, pp. 863–868, 2007.

[32] H. Su, X. Wang, and Z. Lin, “Flocking of multi-agents with a virtual leader,” *IEEE Transactions on Automatic Control*, vol. 54, no. 2, pp. 293–307, 2009.

[33] W. Yu, G. Chen, and M. Cao, “Distributed leader-follower flocking control for multi-agent dynamical systems with time-varying velocities,” *Systems & Control Letters*, vol. 59, no. 9, pp. 543–552, 2010.

[34] G. Wen, Z. Duan, Z. Li, and G. Chen, “Flocking of multi-agent dynamical systems with intermittent nonlinear velocity measurements,” *International Journal of Robust and Nonlinear Control*, vol. 22, no. 16, pp. 1790–1805, 2012.

[35] J. Zhu, J. Lu, and X. Yu, “Flocking of multi-agent non-holonomic systems with proximity graphs,” *IEEE Transactions on Circuits and Systems I: Regular Papers*, vol. 60, no. 1, pp. 199–210, 2013.

[36] S. Martinez, J. Cortes, and F. Bullo, “Motion coordination with distributed information,” *IEEE Control Systems Magazine*, vol. 27, no. 4, pp. 75–88, 2007.

[37] M. Mesbahi and M. Egerstedt, *Graph Theoretic Methods in Multiagent Networks*. Princeton University Press, 2010.

[38] K. Sugihara and I. Suzuki, “Distributed algorithms for formation of geometric patterns with many mobile robots,” *Journal of Robotic Systems*, vol. 13, no. 3, pp. 127–139, 1996.

[39] I. Suzuki and M. Yamashita, “Distributed anonymous mobile robots: Formation of geometric patterns,” *SIAM Journal on Computing*, vol. 28, no. 4, pp. 1347–1363, 1999.

[40] X. Défago and A. Konagaya, “Circle formation for oblivious anonymous mobile robots with no common sense of orientation,” in *Proceedings of the 2nd ACM International Workshop on Principles of Mobile Computing*, pp. 97–104, 2002.

[41] B. Katreniak, “Biangular circle formation by asynchronous mobile robots,” in *Structural Information and Communication Complexity*, pp. 185–199, Springer, 2005.

[42] Y. Dieudonné, O. Labbani-Igbida, and F. Petit, "Circle formation of weak mobile robots," *ACM Transactions on Autonomous and Adaptive Systems*, vol. 3, no. 4, p. 16, 2008.

[43] J. P. Desai, J. P. Ostrowski, and V. Kumar, "Modeling and control of formations of nonholonomic mobile robots," *IEEE Transactions on Robotics and Automation*, vol. 17, no. 6, pp. 905–908, 2001.

[44] R. Olfati-Saber and R. M. Murray, "Distributed cooperative control of multiple vehicle formations using structural potential functions," in *Proceedings of the 15th IFAC World Congress*, pp. 346–352, 2002.

[45] T. Eren, P. N. Belhumeur, B. D. Anderson, and A. S. Morse, "A framework for maintaining formations based on rigidity," in *Proceedings of the 15th IFAC World Congress*, pp. 2752–2757, 2002.

[46] D. V. Dimarogonas and K. H. Johansson, "On the stability of distance-based formation control," in *Proceedings of the 47th IEEE Conference on Decision and Control*, pp. 1200–1205, 2008.

[47] L. Krick, M. E. Broucke, and B. A. Francis, "Stabilisation of infinitesimally rigid formations of multi-robot networks," *International Journal of Control*, vol. 82, no. 3, pp. 423–439, 2009.

[48] F. Dorfler and B. Francis, "Geometric analysis of the formation problem for autonomous robots," *IEEE Transactions on Automatic Control*, vol. 55, no. 10, pp. 2379–2384, 2010.

[49] K.-K. Oh and H.-S. Ahn, "Formation control of mobile agents based on inter-agent distance dynamics," *Automatica*, vol. 47, no. 10, pp. 2306–2312, 2011.

[50] Z. Lin, L. Wang, Z. Han, and M. Fu, "Distributed formation control of multi-agent systems using complex laplacian," *IEEE Transactions on Automatic Control*, vol. 59, no. 7, pp. 1765–1777, 2013.

[51] J. A. Fax and R. M. Murray, "Information flow and cooperative control of vehicle formations," *IEEE Transactions on Automatic Control*, vol. 49, no. 9, pp. 1465–1476, 2004.

[52] M. Ji and M. Egerstedt, "Distributed coordination control of multiagent systems while preserving connectedness," *IEEE Transactions on Robotics*, vol. 23, no. 4, pp. 693–703, 2007.

[53] W. Ren and E. Atkins, "Distributed multi-vehicle coordinated control via local information exchange," *International Journal of Robust and Nonlinear Control*, vol. 17, no. 10-11, pp. 1002–1033, 2007.

[54] D. Gu, "A differential game approach to formation control," *IEEE Transactions on Control Systems Technology*, vol. 16, no. 1, pp. 85–93, 2008.

[55] Y. Cao and W. Ren, "Sampled-data formation control under dynamic directed interaction," in *Proceedings of the American Control Conference*, pp. 5186–5191, 2009.

[56] Y. Cao, W. Ren, and Z. Meng, "Decentralized finite-time sliding mode estimators and their applications in decentralized finite-time formation tracking," *Systems & Control Letters*, vol. 59, no. 9, pp. 522–529, 2010.

[57] M. Ou, H. Du, and S. Li, "Finite-time formation control of multiple nonholonomic mobile robots," *International Journal of Robust and Nonlinear Control*, vol. 24, no. 1, pp. 140–165, 2014.

[58] A. Faruqui and S. Sergici, "Household response to dynamic pricing of electricity: a survey of 15 experiments," *Journal of Regulatory Economics*, vol. 38, no. 2, pp. 193–225, 2010.

[59] D. P. Spanos, R. Olfati-Saber, and R. M. Murray, "Dynamic consensus for mobile networks," in *Proceedings of the 16th IFAC World Congress*, 2005.

[60] R. Ulicheney, *Digital Halftoning*. MIT Press, 1987.

[61] "Standard image data base." `http://sipi.usc.edu/database/`.

[62] F. Bullo, J. Cortés, and S. Martínez, *Distributed Control of Robotic Networks*. Princeton University Press, 2009.

[63] Z. Wang and A. C. Bovik, "Mean squared error: love it or leave it? a new look at signal fidelity measures," *IEEE Signal Processing Magazine*, vol. 26, no. 1, pp. 98–117, 2009.

[64] B. Q. Feng, "Equivalence constants for certain matrix norms," *Linear Algebra and its Applications*, vol. 374, pp. 247–253, 2003.

[65] A. Jokić, M. Lazar, and P. van den Bosch, "Real-time control of power systems using nodal prices," *International Journal of Electrical Power & Energy Systems*, vol. 31, no. 9, pp. 522–530, 2009.

[66] F. Oldewurtel, A. Ulbig, A. Parisio, G. Andersson, and M. Morari, "Reducing peak electricity demand in building climate control using real-time pricing and model predictive control," in *Proceedings of the 49th IEEE Conference on Decision and Control*, pp. 1927–1932, 2010.

[67] M. Roozbehani, M. Dahleh, and S. Mitter, "On the stability of wholesale electricity markets under real-time pricing," in *Proceedings of the 49th IEEE Conference on Decision and Control*, pp. 1911–1918, 2010.

[68] P. Samadi, A. H. Mohsenian-Rad, R. Schober, V. W. S. Wong, and J. Jatskevich, "Optimal real-time pricing algorithm based on utility maximization for smart grid," in *Proceedings of the 1st IEEE International Conference on Smart Grid Communications*, pp. 415–420, 2010.

[69] "Statistics bureau of japan." `http://www.stat.go.jp/english/data/kokusei/2010/summary.htm`.

[70] X. Fang, S. Misra, G. Xue, and D. Yang, "Smart grid – the new and improved power grid: a survey," *IEEE Communications Surveys & Tutorials*, vol. 14, no. 4, pp. 944–980, 2012.

[71] J. Cortes, S. Martinez, and F. Bullo, "Spatially-distributed coverage optimization and control with limited-range interactions," *ESAIM: Control, Optimisation and Calculus of Variations*, vol. 11, no. 4, pp. 691–719, 2005.

[72] T. Mitsa and K. L. Varkur, "Evaluation of contrast sensitivity functions for the formulation of quality measures incorporated in halftoning algorithms," in *Proceedings of the IEEE International Conference on Acoustics, Speech, and Signal Processing*, vol. 5, pp. 301–304, 1993.

[73] R. A. Horn and C. R. Johnson, *Matrix Analysis*. Cambridge University Press, 1985.

[74] H. J. Marquez, *Nonlinear Control Systems: Analysis and Design*. Wiley-Interscience, 2003.

Published Papers by Author

Chapter 3

- S. Izumi, S. Azuma, and T. Sugie, “Stabilization by controller networks,” in *Proceedings of the American Control Conference,* pp. 2339–2344, 2013.

Chapter 4

- S. Izumi, S. Azuma, and T. Sugie, “Real-time pricing based on networked estimators,” in *Proceedings of the 53rd IEEE Conference on Decision and Control,* pp. 2441–2446, 2014.

Chapter 5

- S. Azuma, S. Izumi, and T. Sugie, “Halftone mass games by fixed number of mobile robots,” *Transactions of the Institute of Systems, Control and Information Engineers,* vol. 25, no. 4, pp. 94–100, 2012 (in Japanese).

- S. Izumi, S. Azuma, and T. Sugie “Robotic mass games by distributed hybrid controllers,” in *Proceedings of the 4th IFAC Conference on Analysis and Design of Hybrid Systems,* pp. 339–343, 2012.

- S. Izumi, S. Azuma, and T. Sugie “Robotic mass games over r-disk proximity networks,” *Transactions of the Society of Instrument and Control Engineers,* vol. 49, no. 7, pp. 720–726, 2013 (in Japanese).

- S. Izumi, S. Azuma, and T. Sugie “Distributed hybrid controllers for multi-agent mass games by a variable number of player agents,” *Asian Journal of Control,* vol. 17, no. 3, 2015, to appear.

Related Paper

- S. Izumi, S. Azuma, and T. Sugie, “Coverage control inspired by bacterial chemotaxis,” in *Proceedings of the 33rd IEEE Symposium on Reliable Distributed Systems,* pp. 34–39, 2014.